UNIVERSITÀ
DEGLI STUDI
DI PADOVA

Head Office: Università degli Studi di Padova

Department of General Psychology and Padova Neuroscience Center

---

Ph.D. COURSE IN: Neuroscience

SERIES: XXXVI

MODULATIONS OF SPATIAL PROCESSING THROUGH ATTENTIONAL LOAD

Coordinator: Prof. Antonino Vallesi

Supervisor: Prof. Mario Bonato

Co-Supervisor: Prof. Dante Mantini

Ph.D. student: Maria Silvia Saccani

ABSTRACT

Spatial processing is implemented by selective attention mechanisms and allows us to effectively deal with the broad flow of visual information in a seemingly effortless and highly efficient way. Yet, spatial processing efficiency seems to be influenced by levels of attentional load. The common thread weaving through the diverse contributions that will be presented in this thesis is a detailed investigation into load-induced spatial processing modulations. To do that we adopted a multitasking approach, grounded on the hypothesis that different tasks, despite their distinct nature and specific demands, are characterized by the common use of relatively unspecific yet limited attentional resources. Therefore, when the attentional load increases, for example because of dual-tasking, performance may be impacted.

Firstly, we investigated load-induced spatial processing modulations in the damaged cognitive system. Specifically, we tested the impact of attentional load upon spatial processing in an ultra-chronic right hemisphere damaged patient. Despite his ceiling performance in classic paper and pencil test, he showed biases toward the ipsilesional space when attentional load was increased. As understanding the performance of the "baseline system" is essential for assessing the extent of impairment in patients, we also investigated load-induced spatial processing modulations in healthy adults. In this case we employed different versions of a rather complex dual-task paradigm, involving the presentation of stimuli capable of eliciting an audiovisual integration illusion (i.e., sound-induced flash illusion). Although participants showed increased illusion rates when attentional load was increased, there were no differences between left- and right-sided stimuli. Finally, we investigated neural correlates of load-induced spatial processing modulations in healthy adults. Specifically, we employed a dual-task paradigm identical to the one used in the previous study and recorded electroencephalography during resting-state and while the participants were completing the task. Analysing resting-state data, we have uncovered significant correlations between task performance and intrinsic functional connectivity networks related to auditory and visual processing, as well as the allocation of attentional resources in space. Additionally, analysing Event-Related Potentials, we have identified N1, N2, and P3 modulations associated with the presentation of stimuli eliciting the sound-induced flash illusion during different levels of attentional load, with N1 modulations differing depending on the side of the stimuli.

INDEX

RATIONALE AND SUMMARY OF THE THESIS WORK

In today's digital age, we frequently encounter a vast amount of visual information that surpasses our ability to process it. This is evident in our daily interactions with various digital tools and technologies. For instance, while scrolling through social media feeds, we are bombarded with a constant stream of images and videos. Similarly, in urban environments, digital billboards and screens display a continuous loop of visual content. Even our workspaces have transformed; with multiple tabs open on computer screens, the volume of visual data we are expected to process has increased exponentially. Luckily enough, humans are equipped with very efficient spatial processing abilities, to the extent that we continuously use them without even realizing how pervasive their presence is. Spatial processing is implemented by selective attention mechanisms and allows us to effectively deal with this broad flow of visual information in a seemingly effortless and highly efficient way (Peelen & Kastner, 2014). More specifically, thanks to these selective attention mechanisms, under normal circumstances, we can process the most salient or potentially important stimuli within a specific location in space, while ignoring all others (Moore & Zirnsak, 2017; Peelen & Kastner, 2014; Vecera & Rizzo, 2003). Yet, spatial processing efficiency can be negatively affected, by various contextual factors, such as levels of alertness, vigilance, drowsiness, or fatigue (Bellgrove et al., 2004; Benwell et al., 2013; Dodds et al., 2008; Dufour et al., 2007; Fimm et al., 2006; Manly et al., 2005). Crucially for the present work, spatial processing efficiency seems also to be influenced by levels of attentional load. This is proved by the emergence of spatial processing modulations when spatial processing is made more challenging through additional demands (Bonato et al., 2010; Dodds et al., 2008; Lisi et al., 2015; Naert et al., 2018; Peers et al., 2006; Pérez et al., 2008, 2009). This influence could be of utmost importance in everyday life. Consider, for instance, driving a car in heavy traffic: you must selectively process relevant stimuli in particular locations, such as pedestrians or other vehicles on the road, while disregarding others, like the surrounding scenery. When you engage in an additional task, such as talking on the phone, attentional load will increase. If this actually induces spatial processing modulations, it could have exceedingly hazardous consequences in such a situation (Lamble et al., 1999).

Load-induced spatial processing modulations are commonly investigated, exploiting a *multitasking approach*. For instance, it is possible to design dual-tasks that pair a primary task, which requires spatial processing abilities, with a concurrent secondary task, that allows to modulate attentional load. Primary tasks involving spatial processing abilities can vary from detection of targets on a

screen to navigating in a controlled virtual environment. Secondary tasks can be even more heterogeneous, ranging from the cognitive domain to the motor domain, as they are generally intended to divide the participant's attention. Therefore, under such conditions, spatial processing abilities can be assessed while attentional resources are not entirely devoted to spatial processing (Bonato, 2012; Saccani et al., 2022).

The multitasking approach has different advantages when studying clinical populations, such as patients with unilateral brain damage. These patients very often show spatial processing deficits for the space contralateral to the lesion (Corbetta & Shulman, 2011; Damasio et al., 1980; Husain, 2019). These deficits cannot be ascribed to sensory or motor impairments, but rather stem from a failure of the selective attention mechanisms, that after the insult are no longer symmetric but, rather, biased toward the space ipsilateral to the lesion (Heilman et al., 2002). Some patients may be unaware of stimuli in the contralesional space only when another stimulus is simultaneously presented in the ipsilesional space (i.e., extinction) or, in the most severe cases, even when only one stimulus is presented in the contralesional space (i.e., neglect) (Heilman et al., 2002). The presence and severity of these contralesional spatial processing deficits typically decrease significantly with time from stroke (Durfee & Hillis, 2023). However, it has been proposed the existence of a discrepancy between “apparent” and “genuine” recovery that depends on the type of test used to quantify patients’ performance. When, as in the vast majority of studies, recovery is assessed solely through classic paper-and-pencil tests, patients very often show little or no failures of contralesional space processing, suggesting they were able to compensate for their deficits, and making apparent recovery potentially misleading. In contrast, in the minority of studies assessing recovery with specific tests that prevent compensation by resorting to the multitasking approach, seemingly unimpaired patients often present a certain failure rate in contralesional space processing, unveiling apparent and not genuine recovery. It follows that under multitasking conditions, when recovery occurs, it is more likely to be reliable (Bonato, 2012).

The multitasking approach is very useful also when studying healthy populations as it provides valuable insights into how attentional resources are allocated in space. The findings from such studies are crucial in understanding how individuals cope with complex environments and have practical applications that can enhance efficiency, safety, and user experience in a multitude of real-world settings.

The multitasking approach is grounded on the hypothesis that different tasks, despite their distinct nature and specific demands, are characterized by the common use of relatively unspecific (i.e.,

domain-general) attentional resources. This pool of attentional resources, while flexible, is limited; it can be thought of as an attentional budget that must be allocated across all the tasks one is attempting to accomplish simultaneously. When the attentional load increases, for example because of dual-tasking, this general yet limited pool of resources is depleted, potentially affecting the performance.

The aim of this thesis was to explore load-induced spatial processing modulations during multitasking considering the damaged cognitive system, where these modulations are often more pronounced, as well as the unimpaired cognitive system.

Here, I present a summary of each chapter that might assist the reader in following the narrative more effectively. Note that a specific theoretical introduction pertinent to the topic of each chapter will be provided at the beginning of each chapter.

In ***Chapter 1*** is presented a single-case study, in which we examined how spatial processing in an ultra-chronic right hemisphere damaged patient is influenced by attentional load during multitasking. We employed classic paper-and-pencil tests along with a new computerized dual-task paradigm. The latter combined a spatial processing primary task, which required spatial processing abilities to report the position of appearance of lateralized visual targets, with a concurrent secondary task, that allowed to manipulate attentional load in a top-down manner as required categorizing visual/auditory stimuli. Additionally, we manipulated primary task difficulty in a bottom-up manner, varying lateralized target dimensions.

Paper-and-pencil tests did not reveal contralesional omissions. Differently, the dual-task paradigm demonstrated greater sensitivity in detecting subtle biases toward the ipsilesional space. Surprisingly, the effect was not influenced by the fact that primary task and secondary task stimuli underwent asynchronous presentation (i.e., primary task stimuli were presented immediately before secondary task stimuli). This means that the attentional load increase due to dual-tasking was so disruptive to “cancel from awareness” those stimuli which had been already visually processed. Additionally, when the target's radius was exceptionally small and became difficult to perceive, biases toward the ipsilesional space increased significantly, even if in this condition the effects of multitasking became less prominent. These findings suggest that very different manipulations, the first involving top-down and primarily cognitive factors and the second involving bottom-up and purely perceptual aspects, can interact to jointly modulate the level of required

resources and can be exploited to test very subtle (yet potentially hazardous) deficits which are almost exclusively contralesional.

Understanding the performance of the "baseline system" is essential for assessing the extent of impairment in patients. Therefore, in ***Chapter 2*** we presented a study, in which we examined how spatial processing in the unimpaired cognitive system is influenced by different levels of attentional load during multitasking. We conducted two separate experiments with new dual-task paradigms on healthy adults, by using web-based data collections, which facilitated the participation of a relatively large number of participants (101 in Experiment 1 and 98 in Experiment 2). We employed a primary audiovisual integration task, which involved presenting stimuli capable of eliciting the sound-induced flash illusion (i.e., task-relevant flashes accompanied by an incongruent number of sounds) on either the left or right side of the screen. This task enabled us to investigate audiovisual integration, but also indirectly provided an opportunity to explore spatial processing within a highly complex context. This task was coupled in the two experiments with two distinct concurrent secondary tasks to manipulate attentional load.

In both experiments, we replicated the increase of sound-induced flash illusion under high attentional load, which challenges the notion of an early, completely automatic and pre-attentive onset of the illusion. However, this effect was identical for left- and right-sided flashes, which speak against the existence of load-induced spatial processing asymmetries in the unimpaired cognitive system, at least in the context of audiovisual integration illusions. Therefore, these findings seem to suggest that the unimpaired cognitive system and the damaged cognitive system are not only quantitatively but also qualitatively distinct.

The conceptualization of the project presented in this chapter was preregistered at:
https://l1nq.com/ProjectConceptualization

In ***Chapter 3*** we presented a study, in which we examined how spatial processing in the unimpaired cognitive system is influenced by different levels of attentional load during multitasking, but this time focusing on the neural level. We conducted an experiment using a computer-based dual-task paradigm identical to one of the two used in Chapter 2. At the same time, we recorded high-density electroencephalography (EEG) activity during resting-state and simultaneously with the task, to investigate electrophysiological predictors and correlates of task performance. Firstly, we investigated whether "behavioural indexes", particularly task performance, could be predicted

using “brain indexes”. These brain indexes were average functional connectivity values within specific networks, extracted from EEG recordings during resting-state. Although functional connectivity is typically derived from functional Magnetic Resonance Imaging rather than EEG recordings, we were able to conduct such analysis, using an innovative approach by Liu et al. (2017). Subsequently, we investigated Event-Related Potentials (ERPs) during in-task EEG recordings. Specifically, our focus was on identifying ERP modulations linked to the enhanced perception of sound-induced flash illusions under high attentional load. Additionally, we examined whether these potential ERP modulations differed following left-sided or right-sided flashes. This was aimed at determining whether load-induced spatial processing asymmetries, although not apparent in behavioural responses, could be discerned through ERP responses.

We have uncovered noteworthy correlations between behavioural indexes and functional connectivity, predominantly within networks pertinent to auditory and visual processing, along with the allocation of attentional resources in space. Moreover, we have identified N1, N2, and P3 modulations associated with the presentation of stimuli eliciting the sound-induced flash illusion during different levels of attentional load, with N1 modulations differing depending on the side of the flashes.

CHAPTER 1

UNVEILING CONTRALESIONAL OMISSIONS SIX YEARS AFTER STROKE. COMBINED EFFECTS OF TOP-DOWN AND BOTTOM-UP MULTITASKING

1.1 Overview of the chapter

The present single-case study examined how spatial processing in an ultra-chronic right hemisphere damaged patient is influenced by attentional load during multitasking. We employed classic paper-and-pencil tests along with a new version of a computerized dual-task paradigm already employed in numerous studies. The latter combined a spatial processing primary task, which required spatial processing abilities to report the position of appearance of lateralized visual targets, with a concurrent secondary task, that allowed to manipulate attentional load in a top-down manner as required categorizing visual/auditory stimuli. Additionally, we manipulated primary task difficulty in a bottom-up manner, varying lateralized target dimensions.

Paper-and-pencil tests did not reveal contralesional omissions. Differently, the dual-task paradigm demonstrated greater sensitivity in detecting subtle biases toward the ipsilesional space. Surprisingly, the effect was not influenced by the fact that primary task and secondary task stimuli underwent asynchronous presentation (i.e., primary task stimuli were presented immediately before secondary task stimuli). This means that the attentional load increase due to dual-tasking was so disruptive to "cancel from awareness" those stimuli which had been already visually processed. Additionally, when the target's radius was exceptionally small and became difficult to perceive, biases toward the ipsilesional space increased significantly, even if in this condition the effects of multitasking became less prominent. These findings suggest that very different manipulations, the first involving top-down and primarily cognitive factors and the second involving bottom-up and purely perceptual aspects, can interact to jointly modulate the level of required resources and can be exploited to test very subtle (yet potentially hazardous) deficits which are almost exclusively contralesional.

1.2 Introduction

Unilateral brain damage in heterogeneous cortical and subcortical brain regions often leads to the disruption of the neural and cognitive systems subserving spatial processing abilities, resulting in spatial processing deficits for the space contralateral to the lesion (Corbetta & Shulman, 2011; Damasio et al., 1980; Husain, 2019). These deficits cannot be ascribed to sensory or motor impairments, but rather stem from a failure of selective attention mechanisms, that after the insult are no longer symmetric but, rather, biased toward the space ipsilateral to the lesion (Heilman et al., 2002). Some patients may be unaware of stimuli in the contralesional space only when another stimulus is simultaneously presented in the ipsilesional space (i.e., extinction) or, in the most severe cases, even when only one stimulus is presented in the contralesional space (i.e., neglect) (Heilman et al., 2002). This unawareness affecting contralesional hemispace can manifest itself in different modalities (e.g. visual, auditory, tactile; Guilbert, 2023; Jacobs et al., 2012), reference frames (e.g. egocentric, allocentric; Guilbert, 2023; Upshaw et al., 2019), and spatial frames (e.g. personal, peripersonal, extrapersonal space; Guilbert, 2023). Additionally, this unawareness translates into daily life challenges, such as difficulties in autonomously moving and in judging distances that might cause for example to bump into objects or obstacles on the neglected side. Such symptoms not only impact an individual's independence but also their safety, making contralesional spatial processing deficits among the most debilitating post-stroke conditions (Spaccavento et al., 2017).

The frequency and severity of these contralesional spatial processing deficits typically vary according to the affected hemisphere (Durfee & Hillis, 2023). (Left) neglect following right hemisphere damage is thought to be more common and severe than (right) neglect following left hemisphere damage (Esposito et al., 2021; Ten Brink et al., 2017; but see: Blini et al., 2016). However, for the perspective of clinical care, (right) neglect following left hemisphere damage cannot be considered rare (Esposito et al., 2021). Moreover, the impact of neglect on rehabilitation outcomes is comparable between (left) neglect following right hemisphere damage and (right) neglect following left hemisphere damage (Wee & Hopman, 2008; Yoshida et al., 2022). Additionally, the presence and severity of these contralesional spatial processing deficits typically decrease significantly with time from stroke (Durfee & Hillis, 2023). Shortly after the insult, in the acute phase, neglect is often prominently evident: the individual's gaze, eye-in-head and head-on-trunk positions deviate towards the ipsilesional space, both during active exploration and at rest. However, later on, in the post-acute phase, this deviation generally diminishes until the deficit either

completely recovers or until residual subtler behavioural signs become chronic (Fruhmann Berger et al., 2008). More specifically, recovery rates for acute neglect were reported to be as high as 60 to 90% within 3 to 12 months after the injury (Karnath et al., 2011). However, it has been proposed the existence of a discrepancy between "apparent" and "genuine" recovery that depends on the type of test used to quantify patients' performance. When, as in the vast majority of studies, recovery is assessed solely through classic paper-and-pencil tests, patients very often show little or no failures of contralesional space processing, suggesting they were able to compensate for their deficits, and making apparent recovery potentially misleading. In contrast, in the minority of studies assessing recovery with specific computerized tests that prevent compensation, for instance, by resorting to multitasking, seemingly unimpaired patients often present a certain failure rate in contralesional space processing, unveiling apparent and not genuine recovery. It follows that, under multitasking conditions, when recovery occurs, it is more likely to be reliable (Bonato, 2012).

The paper-and-pencil tests commonly used to quantify patients' performance include bisection tests, cancellation tests, but also copying of shapes and figures and drawing symmetrical figures like a clock face or a butterfly. In the bisection test, participants are asked to mark the midpoint of a line and a displacement of the bisection mark towards the ipsilesional space is interpreted as an indication of neglect. On the other hand, cancellation tests require participants to cross out all target items on a sheet and failure to detect items in the ipsilesional space signifies neglect. For instance, the lines cancellation test consists of 40 target lines distributed across seven rows that patients must cross out (Albert, 1973). More complex tests, such as letter cancellation (Weintraub & Mesulam, 1985), star cancellation (Halligan et al., 1989) and bell cancellation tests (Gauthier et al., 1989) present instead target items mixed with various distractor items. Among others, Ferber and Karnath (Ferber & Karnath, 2001) compared the accuracy of different paper-and-pencil tests in identifying neglect. They noted that displacements in line bisection might not solely indicate neglect but could be determined by other factors, such as hemianopia (Barton & Black, 1998) or the hand used to respond (Brodie & Pettigrew, 1996). Additionally, in their study, cancellation tests, particularly letter and bell cancellation tests, proved to be the most effective in identifying neglect (Ferber & Karnath, 2001). Various attempts to improve cancellation tests sensitivity included, for example, increasing the number and similarity of target and distractor stimuli (Aglioti et al., 1997; Basagni et al., 2017; Sarri et al., 2009) and using time limits (Priftis et al., 2019). Regardless of which paper-and-pencil test is deemed the most sensitive, all such tests suffer from at least three rather important limitations: first, their low difficulty level can result in ceiling effects; second, their unchanged

format across sessions may allow for significant learning; third, they don't accurately represent the dynamic nature of everyday environments. Patients can therefore easily devise strategies to compensate for their difficulties in bisection tests and cancellation tests, leading to prematurely "normalized" scores. In conclusion, while paper-and-pencil tests may be optimal for diagnosing severe neglect, they are not ideal for detecting subclinical neglect, which can nonetheless result in functional disabilities in daily life (Bonato & Deouell, 2013).

Computerized tests have proven to be a more promising method to quantify patients' performance. First of all, computerized tests allow to present stimuli for brief durations and record response latencies with millisecond precision. As a result, they can detect not just the most dramatic failures of contralesional space processing, but also the simple delayed processing of the contralesional space (Schendel & Robertson, 2002). The first proposals in this sense date back to more than 40 years ago although computerized tests use is not yet established at the clinical level. For example, Posner and colleagues (M. Posner et al., 1984) used computerized tests to assess the performance of patients with right or left hemisphere damage. They introduced paradigms in which patients were tasked with detecting targets briefly displayed in one of two lateralized boxes, while response latencies were collected. Results showed slower responses to contralesional sided targets, particularly if preceded by ipsilesional sided cues (M. Posner et al., 1984). Notably, this delay was observed even in patients who exhibited mild or no neglect based on paper-and-pencil tests (Friedrich & Margolin, 1993; M. Posner et al., 1984) and both in the chronic and acute phase (Rengachary et al., 2009). Furthermore, when all the stimuli were within the same hemifield, patients with right hemisphere damage were slower to respond to the leftmost targets (Làdavas et al., 1990). Deouell and colleagues (Deouell et al., 2005) directly compared computerized and paper-and-pencil tests to assess the performance of patients with right or left hemisphere damage. Specifically, they employed the Starry Night Test (SNT), in which patients were tasked with detecting targets briefly displayed in several spatial positions on a dynamically changing background full of distractors, while response latencies were collected. As a term for comparison, they have employed the Behavioral Inattention Test (BIT; Wilson et al., 1987), arguably considered the "gold standard" paper-and-pencil battery for neglect diagnosis (Halligan et al., 1989). Results confirmed the contralesional delay already reported in previous studies (at the group level only for patients with right hemisphere damage) and showed that SNT was more sensitive than BIT, identifying significantly delayed responses to contralesional sided targets in half of the patients with BIT scores within the non-pathological range (Deouell et al., 2005).

Another important characteristic of computerized tests is that they can be customized based on the individual's level of performance at a specific time. For instance, adaptive procedures can be implemented wherein specific stimulus parameters, such as duration, contrast, intensity, or position, are adjusted until a target level of performance is achieved (e.g., a 500-ms duration yielding 75% accuracy). As a result, they can mitigate learning or ceiling effects (List et al., 2008).

Crucially for the present investigation, a further advantage of computerized tests is that they allow the implementation of scenarios requiring the engagement of different levels of attentional resources, up to their full deployment in the most demanding conditions. In such contexts, there is no room for compensatory strategies to develop. One method to fully engage attentional resources consists in adopting a *multitasking approach*. For instance, it is possible to design dual-tasks that pair a primary task, which requires spatial processing abilities, with a concurrent secondary task, that allows to modulate attentional load. Under such conditions, spatial processing abilities can be assessed while attentional resources are divided between the two parallel tasks. This limits to different extents the resources available for compensating spatial processing deficits, making difficult to inhibit the initial orientation towards the ipsilesional space and subsequently redirect attention towards the contralesional space (Bonato, 2012; Saccani et al., 2022). The multitasking approach, in addition to preventing compensatory strategies, closely mirrors real-life situations that are typically complex, filled with distractions and require the concurrent execution of multiple tasks (Bonato, 2012; Saccani et al., 2022). In a multiple single-case study, Bonato and colleagues (2010) used a computerized test, and specifically a dual-task paradigm, to assess the performance of four patients with right hemisphere damage and one with left hemisphere damage (note that only one of them had a pathological BIT score). In the primary task, which required spatial processing abilities, participants were asked to report the position of appearance of lateralized (left, right, or bilateral) visual targets. The size of these targets remained consistent at 0.8° of visual angle, while their duration was set with an adaptive procedure before starting the experiment (upper and lower limits set respectively to 50 and 700 ms). Concurrently, the secondary task demanded the categorization of letters presented visually in the centre of the screen or numbers presented auditorily. Both primary and secondary task stimuli were presented simultaneously. In the single-task condition, participants simply had to identify the position of the lateralized targets. In the visual dual-task condition, they were required to report both the position of the lateralized targets and the identity of visually presented letters. Similarly, in the auditory dual-task condition, participants had to report the position of the lateralized targets and had to count by two (twice) based on the identity of the

auditorily presented numbers. The manipulation was therefore purely top-down, based on the presence/absence of concurrent task demands. Results showed that all patients had a higher number of contralesional omissions when presented with bilateral targets (i.e., extinction) during both auditory and visual dual-task conditions, but not in the single-task condition. Moreover, three patients had a higher number of contralesional omissions when presented with unilateral targets (i.e., neglect) during either the auditory or visual dual-task condition, but not in the single-task condition. In contrast, the performance of neurologically intact control participants was symmetric and unaffected by the dual-task manipulation (Bonato et al., 2010). Notably, these findings were replicated in group studies both in the case of patients with right hemisphere damage (Bonato et al., 2013) and extended to (right) neglect and extinction in patients with left hemisphere damage(Blini et al., 2016). These findings were confirmed in two longitudinal studies examining the performance of a 63-year-old woman who had suffered a stroke, impacting a substantial portion of her right middle cerebral artery (Bonato, 2015; Bonato et al., 2012). She underwent testing with paper-and-pencil tests, a dual-task paradigm similar to that described by Bonato and colleagues (2010) and ecological observations at her home for three years after stroke (Bonato, 2015; Bonato et al., 2012). Paper-and-pencil tests did not reveal biases toward the ipsilesional space, even when they were specifically modified using strategies potentially exacerbating neglect, such as performing the test while counting backwards. Differently, the dual-task paradigm, especially during the dual-task conditions, as well as the ecological observations, demonstrated the greatest sensitivity in detecting subtle biases toward the ipsilesional space, until month 6 after stroke. Notably, the uncommon absence of any motor deficits allowed the researchers to dismiss left leg/arm weakness as a reason for her bumping into objects on her left therefore ascribing to neglect her everyday life difficulties (Bonato et al., 2012). Ceiling performance in the dual-task paradigm was reached at month 12 and maintained until month 29 after stroke. At that point, target diameter was reduced from 0.8° of visual angle to 0.3° of visual angle and the subtle biases toward the ipsilesional space re-emerged mostly during dual-task conditions until month 41 (Bonato, 2015). It has also been observed that Bonato and colleagues' (2010) dual-task paradigm with stimuli positioned vertically (lower/upper) can reveal even the presence of non-lateralized spatial processing biases (e.g. also along the vertical axis) (Andres et al., 2019). Moreover, it has been recently demonstrated that Bonato and colleagues' (2010) dual-task paradigm outperforms cancellation tasks, even when the latter are presented on a large screen (Villarreal et al., 2022).

All these findings converge in suggesting that patients with apparently recovered forms of neglect may, instead, simply use compensatory strategies to counterbalance contralesional spatial processing deficits. The existence of apparently recovered forms of neglect implies that, despite the prevailing conceptualization of neglect as a binary presence-absence phenomenon, the symptoms of neglect may actually vary along a continuum of severity levels. In addition to theoretical consequences, the existence of apparently recovered forms of neglect determines a number of important clinical implications, as patients in the chronic phase may be allowed to return to their pre-morbid activities where they may be at risk (e.g., driving, road crossing or use of dangerous objects/devices). Fortunately, discovering these subtle deficits is possible and seems to be primarily a matter of using the right (resource-consuming) task.

1.3 Aim and hypothesis

In the present single-case study, we tested a new variant of the dual-task paradigm, whereby primary task stimuli (i.e., lateralized targets) and secondary task stimuli (i.e., stimuli for the top-down load manipulation) presentation were asynchronous. At the same time, we introduced a new bottom-up manipulation of primary task difficulty, that focused on varying lateralized target dimensions. Therefore, this approach enabled us to integrate top-down and bottom-up manipulations. Capitalizing on previous findings by Bonato and colleagues (2012) and by Bonato (2015) we were relatively confident that combining these manipulations would have been sufficiently challenging to exacerbate contralesional spatial processing deficits even several years post-stroke, when biases toward the ipsilesional space, if present, typically manifest as exceptionally subtle.

Our participant was a 65-year-old man who had suffered a stroke, affecting his right capsular and frontal nucleus, six years before testing and who was therefore in an ultra-chronic phase of the condition at the time of testing. He underwent classic paper-and-pencil tests and the new variant of the computerized dual-task paradigm. Similar to previous studies, the dual-task combined a primary task, which required spatial processing abilities to report the position of appearance of lateralized visual targets, with a concurrent secondary task, that allowed to modulate attentional load as required categorizing visual/auditory stimuli. In the single-task condition, the patient simply had to identify the position of the lateralized targets, while in the dual-task conditions, he was required to report both the position of the lateralized targets and the identity of visual/auditory stimuli. The

two main differences with previous studies were: 1) lateralized targets appeared immediately before and not concurrently with visual/auditory stimuli and 2) lateralized targets progressively varied in radius from 0.8° to 0.3° and 0.1° of visual angle. The first change was introduced to investigate whether, contralesional spatial processing deficits, if present, could be exacerbated by a top-down increase of attentional load occurring in the absence of perceptual overlap between primary and secondary task stimuli. The second change was introduced to investigate how primary task difficulty (manipulated bottom-up) as well as the interaction between primary task difficulty and increased attentional load might influence contralesional spatial processing deficits severity and rate.

We expected (H1) a ceiling performance of the patient in classic paper-and-pencil tests associated with the re-emergence of biases toward the ipsilesional space in the computerized dual-task paradigm despite the asynchronous presentation of primary and secondary tasks stimuli and especially during the dual-task conditions. Moreover, we expected (H2) an increase of the biases toward the ipsilesional space following the reduction of lateralized target's radius leading to increased primary task difficulty.

The existence of these nuanced contralesional spatial processing deficits, which are compensated for under normal conditions but become evident during multitasking, would suggest that compensatory mechanisms might not be limited to just the initial months after a stroke. They could instead persist longer, possibly for years.

1.4 Method

Participants

The patient was a 65-year-old right-handed man with 13 years of education. He suffered a first stroke, which resulted in a haemorrhage in the right capsular nucleus. Three months later, he experienced a second stroke, leading to an intraparenchymal haemorrhage in the pontine region. At stroke onset, the patient showed clinical signs of left neglect and total hemiplegia. He was hospitalized for 11 months. A CT scan performed one year after stroke, highlighted an extended hypodense region in both the right capsular and frontal nucleus, as well as in the pontine region. The patient's lesion was manually reconstructed using MRICron Software (v 1.0.2; Rorden et al., 2007). Subsequently, both the patient's CT scan and the reconstructed lesion were normalized to

an age-appropriate template brain using the SPM Clinical Toolbox (Rorden et al., 2012) (see Figure 1.1). Following this normalization, the volume of the lesion was calculated with MRICron Software (v 1.0.2; Rorden et al., 2007), resulting in a measurement of 49.47 cm^3.

The patient was referred to us 6 years after the stroke. Family members reported significant improvements in contralesional spatial processing deficits at the cognitive level since the onset of the stroke. However, the same could not be said for the motor level, as the patient still relied on a wheelchair for mobility. This limitation prevented him from returning to his job as an industrial designer. He was fully aware of his deficits, which, according to clinicians, may have aided him in developing compensatory strategies. Indeed, following the stroke, he authored several short books, some of which focused on his experiences as a stroke patient.

The patient's performance in the dual-task paradigm was compared to that of four right-handed neurologically intact control participants (mean age: 67 years; age range: 61-81 years; mean education: 8.5 years; education range: 5-13 years; m: 3).

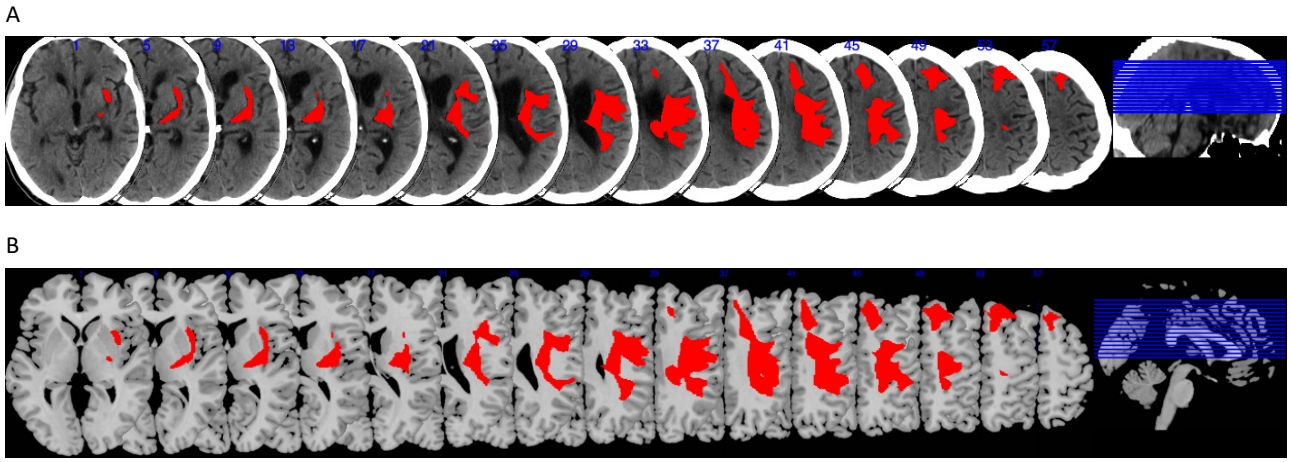

Figure 1.1. Patient's lesion at one year from stroke onset. Panel A *display patient's CT scan and the reconstructed lesion normalized to an age-appropriate template brain.* ***Panel B*** *displays a Montreal Neurological Institute template and the patient's reconstructed lesion superimposed onto it, highlighting the precise anatomical location and extent of the lesion within standardized brain coordinates.*

Experimental protocol

The experimental protocol was approved by the Ethics Committee for Psychological Research of the University of Padua (protocol n. 3824) and was conducted according to the principles expressed in the Declaration of Helsinki.

Paper-and-pencil tests

The patient was administered a set of standardized and ad-hoc neuropsychological paper-and-pencil tests for general cognitive screening and neglect assessment.

Paper-and-pencil standardized tests encompassed the Montreal Cognitive Assessment (MoCA, Nasreddine et al., 2005) for assessing cognitive abilities globally, the conventional part of the Behavioural Inattention Test (BIT; Wilson et al., 1987) for assessing neglect for the peripersonal space and Fluff test (Cocchini et al., 2001; Cocchini & Beschin, 2022) for assessing neglect for the personal space.

Similarly, to Bonato and colleagues (2012), paper-and-pencil ad-hoc tests were administered to exploratively evaluate whether neglect-like performance would be exacerbated by resorting to increased attentional load but without resorting to computerized tests. In a first ad-hoc test we asked the patient to bisect 10 lines 10 cm long, firstly as single-task and then while simultaneously subtracting by 3 from 1000. In a second ad-hoc test we asked the patient to repeat the procedure of the fluff test, while simultaneously subtracting by 3 from 950.

Dual-task paradigm

The patient was administered a dual-task paradigm adapted from Blini et al. (2016) and Bonato et al. (2019). It combined a primary task, which required spatial processing abilities, with a concurrent secondary task, that allowed to modulate attentional load.

The dual-task paradigm was designed to allow both offline and web-based data collection. As such, it was programmed using HyperText Markup Language (HTML), Cascading Style Sheets (CSS) and jsPsych, an open-source JavaScript library that provides a flexible framework for building psychological experiments that can be conducted not only in traditional laboratory settings but also online (de Leeuw, 2015; de Leeuw et al., 2023). The dual-task paradigm was subsequently uploaded to a local computer, with JATOS installed, an open-source web application that streamlines the management of web-based data collections but that can be also used offline (Lange et al., 2015). Data collection was conducted entirely in person and offline.

During each trial, the patient was firstly presented with a black screen lasting for 1000 ms. It followed a white fixation cross set against a black background, positioned in the centre of the screen and measuring 0.76°. It remained on the screen for 800 ms and flickered in the last 200 ms before the target was presented to redirect the patient's attention to the centre of the screen. Immediately

afterwards, the patient was presented with lateralized targets, consisting in white discs set against a black background and lasting for 100 ms. They could be displayed following four different target conditions: either unilaterally (on the left or right side of the screen, with a 13.4° eccentricity) or bilaterally (simultaneously on both sides of the screen, maintaining the 13.4° eccentricity on each). Additionally, to detect any potential response biases, “catch” trials were incorporated, where no actual target was shown. It followed a visual symbol (triangle, square, or circle) displayed in the centre of the screen, written with an Arial font of 140 pixels in advance width and lasting for 100 ms together with an environmental sound (train whistle, doorbell, or hammer) played through bilateral speakers. At the end of each trial, the patient was presented with a noisy screenshot lasting until the beginning of the following trial to minimize retinal after-image (see Figure 1.2). Across three different load conditions the stimuli remained constant and only the instructions varied. Specifically, in the single-task condition, the patient was exclusively asked to report the target(s) position (e.g., “right,” “left,” “both,” or “no target”). In contrast, during the visual dual-task or auditory dual-task conditions, the patient was first asked to report the target(s) position and then to identify the presented visual symbol or environmental sound. The manipulation was therefore purely top-down, based on the presence/absence of concurrent task demands.

The dual-task paradigm comprised 3 blocks, each containing 36 trials (i.e., a total of 108 trials encompassing 3 load conditions X 4 target conditions). Load conditions (single-task, visual dual-task, auditory dual-task) were varied from block to block, following this fixed alternating order: single-task condition, visual dual-task condition and auditory dual-task condition. Each target condition (left, right, bilateral, catch), as well as all possible combinations of symbols and sounds, were presented within each block, balanced in frequency and with randomized order. The dual-task paradigm was administered twice (i.e., a total of 216 trials) for each of three different target's radius conditions: 0.8°, 0.3°, and 0.1° (i.e., a total of 648 trials in total).

Instructions were explained verbally and presented on the screen before starting each block. A practice phase consisting of 36 trials was carried out before starting the first block. Shorter practice phases consisting of 4 trials were carried out before starting respectively the second block and third block. Exclusively during these practice phases, the patient received visual feedback related to his responses, with 'correct' displayed in green and 'wrong' in red on the screen. The patient has been tested in a quiet room, seated in his wheelchair approximately 60 cm away from a 15-inch laptop monitor. To minimize response demands on the patient he provided verbal responses that were coded by the experimenter using a computer keyboard. The patient was allowed to rest after each

trial, if necessary. The patient eye movements were monitored by a second experimenter and trials affected by these movements were immediately discarded and repeated.

The controls were administered the dual-task paradigm with target's radius set at 0.1° twice, under conditions identical to those in which the patient was tested.

The dual-task paradigm was completed in about 30 min by the patient and controls.

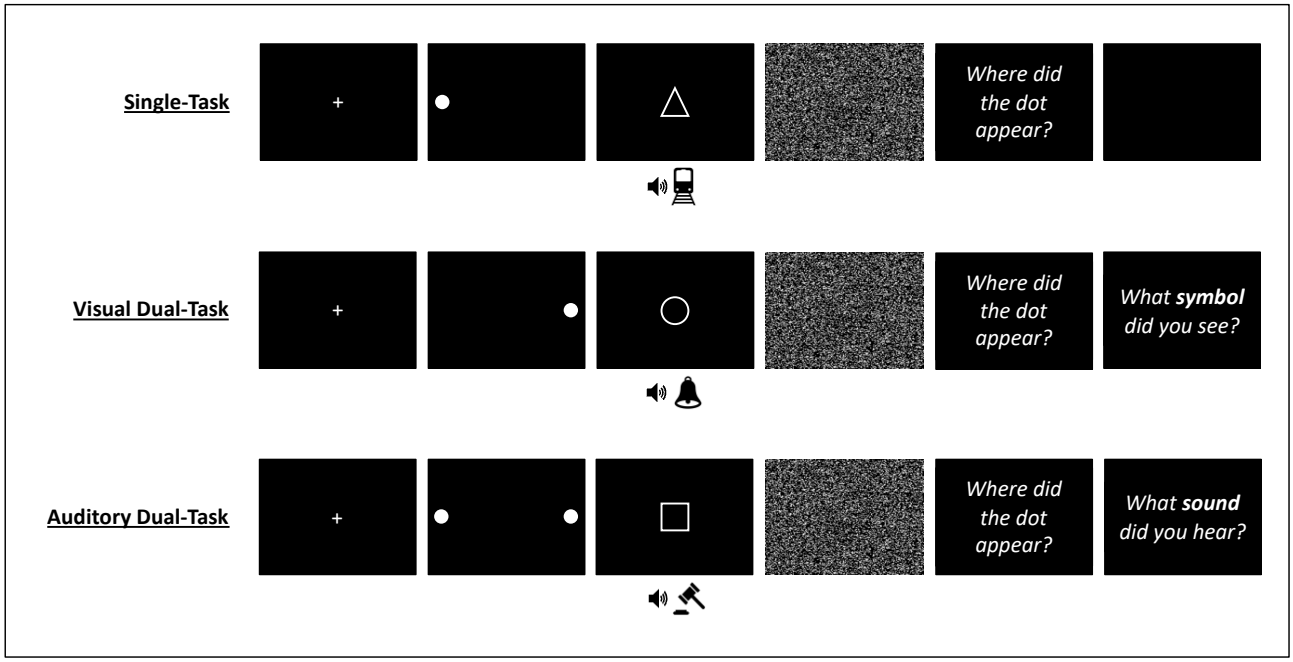

Figure 1.2. Dual-task paradigm, combining a primary task, which required spatial processing abilities, with a concurrent (visual or auditory) secondary task, that allowed to modulate attentional load. *The figure shows a trial of the single-task and left target conditions, a trial of the visual dual-task and right target conditions and a trial of the auditory dual-task and bilateral target conditions.*

Session's order

The patient was tested across four sessions, each with a temporal distance between two and three months and each lasting a couple of hours. During the first session, the patient's medical history was collected, he was administered the conventional part of the BIT (Wilson et al., 1987) and the first repetition of the dual-task paradigm with target's radius set at 0.8°. During the second session the patient was administered the first repetition of the dual-task paradigm with target's radius set at 0.3° and the MoCA (Nasreddine et al., 2005). During the third session the patient was administered the first repetition of the dual-task paradigm with target's radius set at 0.1°, the ad-hoc bisection test without load and with added load, the fluff test (Cocchini et al., 2001; Cocchini & Beschin, 2022) and the ad-hoc version of the same test with added load, and the second repetition of the dual-task paradigm with target's radius set at 0.1°. During the fourth session the patient was

administered with the second repetition of the dual-task paradigm with target's radius set at 0.8° and the second repetition of the dual-task paradigm with target's radius set at 0.3°.
The controls were all tested in a single session.

Analysis

Data from paper-and-pencil standardized tests were scored based on standardized cut-offs, while data from ad-hoc tests were assessed qualitatively.
Dual-task paradigm data from the two repetitions for each of the three different target's radius conditions were combined and analysed together.
First of all, we analysed secondary task accuracy (i.e., accuracy in categorizing visual/auditory stimuli). Specifically, we contrasted it in different target conditions (right vs left and right vs bilateral), considering exclusively the visual dual-task condition and the target's radius set at 0.3°. This focus was prompted by an unexpected decrease in performance observed during the visual inspection of the data. This was performed using R Statistical Software (v 4.2.2; R Core Team, 2022) and Fisher's exact test (Upton, 1992), considering correct vs incorrect responses.
Subsequently, trials in which incorrect responses were made to the secondary task were excluded from further analysis. This exclusion was necessary because it was not possible to verify whether participants were paying attention during these specific trials. For patient data, 16 trials were excluded in the dual-task paradigm version with the target's radius set at 0.8°, 20 trials were excluded in the version with the target's radius set at 0.3°, and 11 trials were excluded in the version with the target's radius set at 0.1°. For all control data, 9 trials were excluded.
After that, we analysed primary task accuracy (i.e., accuracy in reporting the position of appearance of lateralized visual targets). We contrasted it in different target conditions (right vs left and right vs bilateral), across the various load conditions and target's radius conditions. This was performed using RSDT_ES.EXE software (Crawford et al., 2010; Crawford & Garthwaite, 2005), which applies the Revised Standardized Difference Test (RSDT, Crawford et al., 1998) to test whether the difference between an individual's standardized scores on two tests (X and Y) is significantly different from the differences observed in a control sample (Crawford et al., 2010). Only comparisons between conditions differing by at least 20% were computed. This decision was informed by a specific goal: to emphasize the identification and analysis of larger effect sizes that hold both statistical significance and clinical importance, while reducing the total number of

comparisons and thus the risk of false positives and the need for stronger adjustment for multiple comparisons. All comparisons underwent adjustment for multiple comparisons using R Statistical Software (v 4.2.2; R Core Team, 2022) and the false discovery rate method (Glickman et al., 2014).

1.5 Results

Paper-and-pencil tests

The patient presented a good global level of cognitive abilities, according to his overall performance in the MoCA (score of 28/30, cutoff < 26). The subtests assessing visuo-spatial and executive functions, naming, attention, language, fluency, abstract thinking and orientation were all performed at ceiling. The only two errors were made in the delayed memory subtest (score 3/5).
The patient had no neglect according to his errorless performance at the conventional BIT (score of 146/146, cutoff < 129). All subtests were performed at ceiling. Additionally, the patient did not present neglect for the personal space according to his performance in the fluff test: he successfully removed all 9 ipsilesional targets and 15 contralesional targets (i.e., bias of 0.0, indicating performance within the normal range). Finally, the patient did not present any bias for the ipsilesional space even when load was increased in the ad-hoc tests.

Dual-task paradigm

Secondary task

Overall, patient accuracy in the secondary task (i.e., accuracy in categorizing visual/auditory stimuli) was: 80% in the visual dual-task condition and 100% in the auditory dual-task condition. Overall, controls accuracy in the secondary task was: 97% in the visual dual-task condition and 99% in the auditory dual-task condition.
When it was analysed whether patient accuracy in the secondary task was modulated by the different target conditions (right vs left and right vs bilateral) considering exclusively the visual dual-task condition and the target's radius set at 0.3°we found that both comparisons reached significance. More specifically, patient's accuracy in reporting the visual symbols was higher in case of left targets (correct answers: 17, errors: 1) compared to right targets (correct answers: 10, errors:

8) (p = 0.018). Similarly, patient's accuracy in reporting the visual symbols was higher in case of left targets (correct answers: 17, errors: 1) compared to bilateral targets (correct: 8, errors: 10) (p = 0.003) (see Figure 1.3).

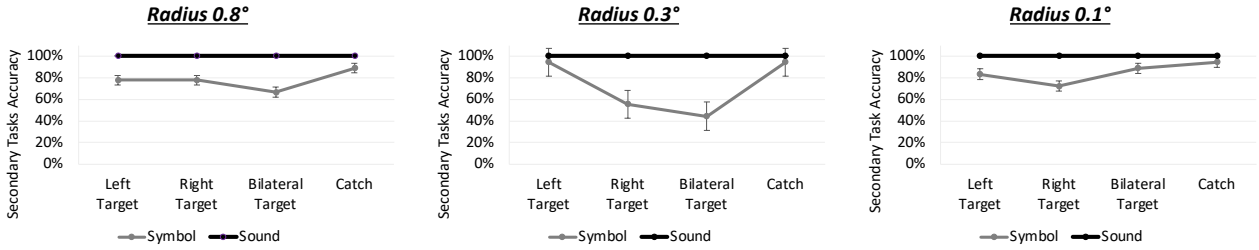

Figure 1.3. Secondary Tasks Accuracy (as percentage) as a function of target's radius conditions (0.8°, 0.3°, 0.1°) and target conditions (left, right, bilateral, catch).

Primary Task

Overall, patient accuracy in the primary task (i.e., accuracy in reporting the position of appearance of lateralized visual targets) was: 87% in the single-task condition, 85% in the visual dual-task condition and 88% in the auditory dual-task condition. Averaged performance across target's radius conditions and load conditions showed near ceiling accuracy for targets presented within the right hemispace (97 % correct) as well as for catch trials (96 % correct). In striking contrast, several errors emerged for left (23 %) as well as for bilateral targets (25 %). Overall, controls accuracy in primary task: was 100% in the single-task condition as well as in the visual dual-task condition and 99% in the auditory dual-task condition. Averaged performance across load conditions showed ceiling accuracy for all target conditions (right: 100% correct, catch: 99% correct, left: 100% correct, bilateral: 100% correct).

When it was analysed whether patient accuracy in the primary task was modulated by the different target conditions (right vs left and right vs bilateral), across the various load conditions and target's radius conditions the following nine comparisons showed a difference greater than 20%.

Target's radius 0.8°. In the dual-task paradigm version with the target's radius set at 0.8°, the patient's accuracy in the visual dual-task condition was higher for the right targets (100%) than for the left targets (71%) (t (3) = 3.321, p= 0.037[1]), indicating signs of neglect. In the auditory dual-task

[1] The reported p-values are corrected for multiple comparisons using the false discovery rate method (Glickman et al., 2014). This method employs a step-up approach. It takes the smallest raw p-value and multiplies it by n, the number of comparisons, to get a temporary adjusted p-value. Then it takes the second smallest raw p-value and multiplies it by n-1 and so on. Whenever a higher-ranking temporary p-value is lower than the ones below it, it replaces all lower-ranking p-values. It follows that it is possible to have uniform adjusted p-values after the correction.

condition, he was more accurate with the right targets (100%) compared to the bilateral targets (72%) (*t* (3) = 3.236, *p* = 0.037), suggesting signs of extinction (note that among the error responses in case of bilateral targets, 60% of responses were “right” and 40% of responses were “catch”)(see Figure 1.4 and Figure 1.7 for a comprehensive representation).

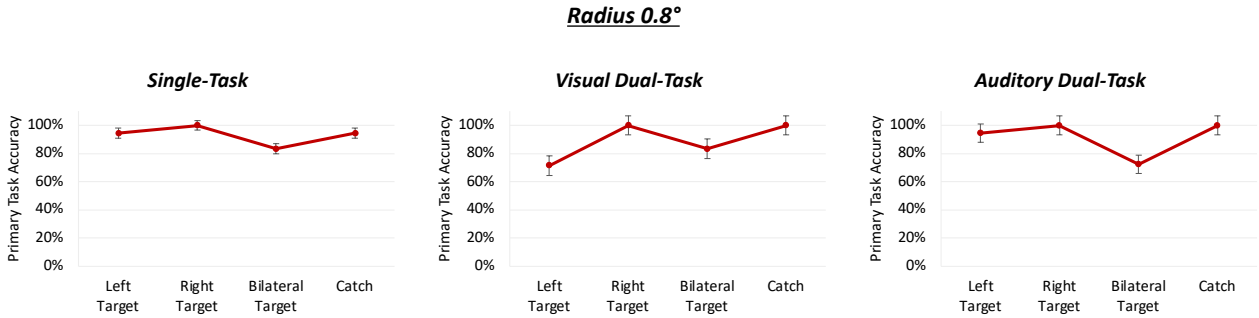

Figure 1.4. Primary Tasks Accuracy (as percentage) for target's radius 0.8°, as a function of load conditions (single-task, visual dual-task, auditory dual-task) and target conditions (left, right, bilateral, catch).

Target’s radius 0.3°. When the target's radius was set at 0.3°, the patient's accuracy in the single-task condition as well as in the visual dual-task condition was higher for the right targets (respectively: 100%, 90%) than for the bilateral targets (respectively: 78%, 63%) (respectively: *t* (3) = 2.692, *p*= 0.037, *t* (3) = 3.150, *p* = 0.037), suggesting signs of extinction(note that among the error responses in case of bilateral targets, 100% of responses were “right” in the single-task condition and also in the visual dual-task condition). In the auditory dual-task condition, he displayed higher accuracy with the right targets (94%) than with the left targets (72%) (*t* (3) = 2.692, *p*= 0.037), indicating signs of neglect (see Figure 1.5 and Figure 1.7 for a comprehensive representation).

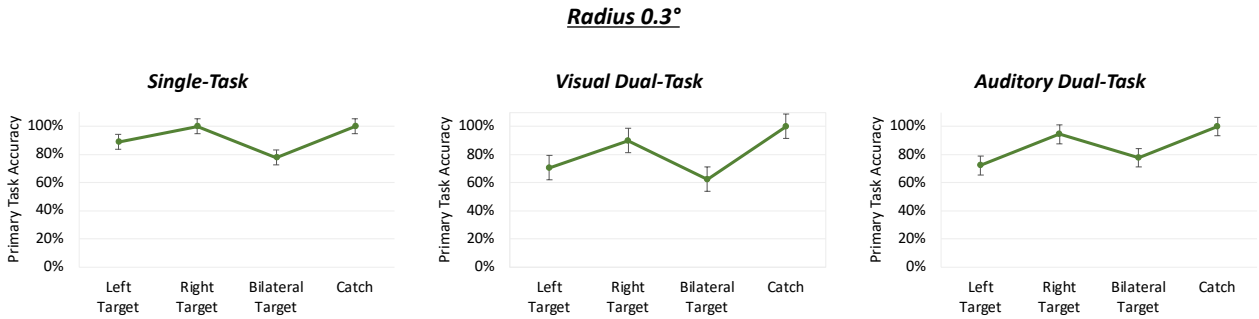

Figure 1.5. Primary Tasks Accuracy (as percentage) for target's radius 0.3°, as a function of load conditions (single-task, visual dual-task, auditory dual-task) and target conditions (left, right, bilateral, catch).

Target’s radius 0.1°. When the target's radius was set at 0.1°, the patient's accuracy in the single-task condition was higher for the right targets (94%) than for the bilateral targets (56%) (*t* (3) = 4.023, *p*= 0.037), as well as for the right targets (94%) than for the left targets (61%) (*t* (3) = 3.646,

p= 0.037), therefore indicating signs of extinction and neglect already in the easiest condition (note that among the error responses in case of bilateral targets, 87.5% of responses were “right” while for one trial the patient refused to answer). Similarly, in the visual dual-task condition, he was more accurate with the right targets (100%) than with the bilateral targets (75%) (*t* (3) = 2.972, *p*= 0.037), as well as with the right targets (100%) than with the left targets (60%) (*t* (3) = 4.167, *p*= 0.037) (note that among the error responses in case of bilateral targets, 100% of responses were “right”) (see Figure 1.6 and Figure 1.7 for a comprehensive representation).

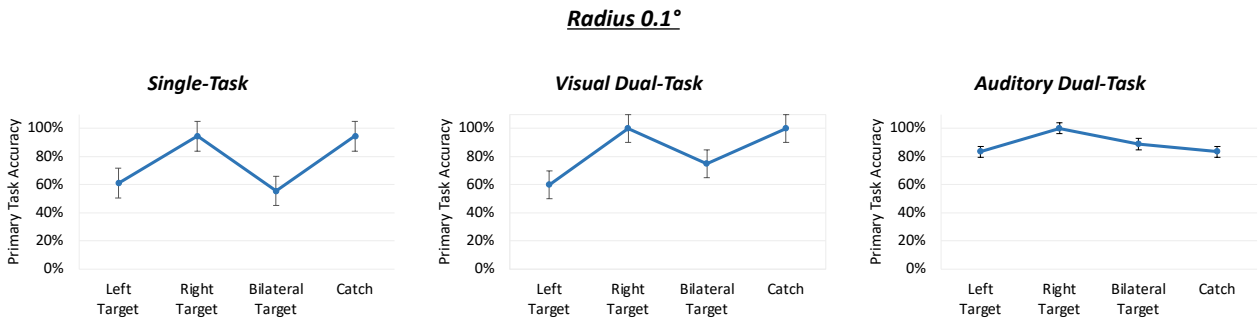

Figure 1.6. Primary Tasks Accuracy (as percentage) for target's radius 0.1°, as a function of load conditions (single-task, visual dual-task, auditory dual-task) and target conditions (left, right, bilateral, catch).

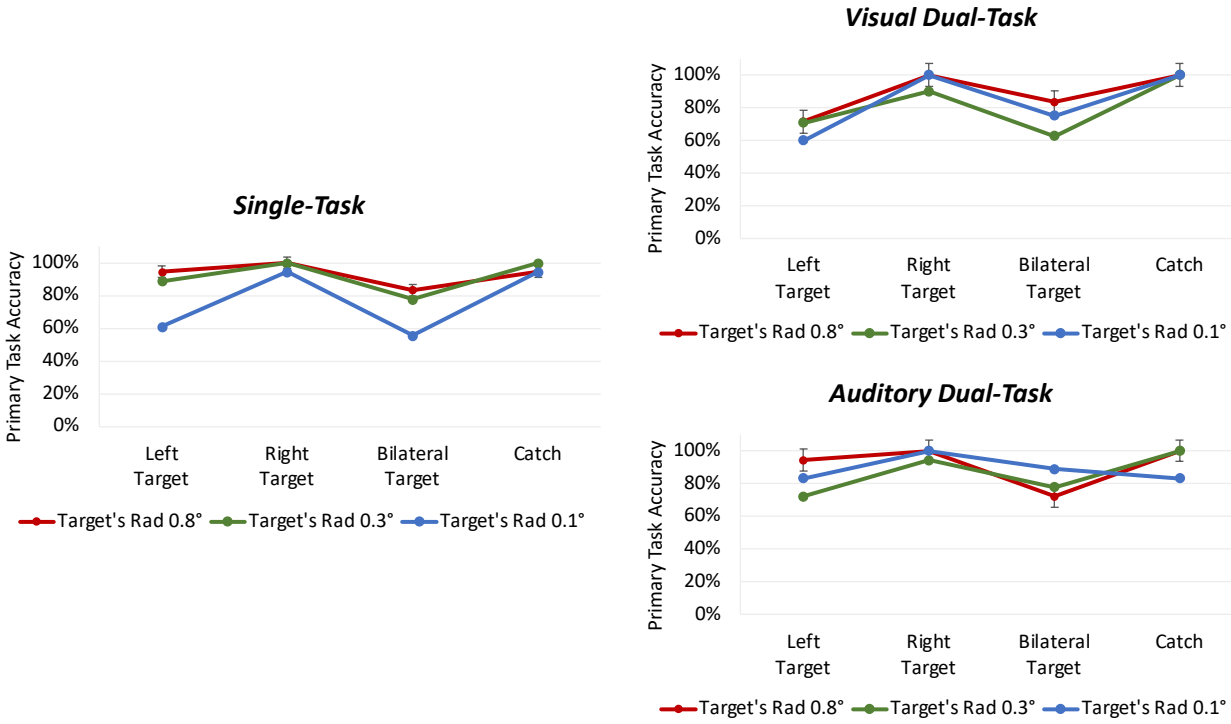

Figure 1.7. Comprehensive representation of Primary Tasks Accuracy (as percentage) for all target's radius conditions (0.8°, 0.3°, 0.1°), as a function of load conditions (single-task, visual dual-task, auditory dual-task) and target conditions (left, right, bilateral, catch).

1.6 Discussion

In the present single-case study, we explored an innovative version of the dual-task paradigm. In this variation, we presented primary task stimuli (i.e., lateralized targets) and secondary task stimuli for the top-down load manipulation asynchronously. This allowed excluding the possibility that dual-tasking omissions were due to a perceptual bottleneck rather than to attentional load-induced effect. Concurrently, we implemented a novel bottom-up manipulation by varying the dimensions of the lateralized targets in the primary task. This method allowed us to effectively combine both top-down and bottom-up manipulations in our approach. We tested with this task a 65-year-old man who had suffered a stroke, affecting his right capsular and frontal nucleus, six years before testing. After such a long time interval from stroke, contralesional spatial processing deficits may not be detectable using classic paper-and-pencil tests. However, biases toward the ipsilesional space might still exist. We propose that what appears as symmetric performance could actually be due to the implementation of compensatory strategies that mask these subtle biases. Therefore, increased task demands, whether through bottom-up or top-down manipulations, should unveil them.

The patient was tested with classic paper-and-pencil tests and a computerized dual-task paradigm. Just like earlier studies, the dual-task combined a primary task, which required spatial processing abilities to report the position of appearance of lateralized visual targets, with a concurrent secondary task, that allowed to modulate attentional load as it required categorizing visual/auditory stimuli. In the single-task condition, the patient simply had to identify the position of the lateralized targets, while in the dual-task conditions, he was required to report both the position of the lateralized targets and the identity of visual/auditory stimuli. Differently from previous studies two new manipulations were additionally present. Firstly, lateralized targets appeared immediately before and not concurrently with visual/auditory stimuli to investigate whether, contralesional spatial processing deficits, if present, could be exacerbated by a top-down increase of attentional load occurring in the absence of perceptual overlap between primary and secondary task stimuli. Secondly, lateralized targets progressively varied in radius from 0.8° to 0.3° and 0.1° of visual angle to investigate how primary task difficulty as well as the interaction between primary task difficulty and increased attentional load might influence contralesional spatial processing deficits severity and rate.

We had the following predictions: (H1) the patient would have a ceiling performance in classic paper-and-pencil tests, while biases toward the ipsilesional space would re-emerge in the computerized dual-task paradigm despite the asynchronous presentation of primary and secondary tasks stimuli and especially during the dual-task conditions; (H2) biases toward the ipsilesional space would increase following the reduction of lateralized targets radius lading to increased primary task difficulty.

Despite the long time interval from stroke, H1 was clearly confirmed. Paper-and-pencil tests did not reveal biases toward the ipsilesional space, even when they were specifically modified using strategies potentially exacerbating neglect. Differently, the dual-task paradigm, demonstrated greater sensitivity in detecting subtle biases toward the ipsilesional space, despite the non-simultaneous presentation of primary and secondary task stimuli. More specifically, when the target's radius was set at 0.8°, the patient demonstrated a high level of accuracy in the single-task condition. However, he exhibited a significant number of omissions for contralesional unilateral targets in the visual dual-task condition and contralesional bilateral targets in the auditory dual-task condition, indicating signs of spatial processing deficits. This finding confirmed once more that the patients with apparently recovered forms of neglect may, instead, simply use compensatory strategies to counterbalance contralesional spatial processing deficits. In such cases, biases toward the ipsilesional space can be observed, but their detection is contingent on the task used, which must consume a significant amount of resources to the extent that compensation becomes impossible. Surprisingly, the effect was not influenced by the fact that primary task stimuli appeared immediately before and not concurrently with secondary task stimuli. This means that the attentional increase due to dual-tasking requirements was so disruptive to “cancel from awareness” those target stimuli which had been already visually processed. The very same target stimuli which were “retrospectively” cancelled from the visual representation of the patient were vividly reported in the absence of multitasking requirements (but only in the case of sufficiently large targets, see later). It remains uncertain to what extent this phenomenon can generalize to other patients. It also remains unclear why the different nature of the dual-tasks (visual vs. auditory) resulted in distinct types of contralateral omissions, with more omissions for unilateral targets in the visual dual-task condition and more omissions for contralateral bilateral targets in the auditory dual-task condition, given that many previous cases have often exhibited more similar patterns in the two dual-tasks types (e.g.: Bonato et al., 2010).

H2 was partially confirmed. More specifically, when the target's radius was reduced to 0.3°, the patient showed a significant number of omissions for contralesional bilateral targets, indicating signs of spatial processing deficits already in the single-task condition. Moreover, he exhibited a significant number of omissions for contralesional bilateral targets in the visual dual-task condition and contralesional unilateral targets in the auditory dual-task condition. Upon reducing the target's radius to 0.1°, the patient's performance in the single-task condition declined even more, and he displayed a significant number of omissions for both contralesional bilateral and unilateral targets. Interestingly, he exhibited a similar performance in the visual dual-task condition, but not in the auditory dual-task condition. This finding confirmed that when the target's radius was exceptionally small and, as a result, the target became difficult to perceive, biases toward the ipsilesional space increased significantly. However, this increase was more pronounced in the single-task condition, while the distinction between the single-task condition and the dual-task conditions, as well as, the effects of multitasking became less prominent. Additionally, omissions for both contralesional bilateral and unilateral targets showed a sort of lower limit/threshold and never went below 50% across all the critical conditions we tested (right vs left and right vs bilateral across various load conditions and target's radius conditions). It remains uncertain whether this threshold pattern is unique to this patient or whether it can be attributed to the long time passed from stroke, given that many previous cases have often exhibited more dichotomous patterns (dramatically impaired vs fully preserved) (e.g.: Bonato et al., 2010). It also remains unclear why, in the most challenging condition where the target's radius was reduced to 0.1°, there was no modulation of the auditory dual-task. We speculate that this null effect could be attributed to a learning effect, as this condition was performed last, to a motivational effect, given that the patient was aware of being in the most difficult condition, or to an interaction of the two.

Interestingly, the accuracy in the secondary task, when it was visual, appeared to be modulated, by the spatial position of the lateralized visual targets and not only vice versa. The presence of a target on the right, be it alone or together with another target on the left, determined a loss of accuracy in identifying the visual symbol in the centre. It seems very likely that, under dual-tasking conditions, the visual symbol on the centre was extinguished as it was contralesional with respect to the target in the right hemispace.

An important point to emphasize is that very different manipulations, the first involving top-down and primarily cognitive factors (i.e., varying the number of tasks to be performed simultaneously), and the second involving bottom-up and purely perceptual aspects (i.e., varying the size of the

target), can interact to jointly modulate the level of required resources. Consequently, they both contribute to shaping the potential reappearance of biases toward the ipsilesional space. Expanding on this idea, it is plausible to speculate that different task requirements are characterized by the common use of relatively unspecific attentional resources. When the attentional load increases either due to dual-task performance or because it's necessary to report the position of an extremely small target (or both), this general yet limited pool of resources is depleted, potentially affecting the ability to compensate for contralesional spatial processing deficits.

A crucial aspect that requires clarification, in addition to assessing the generalizability of these results, is whether load-induced spatial processing asymmetries exist within the unimpaired cognitive system or exclusively arise after a brain lesion. Clarifying this point is essential to determine whether the extremely subtle biases toward the ipsilesional space observed in this patient are indeed remnants of the stroke's impact or rather genuinely asymmetric effects emerging due to the complexity of the testing process. Clarifying this point is challenging, as the absence of load-induced spatial processing asymmetries in neurologically intact matched control participants could be simply attributed to ceiling effects as emerged from our control group performance; therefore, the development of particularly complex tasks is necessary (see Chapter 2).

In conclusion, as an overarching finding, increasing the number of tasks to be performed together and decreasing target diameter were detrimental for the detection of contralesional targets, while performance for ipsilesional targets (and also catch trials) was unaffected by these parameters. The overall picture provided strong empirical support for our interpretation whereby contralesional spatial processing deficits are strongly modulated by the availability of unspecific attentional resources, that allow to implement compensatory strategies. Consequently, computerized resource-demanding dual-tasks appear to be one of the best options available for detecting and monitoring biases towards the ipsilesional space from the onset of a lesion, spanning a very extended period (Bonato, 2012). Unlike other tools, they can be quite challenging. Moreover, they can be adapted according to the severity of the contralesional spatial processing deficits, modulating the number of tasks to be completed at the same time and target to avoid ceiling effects. Furthermore, these tasks more accurately represent the dynamic nature of natural environments characterized by highly intricate situations. At the same time, they are informative because they allow the identification of patients whose spatial processing performance in everyday life can be kept within the boundaries of normality by avoiding dual-task (Bonato, 2012).

1.7 Supplementary

Characteristics of control participants

The control group comprised four right-handed neurologically intact control participants (mean age: 67 years; age range: 61-81 years; mean education: 8.5 years; education range: 5-13 years; m: 3). Detailed registry information for each control participant is presented in Table 1.1. Control 1 may be viewed as an outlier in terms of age, Control 2 in terms of years of education, and Control 3 is the sole female participant in the group. Despite these differences, all participants achieved a ceiling performance in the most challenging conditions of the dual-task paradigm (i.e, dual-task conditions with target's radius set at 0.1°), which was compared against patient data. Secondary Tasks Accuracy (as percentage) as a function of target conditions (left, right, bilateral, catch) is presented for each control participant in Table 1.2. Primary Tasks Accuracy (as percentage) as a function of load conditions (single-task, visual dual-task, auditory dual-task) and target conditions (left, right, bilateral, catch) is presented for each control participant in Table 1.3.

	Age	***Years of Education***	***Biological Sex***
Control1	81	5	M
Control2	61	13	M
Control3	61	6	F
Control4	65	6	M

Table 1.1. Registry information for each control participant.

	Visual Dual-Task				***Auditory Dual-Task***			
	Left Target	***Right Target***	***Bilateral Target***	***Catch***	***Left Target***	***Right Target***	***Bilateral Target***	***Catch***
Control1	88%	100%	100%	100%	100%	100%	100%	100%
Control2	100%	100%	88%	94%	100%	100%	94%	100%
Control3	100%	100%	100%	94%	100%	100%	100%	100%
Control4	100%	94%	100%	94%	100%	100%	100%	100%

Table 1.2. Secondary Tasks Accuracy (as percentage) as a function of target conditions (left, right, bilateral, catch) for each control participant.

	Single-Task				Visual Dual-Task				Auditory Dual-Task			
	Left Target	Right Target	Bilateral Target	Catch	Left Target	Right Target	Bilateral Target	Catch	Left Target	Right Target	Bilateral Target	Catch
Control1	100%	100%	100%	100%	100%	100%	100%	100%	100%	100%	100%	100%
Control2	100%	100%	100%	100%	100%	100%	100%	100%	100%	100%	100%	94%
Control3	100%	100%	100%	100%	100%	100%	100%	100%	100%	100%	100%	94%
Control4	100%	100%	100%	100%	100%	100%	100%	100%	100%	100%	100%	100%

Table 1.3. Primary Tasks Accuracy (as percentage) as a function of load conditions (single-task, visual dual-task, auditory dual-task) and target conditions (left, right, bilateral, catch) for each control participant.

Entire set of primary task comparisons

In primary task analysis we computed and reported a small sample of comparisons to concentrate on findings that deliver clear and substantial insights without inflating the total number of comparisons and thus the risk of false positives and the need for stronger adjustment for multiple comparisons.

The entire set of comparisons is reported in Table 1.4 (without adjustment for multiple comparisons).

Comparisons	Controls		Patient		Test of significance				Effect size	
	Accuracy Test X	Accuracy Test Y	Accuracy Test X	Accuracy Test Y	t	df	p-value		Point	95% CI
Test X = 0.8 *Test Y = 0.3*	100%	100%	92%	87%	0,708	3	0,265	n.s.	1,118	-0,466 - 2,996
Test X = 0.8 *Test Y = 0.1*	100%	100%	92%	83%	1,242	3	0,151	n.s.	2,012	0,026 - 4,577
Test X = 0.3 *Test Y = 0.1*	100%	100%	87%	83%	0,569	3	0,305	n.s.	0,894	-1,001 - 3,034
Test X = 0.8-Single-Task *Test Y = 0.8-Visual Dual-Task*	100%	100%	93%	89%	0,569	3	0,305	n.s.	0,894	-0,537 - 2,55
Test X = 0.8-Single-Task *Test Y = 0.8-Auditory Dual-Task*	100%	0.9	93%	92%	1,242	3	0,151	n.s.	-2,012	-4,145 - -0,441
Test X = 0.8-Visual Dual-Task *Test Y = 0.8-Auditory Dual-Task*	100%	0.9	89%	92%	1,735	3	0,091	n.s.	-2,097	-5,826 - -0,853
Test X = 0.3-Single-Task *Test Y = 0.3-Visual Dual-Task*	100%	100%	92%	83%	1,242	3	0,151	n.s.	2,012	0,026 - 4,577

Test X = 0.3-Single-Task *Test Y = 0.3-Auditory Dual-Task*	100%	0.9	92%	86%	0,569	3	0,305	n.s.	-0,894	-2,361 - 0,363
Test X = 0.3-Visual Dual-Task *Test Y = 0.3-Auditory Dual-Task*	100%	0.9	83%	86%	1,735	2	0,091	n.s.	-2,907	-6,028 - -0,649
Test X = 0.1-Single-Task *Test Y = 0.1-Visual Dual-Task*	100%	100%	76%	84%	1,112	3	0,174	n.s.	-1,789	-4,785 - 0,696
Test X = 0.1-Single-Task *Test Y = 0.1-Auditory Dual-Task*	100%	0.9	76%	89%	2,787	3	0,034	*	-5,143	-10,228 - -1,663
Test X = 0.1-Visual Dual-Task *Test Y = 0.1-Auditory Dual-Task*	100%	0.9	84%	89%	1,965	3	0,072	n.s.	-3,354	-6,765 - -0,957
Test X = 0.8 - Single-Task - Right *Test Y = 0.8 - Single-Task - Left*	100%	100%	100%	94%	0,845	3	0,230	n.s.	1,342	0,051 - 2,976
Test X = 0.8 - Visual Dual-Task - Right *Test Y = 0.8 - Visual Dual-Task - Left*	100%	100%	100%	71%	3,321	3	0,023	*	6,485	2,205 - 12,822
Test X = 0.8 - Auditory Dual-Task - Right *Test Y = 0.8 - Auditory Dual-Task - Left*	100%	100%	100%	94%	0,845	3	0,230	n.s.	1,342	0,051 - 2,976
Test X = 0.8 - Single-Task - Right *Test Y = 0.8 - Single-Task - Bilateral*	100%	100%	100%	83%	2,184	3	0,058	n.s.	3,801	1,174 - 7,604
Test X = 0.8 - Visual Dual-Task - Right *Test Y = 0.8 - Visual Dual-Task - Bilateral*	100%	100%	100%	83%	2,184	3	0,058	n.s.	3,801	1,174 - 7,604
Test X = 0.8 - Auditory Dual-Task - Right *Test Y = 0.8 - Auditory Dual-Task - Bilateral*	100%	100%	100%	72%	3,236	3	0,024	*	6,261	2,123 - 12,386
Test X = 0.3 - Single-Task - Right *Test Y = 0.3 - Single-Task - Left*	100%	100%	100%	89%	1,494	3	0,116	n.s.	2,460	0,608 - 5,034
Test X = 0.3 - Visual Dual-Task - Right *Test Y = 0.3 - Visual Dual-Task - Left*	100%	100%	90%	71%	2,394	3	0,048	*	4,249	0,897 - 8,900
Test X = 0.3 - Auditory Dual-Task - Right *Test Y = 0.3 - Auditory Dual-Task - Left*	100%	100%	94%	72%	2,692	3	0,037	*	4,919	1,373 - 9,994
Test X = 0.3 - Single-Task - Right *Test Y = 0.3 - Single-Task - Bilateral*	100%	100%	100%	78%	2,692	3	0,037	*	4,919	1,614 - 9,772
Test X = 0.3 - Visual Dual-Task - Right *Test Y = 0.3 - Visual Dual-Task - Bilateral*	100%	100%	90%	63%	3,15	3	0,026	*	6,037	1,608 - 12,349
Test X = 0.3 - Auditory Dual-Task - Right *Test Y = 0.3 - Auditory Dual-Task - Bilateral*	100%	100%	94%	78%	2,076	3	0,065	n.s.	3,578	0,838 - 7,407
Test X = 0.1 - Single-Task - Right *Test Y = 0.1 - Single-Task - Left*	100%	100%	94%	61%	3,646	3	0,018	*	7,379	2,305 - 14,786
Test X = 0.1 - Visual Dual-Task - Right *Test Y = 0.1 - Visual Dual-Task - Left*	100%	100%	100%	60%	4,167	3	0,013	*	8,944	3,113 - 17,635
Test X = 0.1 - Auditory Dual-Task - Right *Test Y = 0.1 - Auditory Dual-Task - Left*	100%	100%	100%	83%	2,184	3	0,058	n.s.	3,801	1,174 - 7,604
Test X = 0.1 - Single-Task - Right *Test Y = 0.1 - Single-Task - Bilateral*	100%	100%	94%	56%	4,023	3	0,014	*	8,497	2,719 - 16,966

Test X = 0.1 - Visual Dual-Task - Right *Test Y = 0.1 - Visual Dual-Task - Bilateral*	100%	100%	100%	75%	2,972	3	0,029	*	5,590	1,870 - 11,077
Test X = 0.1 - Auditory Dual-Task - Right *Test Y = 0.1 - Auditory Dual-Task - Bilateral*	100%	100%	100%	89%	1,494	3	0,116	n.s.	2,460	0,608 - 5,034
Test X = 0.8 - Single-Task - Left *Test Y = 0.8 - Visual Dual-Task - Left*	100%	100%	94%	71%	2,787	3	0,034	*	5,143	1,459 - 10,430
Test X = 0.8 - Single-Task - Bilateral *Test Y = 0.8 - Visual Dual-Task - Bilateral*	100%	100%	83%	83%	0	3	0,500	n.s.	0,000	-2,083 - 2,087
Test X = 0.8 - Single-Task - Left *Test Y = 0.8 - Auditory Dual-Task - Left*	100%	100%	94%	94%	0	3	0,500	n.s.	0,000	-1,177 - 1,177
Test X = 0.8 - Single-Task - Bilateral *Test Y = 0.8 - Auditory Dual-Task - Bilateral*	100%	100%	83%	72%	1,494	3	0,116	n.s.	2,460	-0,405 - 6,054
Test X = 0.3 - Single-Task - Left *Test Y = 0.3 - Visual Dual-Task - Left*	100%	100%	89%	71%	2,29	3	0,053	n.s.	4,025	0,747 - 8,531
Test X = 0.3 - Single-Task - Bilateral *Test Y = 0.3 - Visual Dual-Task - Bilateral*	100%	100%	78%	63%	1,965	3	0,072	n.s.	3,354	-0,345 - 8,072
Test X = 0.3 - Single-Task - Left *Test Y = 0.3 - Auditory Dual-Task - Left*	100%	100%	89%	72%	2,184	3	0,058	n.s.	3,801	0,653 - 8,106
Test X = 0.3 - Single-Task - Bilateral *Test Y = 0.3 - Auditory Dual-Task - Bilateral*	100%	100%	78%	78%	0	3	0,500	n.s.	0,000	-2,577 - 2,582
Test X = 0.1 - Single-Task - Left *Test Y = 0.1 - Visual Dual-Task – Left*	100%	100%	61%	60%	0,143	3	0,448	n.s.	0,224	-4,138 - 4,660
Test X = 0.1 - Single-Task - Bilateral *Test Y = 0.1 - Visual Dual-Task - Bilateral*	100%	100%	56%	75%	2,394	3	0,048	*	-4,249	-9,926 - 0,143
Test X = 0.1 - Single-Task - Left *Test Y = 0.1 - Auditory Dual-Task - Left*	100%	100%	61%	83%	2,692	3	0,037	*	-4,919	-10,604 - -0,747
Test X = 0.1 - Single-Task - Bilateral *Test Y = 0.1 - Auditory Dual-Task - Bilateral*	100%	100%	56%	89%	3,646	3	0,018	*	-7,379	-14,998 - -2,065

Table 1.4. Entire set of comparisons for the analysis of primary tasks. *Test of significance: Revised Standardized Difference Test (RSDT, Crawford et al., 1998), without adjustment for multiple comparisons). Effect size: zdcc index (Crawford et al., 2010).*

CHAPTER 2

ATTENTIONAL LOAD CAN IMPACT MULTISENSORY INTEGRATION, WITHOUT LEADING TO SPATIAL PROCESSING ASYMMETRIES

2.1 Overview of the chapter

The present study examined how spatial processing in the unimpaired cognitive system is influenced by different levels of attentional load during multitasking. We conducted two separate experiments on healthy adults, by using web-based data collections, which facilitated the participation of a relatively large number of participants (101 in Experiment 1 and 98 in Experiment 2). We employed a primary audiovisual integration task, which involved presenting stimuli capable of eliciting the sound-induced flash illusion (i.e., task-relevant flashes accompanied by an incongruent number of sounds) on either the left or right side of the screen. This task enabled us to investigate audiovisual integration, but also indirectly provided an opportunity to explore spatial processing within a highly complex context. This task was coupled in the two experiments with two distinct concurrent secondary tasks to manipulate attentional load.

In both experiments, we replicated the increase of sound-induced flash illusion under high attentional load, which challenges the notion of an early, completely automatic and pre-attentive onset of the illusion. However, this effect was identical for left- and right-sided flashes, which speak against the existence of load-induced spatial processing asymmetries in the unimpaired cognitive system, at least in the context of audiovisual integration illusions. These findings seem to suggest that the unimpaired cognitive system and the damaged cognitive system are not only quantitatively but also qualitatively distinct. Consequently, assessing spatial processing in brain-damaged patients under high attentional load does not exacerbate asymmetries existing in the unimpaired cognitive system. Instead, it uncovers very subtle (yet potentially hazardous) deficits which are almost exclusively contralesional.

2.2 Introduction

Spatial processing is implemented by selective attention mechanisms and allows us to effectively deal with the broad flow of visual information in a seemingly effortless and highly efficient way (Peelen & Kastner, 2014). More specifically, thanks to these selective attention mechanisms, under normal circumstances we can process the most salient or potentially important stimuli within a specific location in space, while ignoring all others (Moore & Zirnsak, 2017; Peelen & Kastner, 2014; Vecera & Rizzo, 2003). Yet, spatial processing efficiency, not only in the damaged cognitive system, as outlined in Chapter 1, but also in the unimpaired cognitive system, seems to be negatively affected by levels of attentional load. This is proved by the emergence of spatial processing modulations when spatial processing is made more challenging through additional demands (Bartlett et al., 2020; Benedetto et al., 2013; Dodds et al., 2008; Lisi et al., 2015; Naert et al., 2018; Paladini et al., 2020; Peers et al., 2006; Pérez et al., 2008, 2009). This influence is commonly investigated in the experimental context, again exploiting a multitasking approach. Specifically, also to study the unimpaired cognitive system, it is indeed possible to design dual-tasks that pair a primary task, which requires spatial processing abilities, with a concurrent secondary task that leads attentional load to increase, as all the tasks must be completed simultaneously (Saccani et al., 2022). An ongoing debate within the research field of load-induced spatial processing modulations pertains to the existence of *spatially asymmetric* modulations in the unimpaired cognitive system. While there are indeed no doubts relative to the existence of load-induced spatial processing asymmetries in brain-damaged patients, who show an evident ipsilesional attentional bias, that dramatically impacts the already compromised processing of contralesional stimuli during multitasking (see Chapter 1; see also: Bellgrove et al., 2013; Russell et al., 2013; van Kessel et al., 2013), when it comes to healthy adults, the issue at stake is more subtle. This question holds considerable theoretical and clinical significance. At the theoretical level, it might provide insights into the characteristics of unimpaired cognitive systems. At the clinical level, it might greatly improve the ability to accurately interpret clinical data, as understanding the performance of the "baseline system" is essential for assessing the extent of impairment in a patient.

Load-induced spatial processing asymmetries have been previously reported in healthy adults, who seem to show either a reduction of the typical leftward attentional bias called pseudoneglect or even a rightward attentional bias, which consists in a disadvantage for the processing of left-sided stimuli compared to right-sided stimuli during multitasking (Bartlett et al., 2020; Benedetto et al.,

2013; Naert et al., 2018; Paladini et al., 2020; Peers et al., 2006; Pérez et al., 2008, 2009). For example, Peers and colleagues (Peers et al., 2006) asked participants to perform a visual detection task in which an array of six letters was briefly presented around a central fixation point, firstly individually and then while simultaneously engaging in a spatial or non-spatial auditory discrimination task. In the low attentional load condition, performance in the visual detection task was symmetrical. Differently, in the high attentional load condition, when the two tasks had to be performed together, a significant rightward attentional bias emerged, consisting of increased difficulty in reporting left-sided but not right-sided letters (Peers et al., 2006). Similarly, Naert and colleagues (Naert et al., 2018) required participants to execute a visual detection task of lateralized dots, during an easy or difficult working memory task, that consisted in keeping in mind short or long stimuli sequences. Also in this case, in the low attentional load condition, performance in the visual detection task was symmetrical. In contrast, in the high attentional load condition, when long sequences of stimuli had to be remembered, a significant rightward attentional bias emerged, consisting of increased response times in detecting left-sided but not right-sided dots (Naert et al., 2018; Paladini et al., 2020). Moreover, Pérez and colleagues (Pérez et al., 2008, 2009) paired a temporal order judgement task with an attentional blink task and replicated the attentional load level effect. Participants were presented with a visual target (T1 of the attentional blink task) and after a 280 or 1030 ms delay they were shown with a pair of lateralized stimuli (T2 of the attentional blink task) that had to be temporally ordered. In the low attentional load condition, when T1 was ignored or the lag between T1 and T2 was long, a leftward attentional bias (Pérez et al., 2008) or no bias (Pérez et al., 2009) emerged. In contrast, in the high attentional load condition, when T1 had to be processed plus the lag between T1 and T2 was short, an attention shift towards the right was found: left-sided stimuli were perceived as appearing simultaneously with right-sided stimuli even when they were in fact presented few milliseconds prior to them (Pérez et al., 2008, 2009). Finally, similar results were replicated also in more ecological contexts like a driving simulator (Benedetto et al., 2013) or a virtual maze (Bartlett et al., 2020). However, the abovementioned studies reporting load-induced spatial processing asymmetries in healthy adults are characterized by small sample sizes, which limits the generalizability of their findings. In addition to that, absence of load-induced spatial processing asymmetries in the unimpaired cognitive system has also been reported. For example, Bonato and colleagues (Bonato et al., 2010) tested right-hemisphere damaged patients and left-hemisphere damaged patients with a dual-task paradigm. The primary task involved detecting the appearance of lateralized visual targets, while the concurrent secondary task required

categorizing visual or auditory stimuli (see Chapter 1 for further details). The dual-task condition, (i.e., high attentional load condition) despite being highly sensitive with both right- and left-hemisphere damaged patients, failed multiple times to reveal any significant rightward attentional bias in neurologically intact matched control participants (Blini et al., 2016; Bonato et al., 2010). This lack of bias was observed even when the duration of the lateralized visual targets was extremely brief (i.e., 50 ms) and their size was reduced from 0.8° to 0.3° (Bonato, 2015) and further down to 0.1° in the single-case study detailed in Chapter 1. Similarly, Bellgrove and colleagues (Bellgrove et al., 2013) asked a group of right-hemisphere damaged patients to monitor the colour (i.e., low attentional load condition) or the identity (i.e., high attentional load condition) of a stream of stimuli at fixation while also detecting lateralized targets. The control group of neurologically intact matched control participants showed an effect of attentional load level but, differently from patients who exhibited a rightward attentional bias during the high attentional load condition, didn't show any interaction between attentional load level and target side (Bellgrove et al., 2013). Moreover, Russel and colleagues (C. Russell et al., 2013) asked a group of right-hemisphere damaged patients to complete a visual discrimination task that varied in difficulty and was combined with an attentional blink task. The control group of neurologically intact matched control participants didn't show any effect of attentional load level (C. Russell et al., 2013). Finally, in neurologically intact matched control participants, no discernible effect of attentional load level emerged, even when using a driving simulator (van Kessel et al., 2013). The absence of load-induced spatial processing asymmetries observed in neurologically intact matched control participants could be attributed to several factors. Firstly, patients may have more prominent general processing limitations compared to controls. Additionally, they may experience accelerated declines in efficiency as the task progresses. More importantly, patients may exhibit more pronounced spatial processing difficulties. As a result, dual-tasks that are challenging enough to increase attentional load during spatial processing in patients, may not have the same impact on controls. Therefore, the absence of load-induced spatial processing asymmetries in neurologically intact matched control participants shouldn't be interpreted as the absence of such modulations in the unimpaired cognitive system. Instead, such absence could simply be the result of a ceiling effect. Nevertheless, there are also studies that have specifically tailored the task for healthy adults and reported absence of load-induced spatial processing asymmetries. For example, Lisi and colleagues (Lisi et al., 2015) used a task similar to the one employed by Bonato and colleagues (2010) to test exclusively healthy adults' performance. In this case, to avoid ceiling effects, during the primary task, lateralized visual

targets were masked. Specifically, after targets disappearance, were arranged four other stimuli with the same shape as targets in the corners of a square centred on targets position. Additionally, during the secondary task, it was required to categorize not only visual or auditory stimuli, but also visual *and* auditory stimuli together. Despite that, the interaction between attentional load level and target side did not reach significance. Another of such studies was conducted by Dodds and colleagues (Dodds et al., 2008) utilizing the same task as Peers and colleagues (Peers et al., 2006) to examine exclusively healthy adults' performance. This task proved to be sufficiently sensitive in detecting subtle spatial processing biases in healthy adults, as indexed by a significant effect of time-on-task on spatial processing. Specifically, an attention shift towards the right was observed at the end of the task, but not at the beginning (Dodds et al., 2008). Despite that, the attention shift was not modulated by attentional load level, failing to replicate the previous result (Dodds et al., 2008). Given the mixed findings outlined, it becomes increasingly important to clarify whether spatial processing can be asymmetrically influenced by levels of attentional load during multitasking in the unimpaired cognitive system. However, investigating the performance of healthy adults necessitates the use of a sufficiently challenging task to avoid ceiling effects. To address this issue, we propose the utilization of complex lateralized multisensory stimuli in the experimental design.

Our idea is rooted in previously documented load-induced spatial processing asymmetries during multisensory integration, as shown by Eramudugolla et al. in 2011. In their study participants were exposed to sequences of simultaneous but spatially separated auditory and visual stimuli, while they also had to discriminate centrally presented salient (i.e., high attentional load condition) or not salient (i.e., low attentional load condition) visual patterns. After this exposure, participants showed the ventriloquist aftereffect, that is a long-lasting shift in the localization of auditory stimuli, toward the direction of the visual stimuli presented during the exposure period. Crucially, the aftereffect was significantly enhanced after experiencing high attentional load, but only when the sound localization was shifted toward the right side of space and only for sounds on the right side of space. This result was likely due to a rightward attentional bias that emerged during exposure with salient visual patterns (Eramudugolla et al., 2011). In our current investigation, we plan to leverage another perceptual illusion known as the "sound-induced flash illusion" (SIFI) to investigate load-induced spatial processing asymmetries during multisensory integration in healthy adults. This phenomenon occurs during the simultaneous presentation of different numbers of visual flashes and auditory sounds. Participants' accuracy in reporting the number of perceived flashes is higher when the number of flashes and sounds is congruent, but it drops when they are incongruent, as sounds

influence flashes perception in an illusory way (Shams et al., 2000, 2002). Specifically, when one flash is combined with two sounds, it can lead to the splitting of the visual percept, causing participants to report seeing two flashes (i.e., fission illusion). On the other hand, when two flashes are combined with one sound, it can induce the merging of visual percepts, leading participants to report seeing only one flash (i.e., fusion illusion) (Andersen et al., 2004; Shams et al., 2000, 2002). This effect is highly reliable and has been replicated in numerous studies, even with variations in different parameters (Hirst et al., 2019; Keil, 2020). Yet, despite the overall robustness, there is significant variation among individuals in their susceptibility to the illusion (de Haas et al., 2012) and the average occurrence of the illusion has frequently been found to be approximately 50% (e.g.: Keil et al., 2014). This effect seems to occur at an early perceptual stage, as it is associated with brain activity 35–65 ms after the onset of the flash (Shams et al., 2005) and also with brain activity in the primary visual cortex (Watkins et al., 2006, 2007). However, there is also evidence that it can be influenced by high level top-down cognitive factors (Hirst et al., 2019; Keil, 2020). For example, Anderson and colleagues demonstrated that the generation of the illusion could be influenced by the modality towards which participants direct their attention. Specifically, when they inverted the classic instructions and asked participants to count beeps instead of flashes, a visual stimulus-induced beep illusion was created. The authors interpreted these findings as supporting the directed attention hypothesis, which suggests that the attended modality is the one that dominates perception (Andersen et al., 2004). Moreover, Michail and colleagues (Michail et al., 2021; Michail & Keil, 2018) discovered that the illusion generation might be also influenced by concurrent task demands. They modulated attentional load exposing participants to stimuli eliciting the SIFI, while completing a concurrent n-back task. Results showed that high attentional load led to an increase in the rate of illusions (Michail & Keil, 2018), associated with the engagement of top-down theta and beta frequency bands (Michail et al., 2021). Finally, Wang and colleagues (Wang et al., 2019) found that not only attentive factors, but also expectations could influence the illusion generation. They modulated cognitive expectations by presenting instructions that were either true or false in terms of the proportion of trial types. Results showed that informing participants to expect a larger proportion of single flash trials can decrease the fission illusion, while the modulation was not significant for the fusion illusion (Wang et al., 2019). Crucially for our study, the probability of perceiving the illusion increases when the visual stimuli's eccentricity is greater, possibly because audiovisual integration is more efficient in the periphery compared to the fovea (Chang et al., 2023;

Shams et al., 2001). However, there are no differences in the rate of illusion perception when stimuli eccentricity is increased toward the right or the left side of space (Kamke et al., 2012).

2.3 Aim and hypothesis

Spatial processing efficiency appears to be affected by levels of attentional load. This phenomenon is well-documented in clinical populations, where load-induced spatial processing asymmetries during multitasking are clearly evident. In healthy populations, however, this effect is more subtle and can potentially be masked by ceiling effects.

In order to clarify the existence of load-induced spatial processing asymmetries in the unimpaired cognitive system we conducted two separate experiments employing a computer-based dual-tasking approach with healthy adults. In both experiments, we utilized a primary audiovisual integration task that involved presenting stimuli capable of eliciting the SIFI on either the left or right side of the screen. This task not only allowed to investigate audiovisual integration but also indirectly provided an opportunity to investigate spatial processing within a highly complex context. Depending on the experiment, this primary task was paired with different secondary tasks requiring additional processing, in order to test which manipulation was more effective. In Experiment 1, the primary task was combined with a concurrent secondary verbal or spatial working memory task that enabled us to manipulate attentional load *offline* (i.e., the stimuli used to vary load were presented *before* the lateralized audiovisual integration stimuli). In Experiment 2, the primary task was combined instead with a concurrent secondary visual discrimination task that allowed us to manipulate attentional load *online* (i.e., the stimuli used to vary load were presented *simultaneously* with the lateralized audiovisual integration stimuli). A noteworthy feature of both experiments was the web-based data collection, which facilitated the participation of a large number of participants compared with previous research in the field.

We expected (H1) SIFI to emerge with incongruent stimuli as the result of failed audiovisual integration. Additionally, we expect (H2) the emergence of SIFI to be especially pronounced under high attentional load. In this case, we might be able to conclude that SIFI can be influenced by attention mechanisms. Conversely, if the emergence of SIFI remains unaffected by attentional load levels, we may infer that SIFI took place during an early, automatic and pre-attentive stage. Finally, (H3) to confirm that spatial processing can be asymmetrically influenced by levels of attentional load

during multitasking the emergence of SIFI under high attentional load should be more evident for left-sided stimuli compared to right-sided stimuli (i.e., rightward attentional bias).
Additionally, we expected similar effects across both experimental designs.
The project conceptualization is preregistered at: https://l1nq.com/ProjectConceptualization

2.4 Methods

Participants and Experimental Protocol

Participants were recruited by word of mouth among the acquaintances of the research laboratory members, were unaware of the aims and hypothesis of the experiments and received no compensation.
Initially, participants were sent an email containing comprehensive instructions and a link to complete the experiments. Upon accessing this link, they were firstly presented with the informed consent form, and only those who clicked the designated button to provide explicit informed consent were able to proceed. After that, they encountered the following list of inclusion criteria: age between 18 and 40 years, absence of neurological disorders, absence of severe vision impairments or any other severe medical condition that would prevent from carrying out tasks on the computer and no substance abuse. Only those who confirmed their compliance with the entire list were allowed to go ahead. Subsequently, to prevent potential confounding effects related to handedness, they were asked to respond to an online adaptation of the Edinburgh Handedness Inventory (Oldfield, 1971), and only those who were identified as right-handed could continue.
At this stage, participants were finally required to execute a practice session and the actual testing phase (see detailed description below).
A total of 101 volunteers completed the testing phase of Experiment 1 (mean age: 24.14, age range: 18-34; m: 30) and a total of 98 volunteers completed the testing phase of Experiment 2 (mean age: 22.63, age range: 18-40; m: 34) (statistical power was calculated a priori on the base of preliminary data previously collected in pilot studies and preliminary analysis, with a simulation approach (R Package: simr - v 1.0.7, Green & MacLeod, 2016)). Importantly, to prevent potential confounding effects related to learning, none of the participants took part in both experiments. Moreover, in Experiment 1, to prevent potential confounding effects related to the hand-used to respond, 54 participants responded to lateralized stimuli with their dominant hand, while the remaining

participants used their non-dominant hand. The same approach was followed in Experiment 2, where 49 participants used their dominant hand, and the rest used their non-dominant hand.
Once finished the testing phase, participants were asked to respond to a questionnaire to assess user autonomy and test usability. Specifically, they had to select one or more of the following options: “I carried out the experiment to the best of my ability”, “I was interrupted or distracted while carrying out the experiment”, “I completed the experiment quickly without focusing on the given answers”, “I completed the experiment autonomously”, “A person opened the email, and then I completed the experiment autonomously”, “I completed the experiment autonomously, but a person helped me with the use of the mouse and keyboard”, “I completed the experiment with a person who repeated the instructions to me”, “I completed the experiment with a person who suggested a few answers to me”.
The experimental protocol was approved by the Ethics Committee for Psychological Research of the University of Padua (protocol n. 3824) and was conducted according to the principles expressed in the Declaration of Helsinki.

Experiment 1: Dual-task with “offline” manipulation of attentional load

In Experiment 1 the attentional load manipulation was implemented combining the primary audiovisual integration task with a concurrent secondary verbal or spatial working memory task.
Participants were required to complete *macro-trials*, which consisted in a combination of the two types of trials. Specifically, these macro-trials were formed by a single working memory trial followed by a series of audiovisual integration trials, structured as follows: encoding phase of the working memory trial, audiovisual integration trials and recall phase of the working memory trial. Participants were required to answer to audiovisual integration stimuli after each audiovisual integration trial and to report working memory stimuli at the end of each macro-trial (see Figure 2.1).

Audiovisual integration task. During each audiovisual integration trial, participants firstly were presented with a black fixation cross measuring 0.5° and lasting for 500 ms. This was followed by lateralized flashes and binaural sounds. The lateralized flashes consisted in white discs with diameter measuring 4° and lasting for 16.66 ms (i.e., a refresh rate cycle in commonly used 60 Hz monitors). According to the condition, either one flash (1F) or two flashes (2F) were presented on the left or on the right side of the screen with an eccentricity of 8° with a time lag between the first

and second flash lasting for 50 ms in case of a double presentation. The binaural sounds consisted in hamming windowed sine waveform tones at the frequency of 3.5 kHz and with a duration of 7 ms. According to the condition, either one sound (1S) or two sounds (2S) were presented, in conjunction with the first flash or in conjunction with both the first and the second flash (see Figure 2.2). Thus, four different audiovisual integration stimulus types were presented with flashes appearing on the left or on the right side of the screen: 1F1S-left (one flash on the left + one sound), 2F2S-left, 1F2S-left, 2F1S-left, 1F1S-right, 2F2S-right, 1F2S-right and 2F1S-right. During each audiovisual integration trial, participants were required to focus their attention on the flashes only, while ignoring sounds. They were asked to report the number of perceived flashes, by pressing the space bar once for one flash and twice for two flashes with the index finger (of the dominant or non-dominant hand, depending on the counterbalancing). As soon as participants provided their response, the next audiovisual integration trial started.

Working memory task. During the encoding phase of each working memory trial, participants were presented with sequences of verbal or spatial stimuli. In the case of verbal attentional load, they were shown a sequence of two consonants (low attentional load) or seven consonants (high attentional load) appearing one after the other. These consonants were written in black, with an Arial font of 50 pixels in advance width, and were positioned in the centre of the screen. In the case of spatial attentional load, participants were presented with a sequence of two dots (low attentional load) or six dots (high attentional load) appearing one after the other. The dots were drawn in black, with a diameter of 1°, and were randomly located on the screen. Each consonant or dot was preceded by a grey screen and lasted for 2000 ms. None of the consonant identities or dot positions were repeated within a sequence. The specific number, size, and duration of the stimuli were all adjusted based on preliminary data previously collected in pilot studies. Thus, two attentional load types were presented in combination with two attentional load levels: verbal-low load, verbal-high load, spatial-low load and spatial-high load. During the encoding phase of each working memory trial, thus before performing the series of audiovisual integration trials, participants were required to memorize consonant identities or dot positions. During the recall phase, after having performed the series of audiovisual integration trials, they were then asked to report them, by pressing the keyboard or clicking on the screen with the mouse. In both cases responses were considered correct only when stimuli were reported in the exact order in which they

were presented (tolerance for the spatial task: 100 pixels from the original dot centre). As soon as participants provided their response, the next working memory trial started.

Dual-task procedure. The dual-task consisted of 8 blocks, formed by 5 macro-trials. Each macro-trial was composed by 1 working memory trial and by a series of 16 audiovisual integration trials, organized as follows: encoding phase of the working memory trial, 16 audiovisual integration trials and recall phase of the working memory trial. In total there were 10 trials for each of the four working memory conditions (i.e., verbal-low load, verbal-high load, spatial-low load and spatial-high load), presented in random ordered alternated block by block. As for the audiovisual integration trials, there were 80 trials for each of the eight audiovisual integration conditions (i.e., 1F1S-left, 2F2S-left, 1F2S-left, 2F1S-left, 1F1S-right, 2F2S-right, 1F2S-right and 2F1S-right), presented in random order. Before the testing phase it was conducted a practice session that consisted of 2 macro-trials, one under the verbal-low load condition and one under the spatial-high load.

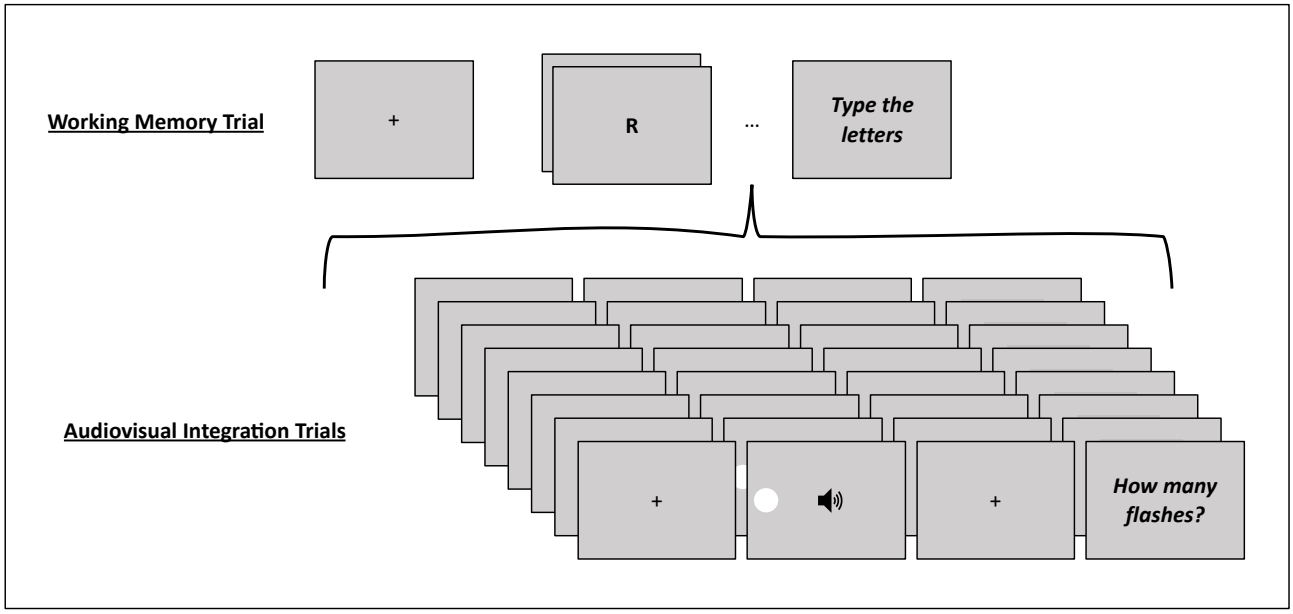

Figure 2.1. Dual-task with "offline" manipulation of attentional load. *Participants were required to complete macro-trials, which consisted in a combination of the two types of trials. Specifically, these macro-trials were formed by a single working memory trial followed by a series of audiovisual integration trials, structured as follows: encoding phase of the working memory trial, audiovisual integration trials and recall phase of the working memory trial. Participants were required to answer to audiovisual integration stimuli after each audiovisual integration trial and to report working memory stimuli at the end of each macro-trial. The figure shows a macro-trial encompassing a working memory trial from the verbal-low load (i.e., request to memorize and then report two consonants) condition and an audiovisual integration trial from the 1F1S-left (i.e., one flash on the left + one sound) condition.*

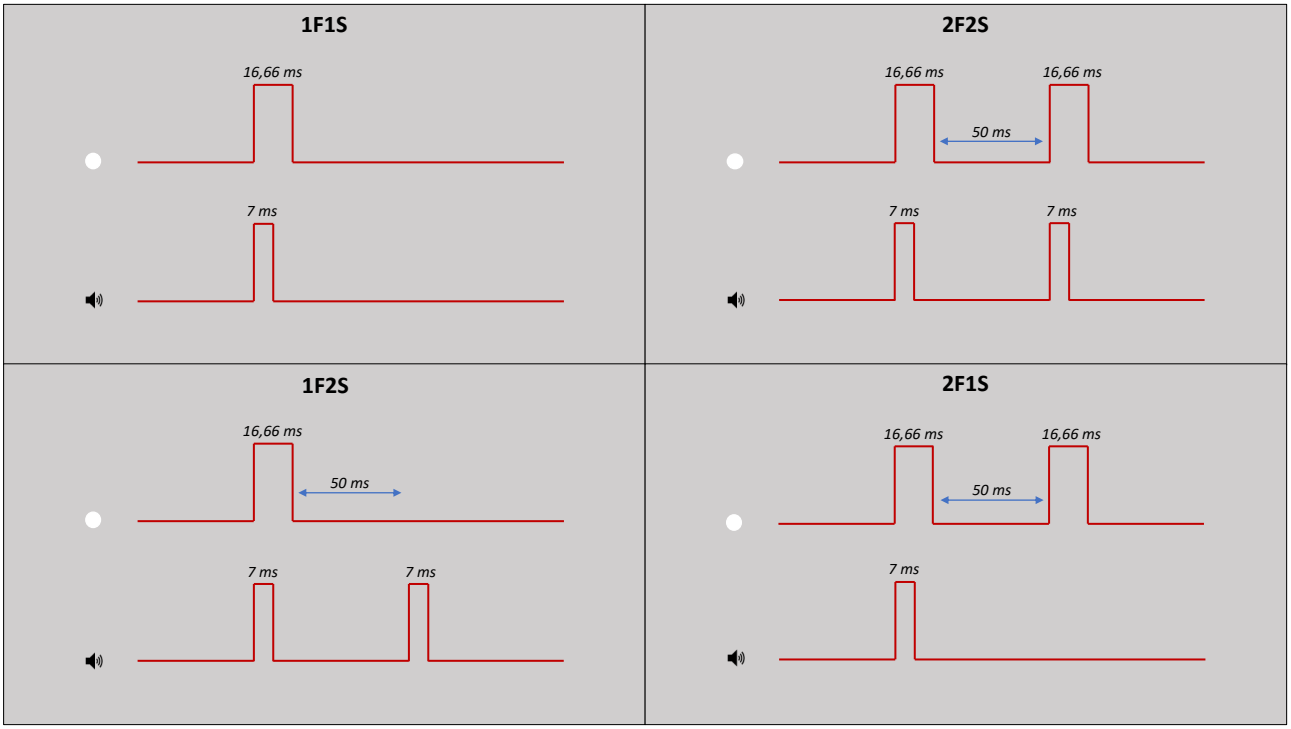

Figure 2.2. Audiovisual integration trial. *In each audiovisual integration trial, participants were concurrently presented with lateralized flashes (lasting 16.66 ms) and binaural sounds (lasting 7 ms). The presentation varied based on the condition: either a single flash (1F) or two successive flashes (2F) were displayed. In the case of the dual flash presentation, there was a 50 ms interval between the first and second flash. Additionally, depending on the condition, either a single sound (1S) or two sounds (2S) were presented in conjunction with the flash(es). In total, four different audiovisual integration stimulus types were possible.*

Experiment 2: Dual-task with "online" manipulation of attentional load

In Experiment 2 the attentional load manipulation was implemented combining the primary audiovisual integration task with a concurrent secondary visual discrimination task. Also in this case, participants were required to complete *macro-trials,* which consisted in a combination of the two types of trials. However, differently from Experiment 1, these macro-trials were formed by an audiovisual integration trial and a visual discrimination trial integrated together, with all the stimuli displayed simultaneously. After each macro-trial, participants were required to answer firstly to audiovisual integration stimuli and then to visual discrimination stimuli (see Figure 2.3).

Audiovisual integration task. Identical to the one used in Experiment 1.

Visual discrimination task. While participants were presented with lateralized flashes and binaural sounds, they were also presented with a central symbol consisting in a blue or red spade or flower shape. These symbols were written with an Arial font of 18 pixels in advance width and lasted for 50 ms. The size and duration of the stimuli were all adjusted based on preliminary data previously

collected in pilot studies. During each visual discrimination trial, participants were required to focus their attention either on the colour of the central symbol (i.e., blue vs red), which is an easier task (low attentional load), or on the shape of the central symbol (i.e., spade vs flower), which is a more difficult and resource consuming task (high attentional load). They were asked to report the colour or the shape, by pressing either the "t" or "y" key with any finger of the hand not used during the audiovisual integration task. Thus, in this case, exclusively manipulating the instructions (i.e., without any perceptual difference between trials), two attentional load levels were presented: low load and high load.

Dual-task procedure. The dual-task consisted of 4 blocks, formed by 160 macro-trials. Each macro-trial was composed by 1 audiovisual integration trial and by 1 visual discrimination trial, organized as follows: participants firstly were presented with a black fixation cross measuring 0.5° and lasting for 500 ms, followed by audiovisual integration stimuli (i.e., lateralized flashes and binaural sounds) together with visual discrimination stimuli (i.e., central symbol). After the stimuli presentation, participants were required to answer firstly to audiovisual integration stimuli and then to visual discrimination stimuli. As soon as participants provided both their responses, the next macro-trial started. In total, there were 320 trials for each of the two visual discrimination conditions (i.e., low load and high load), presented in random ordered alternated block by block. As for the audiovisual integration trials, there were 80 trials for each of the eight audiovisual integration conditions (i.e., 1F1S-left, 2F2S-left, 1F2S-left, 2F1S-left, 1F1S-right, 2F2S-right, 1F2S-right and 2F1S-right), presented in random order. Before the testing phase it was conducted a practice session that comprised 64 macro-trials, evenly divided with 32 under the low load condition and 32 under the high load condition.

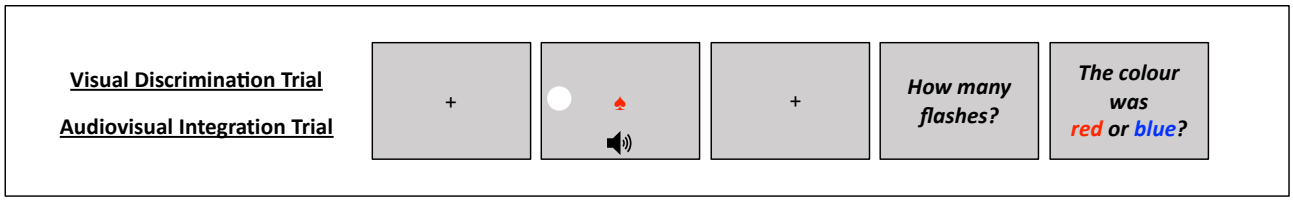

Figure 2.3. Dual-task with "online" manipulation of attentional load. *Participants were required to complete macro-trials, which consisted in a combination of the two types of trials. More specifically, these macro-trials were formed by an audiovisual integration trial and a visual discrimination trial integrated together, with all the stimuli displayed simultaneously. After each macro-trial, participants were required to answer firstly to audiovisual integration stimuli and then to visual discrimination stimuli. The figure shows a macro-trial encompassing an audiovisual integration trial from the 1F1S-Left (i.e., one flash on the left + one sound) condition and a visual discrimination trial from the low load (i.e., colour discrimination request) condition.*

During both experiments stimuli were presented on a grey background. All responses were collected without time constraints. Instructions were repeated at the start of each block, emphasizing the importance of accuracy over speed. It was also clarified that both tasks were important and that higher scores would only be achieved by correctly answering the secondary tasks. This was to ensure that participants didn't focus solely on audiovisual integration trials without any attentional load. Participants were allowed to take breaks at the end of each block.

Materials

Dual-tasks were both programmed using HyperText Markup Language (HTML), Cascading Style Sheets (CSS) and jsPsych, an open-source JavaScript library that provides a flexible framework for building psychological experiments that can be conducted online (de Leeuw, 2015; de Leeuw et al., 2023). The dual-tasks were subsequently uploaded to a web server, with JATOS installed, an open-source web application that streamlines the management of web-based data collections. Specifically, JATOS enables hosting experiment scripts, generating links for completing the experiments and organizing collected data (Lange et al., 2015). The web server was located at the Department of General Psychology of the University of Padua.

To minimize setting variability, several precautions were taken. Firstly, participants were instructed to complete the task in a semi-dark and quiet room, sitting at a distance of 57 cm from the computer screen. They were advised to keep the computer connected to a power source throughout the testing session to avoid abrupt interruptions. They were indicated to close all internet tabs except for the one related to the experiment, which had to be kept in full-screen mode, without being refreshed, and without going back to previous pages. Additionally, they were asked to avoid using Bluetooth devices for audio output and response recording, as these could potentially introduce delays in stimuli presentation and response collection. When using wired devices, they were directed to align the keyboard's space bar with the centre of the screen. Furthermore, to ensure consistent stimulus sizes across varying monitor resolutions, jspsych-resize plugin was used. At the outset of each experiment, this tool required participants to use a ruler to adjust the length of a square-shaped container until it measured 10 cm. After that, the ratio between square width in pixels and in millimetres could be calculated, yielding the logical pixel density (LPD) expressed in pixels per mm, which was used to ensure uniform scaling of the size of all stimuli, regardless of the device in use (Q. Li et al., 2020; Morys-Carter, 2021).

To minimize audio-visual asynchrony, which is one of the less precise aspects of web-based data collections (Bridges et al., 2020), jsPsych's capabilities were expanded by utilizing the "jspsych-psychophysics" plugin (Kuroki, 2021). This tool enhanced visual stimuli timing precision (and consequently, ensured highly accurate audio-visual synchronization) by aligning their presentation with the display refresh through the utilization of the requestAnimationFrame method (Kuroki, 2021). Achieving a level of precision comparable to laboratory settings could only be guaranteed under real-time priority, a factor beyond our control as it is impossible to boost priority using JavaScript in all browsers (Gao et al., 2020). Nevertheless, this limitation did not present a significant concern, given previous findings that the SIFI is resistant to asynchronies within an approximate range of 100 ms (Shams et al., 2000, 2002).

Finally, to avoid unforeseen issues with the rendering of the experimental webpage, the use of mobile phones or tablets, along with any browser other than Chrome, was blocked.

Analysis

Data Preparation and data analysis were performed using R Statistical Software (v 4.2.2; R Core Team, 2022).

Data preparation

Firstly, a rigorous data cleaning procedure was implemented to ensure the quality and reliability of the data. To filter out those who might not have provided genuine responses, participants who declared to have been given suggested answers or did not furnish any feedback in the questionnaire regarding user autonomy and test usability were excluded (n excluded Experiment 1: 3; n excluded Experiment 2: 3). Additionally, to filter out those who may have responded way too quickly without due attention or who may have been engaged in other activities during the experiments, participants who completed the experiment in less than 20 minutes or more than 3 hours were also excluded; these cutoffs were determined based on preliminary data collected in pilot studies, where it emerged that experiments would typically take around 50 minutes for completion (n excluded Experiment 1: 1; n excluded Experiment 2: 3). Moreover, to filter out those who might have encountered inconsistent stimuli duration because of technical issues it was taken into account the "avg_frame_time" parameter, provided by the "jspsych-psychophysics" plugin (Kuroki, 2021). This parameter is an indirect measure of the display refresh rate through the use of the

requestAnimationFrame method. Theoretically, with a display refresh rate set at 60 Hz, the avg_frame_time would be 16.66 ms. However, in cases where the display operates at a refresh rate different from 60 Hz or when there is a high load during stimulus presentation, the avg_frame_time deviates from 16.66 ms. This variance indicates that, in the specific trial considered, the stimulus may not have been presented with the intended timing. For this reason, participants with individual mean avg_frame_time deviated by more than 1.5 standard deviations from the group's average avg_frame_time in at least one audiovisual integration trial type were excluded (n excluded Experiment 1: 3; n excluded Experiment 2: 5). Finally, participants with individual audiovisual integration accuracy scores deviated by more than 1.5 standard deviations from group's average audiovisual integration accuracy in at least one audiovisual integration trial type were excluded (n excluded Experiment 1: 9; n excluded Experiment 2: 8). The same threshold was used for audiovisual integration response times (n excluded Experiment 1: 0; n excluded Experiment 2: 0), working memory accuracy in Experiment 1 and visual discrimination accuracy in Experiment 2 (n excluded Experiment 1: 1; n excluded Experiment 2: 5). All criteria were applied to the original samples of participants who completed the experiments; as a result, some participants were excluded due to meeting multiple criteria. The procedure resulted in final samples consisting of 88 participants in Experiment 1 (mean age: 24.36, age range: 18-34; number of males: 28, number of responders with dominant hand: 48) and 80 participants in Experiment 2 (mean age: 22.74, age range: 18-40; number of males: 26, number of responders with dominant hand: 38). Before performing the statistical procedures, individual trials were further pre-processed according to the following steps: trimming avg_frame_time between 14 and 19 ms and trimming audiovisual integration response times between 100 and 4000 ms. These steps resulted in the removal of 1.01% of all initial trials in Experiment 1 and 2.04% of all initial trials in Experiment 2.

The large number of exclusions is perhaps not surprising in a web-based data collection. Importantly, main effects and interactions highlighted in the following paragraph as relevant for addressing our hypothesis hold when not applying exclusion criteria, which suggests that the conservative exclusion criteria are not inherently biasing the reported results.

Models fitting and hypothesises testing

Statistical procedures capitalized on the use of Linear Mixed-effect Models (LMMs) and Generalized Linear Mixed-effect Models (GLMMs) (R Package: lme4 – v 1.1.31, Bates et al., 2015). These models do not assume independence amongst observations and they also enable the analysis of data in

which observations are nested within participants, without collapsing observations across items or participants; this approach preserves crucial information about variability and enhances the handling of missing data (Brown, 2021). Additionally, they enable the simultaneous specification of fixed and random effects to account for population-level trends and their variations across specific grouping factors (e.g., participants) (Brown, 2021; DeBruine & Barr, 2021). Lastly, through generalized models, it becomes possible to analyse not only continuous independent variables, but also categorical ones (Brown, 2021).

Secondary task accuracy. To assess the efficacy of secondary tasks in inducing attentional load modulations we initially performed a GLMM (family: binomial; distribution: logit). In Experiment 1 the dependent variable was accuracy in the secondary task. The fixed effects included types (verbal, spatial) and levels (low, high) of attentional load. Participants entered the model as a random intercept, to account for the inherent variations among their baseline accuracy during the secondary task. Additionally, blocks entered the model as a random slope nested within participants; this modelling choice was based on a model selection (see Supplementary) and it captured the idea that time on task might have different effects at the individual level. In Experiment 2, the model calculated was identical to the one used in Experiment 1, except for the absence of attentional load types as a fixed effect. In both experiments we expected a main effect of attentional load levels: working memory accuracy (Experiment 1) or visual discrimination accuracy (Experiment 2) would be significantly lower in high attentional load compared to low attentional load. Additionally, in Experiment 1, we explored the potential main effect of attentional load types and the interaction between attentional load types and attentional load levels.

Audiovisual integration accuracy. We then conducted a GLMM (family: binomial; distribution: logit) to investigate H1. In Experiment 1 the dependent variable was audiovisual integration accuracy. The fixed effects included: audiovisual integration stimulus types (1F1S, 2F2S, 1F2S, 2F1S), flash presentation side (left, right), attentional load types (verbal, spatial), attentional load levels (low, high) and hand-used to respond (dominant, non-dominant). Random effects included also in this case participants as a random intercept and blocks as a random slope nested within participants. Additionally, random effects included audiovisual integration stimulus types as random slope nested within participants; also this modelling choice aimed at capturing the previously reported individual variability in audiovisual integration accuracy when considering stimuli generating fission

and fusion illusions (Hirst et al., 2020). In Experiment 2, the model calculated was again identical to the one used in Experiment 1, except for the absence of attentional load types as a fixed effect. In both experiments we expected (H1) a main effect of audiovisual integration stimulus types: audiovisual integration accuracy would be significantly lower and SIFI would emerge in incongruent audiovisual integration stimuli, i.e. 1F2S stimuli and 2F1S stimuli, compared to congruent audiovisual integration stimuli, i.e. 1F1S stimuli and 2F2S stimuli.

Audiovisual integration d-prime. Finally, we implemented a LMM to investigate H2 and H3. In this case the dependent variable audiovisual integration accuracy was transformed using signal detection theory principles (similar to: Watkins et al., 2006; Whittingham et al., 2014), which is a standard approach to investigate sound-induced flash illusion (Keil, 2020). We aggregated audiovisual integration accuracy values from different congruent and incongruent audiovisual integration stimuli to calculate d-prime (d'). A lower d' value indicates poorer discrimination ability, and in the present context it indexes a greater susceptibility to illusions. Congruent 2F2S stimuli and incongruent 1F2S stimuli were used to calculate d' related to fission illusion. In 2F2S the correct response “2” was considered a hit, while the wrong response “1” was considered a miss. In 1F2S stimuli the illusory response “2” was considered a false alarm, while the correct response “1” was considered a correct rejection. Congruent 1F1S stimuli and incongruent 2F1S stimuli were instead used to calculate d' related to fusion illusion. In 1F1S stimuli the correct response “1” was considered a hit, while the wrong response “2” was considered a miss. In 2F1S stimuli the illusory response “1” was considered a false alarm, while the correct response “2” was considered a correct rejection. From these values, d' was computed as

$$d' = z(\text{hit rate}) - z(\text{false alarm rate})$$

adjusting for extreme values with the log-linear rule recommended by Hautus (Hautus, 1995) (R Package: psycho - v 0.6.1, Makowski, 2018). In Experiment 1 the so-calculated audiovisual integration d' entered the LMM as the dependent variable. The fixed effects included: sound-induced flash illusion types (fission, fusion), flash presentation side (left, light), attentional load types (verbal, spatial), attentional load levels (low, high) and hand-used to respond (dominant, non-dominant). Random effects included also in this case participants as a random intercept and blocks as a random slope nested within participants. Additionally, random effects included audiovisual integration illusion types as a random slope nested within participants, following the same rationale

as the inclusion of audiovisual integration stimulus types as random slope nested within participants in the previous model. In Experiment 2, the model calculated was again identical to the one used in Experiment 1, except for the absence of attentional load types as a fixed effect. In both experiments we expected (H2) a main effect of attentional load levels: the emergence of SIFI would be significantly higher with high attentional load compared to low attentional load. Additionally, in both experiments we expected (H3) an interaction between attentional load levels and flash presentation side: the emergence of SIFI would be significantly higher with high attentional load, especially in case of left sided flashes.

For all the models in this study, we performed model assumption checks using "DHARMa"(R Package: DHARMa - v 0.4.6, Hartig, 2022). This package employs a simulation-based approach to analyse residuals for fitted LMMs and GLMMs. The analysis indicated small deviations from expected residuals with no evident pattern. None of the models exhibited evident overdispersion, underdispersion, or heteroscedasticity.

To conduct hypothesis tests, LMMs were assessed through Analysis of Variance (Type III) with Satterthwaite's method for computing degrees of freedom and F statistics (R Package: lmerTest – v 3.1.3, Kuznetsova et al., 2017), while GLMMs were assessed through Analysis of Deviance with Type III Wald test for computing Chi-square statistics (R Package: car - v 3.1.1, Fox J. & Weisberg S., 2019). Post-hoc pairwise comparisons between the levels of fixed factors were tested for main effects and interactions of interest when significant, computing estimated marginal means contrasts (R package: emmeans - v 1.8.3, Russell V. L., 2022) and adjusting for multiple comparisons with the false discovery rate method (Glickman et al., 2014).

2.5 Results

We present below the results pertaining to secondary task accuracy, audiovisual integration accuracy, and audiovisual integration d' for both experiments. We provide details on all the main effects, while we include exclusively those interactions highlighted in the analysis section as relevant for addressing our hypothesis. For each of these main effect and interaction, for what concerns analysis of variance (for LMMs) or analysis of deviance (for GLMMs), we have reported either the Chi-square (for GLMMs) or F value (for LMMs). For post-hoc pairwise comparisons, we have then reported: the difference between estimated means ($\Delta\hat{\mu}$, in log odds ratio scale for GLMMs and in response scale for LMMs), as well as, exclusively for GLMMS, the difference between observed means ($\Delta\mu$ in response scale), the standard error (SE) and associated statistics (*z* test for GLMMs and *t* test for LMMs). Note that odds ratios are the ratios between the frequency with which a correct response occurs in a certain condition and the frequency with which a correct response occurs in another condition.

Experiment 1

Secondary task accuracy

Descriptive statistics for secondary task accuracy (range 0-1) as a function of load types and load levels are summarized in Table 2.1. GLMM for secondary task accuracy is summarized in Table 2.2. Analysis of deviance resulted in the expected main effect of attentional load levels (X^2 (1) = 143.914, $p < .001$), with participants being less accurate in the working memory task in case of high load compared to low load (high vs low: $\Delta\hat{\mu}$ = - 1.7, $\Delta\mu$ = -0.186, SE = 0.098, z = - 17.262, $p < .001$). Additionally, we found a main effect of attentional load types (X^2 (1) = 113.807, $p < .001$) and an interaction between attentional load types and attentional load levels (X^2 (1) = 19.105, $p < .001$), with participants being more accurate in the working memory task with verbal stimuli compared to spatial stimuli under low load (verbal vs spatial: $\Delta\hat{\mu}$ = 1.790, $\Delta\mu$ = 0.119, SE = 0.176, z = 10.172, $p < .001$) as well as under high load (verbal vs spatial: $\Delta\hat{\mu}$ = 0.935, $\Delta\mu$ = 0.151, SE = 0.088, z = 10.668, $p < .001$).

load types			
verbal load		*spatial load*	
load levels			
high load	*low load*	*high load*	*low load*
m= 0. 641 sd = 0.48	m= 0.849 sd = 0.358	m= 0.793 sd = 0.405	m= 0.960 sd = 0.174

Table 2.1. Experiment 1: descriptive statistics for secondary task accuracy (range 0-1).

Predictors	*Odds Ratios*	*SE*	*CI*
intercept	1.84	0.16	1.56 – 2.18
load type (verbal vs spatial)	2.55	0.22	2.14 – 3.02
load level (low vs high)	3.55	0.38	2.89 – 4.37
load type (verbal) X load level (low)	2.35	0.46	1.60 – 3.45
Marginal R^2 = 0.177; *AIC* = 13823.151			

Table 2.2. Experiment 1: GLMM for secondary task accuracy output.

Audiovisual integration accuracy

Descriptive statistics for audiovisual integration accuracy (range 0-1) as a function of flash presentation side, audiovisual integration stimulus types, load types and load levels are summarized in Table 2.3. GLMM for audiovisual integration accuracy is summarized in Table 2.4. Analysis of deviance highlighted the expected main effect of audiovisual integration stimulus types (X^2 (3) = 137.704, p < .001). Participants were less accurate with incongruent 1F2S stimuli than with congruent 1F1S stimuli (1F2S vs 1F1S: $\Delta\hat{\mu}$ = - 3.413, $\Delta\mu$ = -0.438, SE = 0.204, z = - 16.769, p < .001) indexing the presence of fission illusion (i.e., due to the delivery of two sounds two flashes were perceived although only one was presented). Similarly, they were less accurate with incongruent 2F1S stimuli than with congruent 2F2S stimuli (2F1S vs 2F2S: $\Delta\hat{\mu}$ = -3.137, $\Delta\mu$ = -0.405, SE = 0.212, z = - 14.819, p < .001) indexing the presence of fusion illusion (i.e., due to the delivery of one sound only one flash was perceived although two were presented). There were no differences in accuracy between the congruent 1F1S stimuli and 2F2S stimuli (1F1S vs 2F2S: $\Delta\hat{\mu}$ = 0.192, $\Delta\mu$ = 0.011, SE = 0.236, z = 0.813, p = 0.499), as well as between the incongruent 1F2S stimuli and 2F1S stimuli (1F2S vs 2F1S: $\Delta\hat{\mu}$ = -0.084, $\Delta\mu$ = -0.022, SE = 0.251, z = -0.335, p = 0.738) (see Figure 2.4). We can therefore conclude that the main effect of audiovisual integration stimulus types was due to the significant

differences between congruent and incongruent stimuli. Moreover, the main effect of flash presentation side was not significant (X^2 (1) = 1.967, p = 0. 161) and also the main effect of attentional load levels was not significant (X^2 (1) = 1.1355, p = 0.287), while the main effect of attentional load types was significant (X^2 (1) = 12.192, p = < .001).

				flash presentation side							
				left				*right*			
				audiovisual integration stimulus types							
				1F1S	*1F2S*	*2F1S*	*2F2S*	*1F1S*	*1F2S*	*2F1S*	*2F2S*
load types	*verbal load*	***load levels***	*low load*	m= 0.934 sd = 0.249	m= 0.503 sd = 0.5	m= 0.508 sd = 0.5	m= 0.921 sd = 0.269	m= 0.946 sd = 0.226	m= 0.485 sd = 0.5	m= 0.479 sd = 0.5	m= 0.916 sd = 0.277
			high load	m= 0.868 sd = 0.338	m= 0.480 sd = 0.5	m= 0.522 sd = 0.5	m= 0.88 sd = 0.325	m= 0.878 sd = 0.327	m= 0.490 sd = 0.5	m= 0.487 sd = 0.5	m= 0.87 sd = 336
	spatial load	***load levels***	*low load*	m= 0.939 sd = 0.238	m= 0.478 sd = 0.5	m= 0.498 sd = 0.5	m= 0.916 sd = 0.277	m= 0.934 sd = 0.248	m= 0.470 sd = 0.499	m= 0.467 sd = 0.499	m= 0. 916 sd = 0.277
			high load	m= 0.915 sd = 0.278	m= 0.453 sd = 0.498	m= 0.52 sd = 0.5	m= 0.909 sd = 0.287	m= 0.908 sd = 0.289	m= 0.458 sd = 0.498	m= 0.509 sd = 0.5	m= 0.905 sd = 0.293

Table 2.3. Experiment 1: descriptive statistics for audiovisual integration accuracy (range 0-1).

Predictors	*Odds Ratios*	*SE*	*CI*
intercept	22.95	6.41	13.27 – 39.69
flash presentation side (right vs left)	0.76	0.15	0.51 – 1.12
audiovisual integration stimulus types (1F2Svs 1F1S)	0.03	0.01	0.02 – 0.06
audiovisual integration stimulus types (2F1S vs 1F1S)	0.03	0.01	0.01 – 0.07
audiovisual integration stimulus types (2F2S vs 1F1S)	0.66	0.24	0.32 – 1.35
load type (verbal vs spatial)	0.51	0.10	0.34 – 0.74
load level (low vs high)	1.26	0.28	0.82 – 1.94
Marginal R^2 = 0.458; *AIC* = 40430.998			

Table 2.4. Experiment 1: GLMM for audiovisual integration accuracy output.

Audiovisual integration d-prime

Descriptive statistics for audiovisual integration d' as a function of flash presentation side, audiovisual integration stimulus types, load types and load levels are summarized in Table 2.5. LMM for audiovisual integration d' is summarized in Table 2.6. Analysis of variance highlighted the expected main effect of attentional load levels (F (1, 867.70) = 24.238, $p < .001$), with participants having higher illusion rates in case of high load compared to low load (high vs low: $\Delta\hat{\mu}$ = -0.123, SE: 0.027, t (488) = - 4.495, $p < .001$). However, the interaction we predicted between attentional load levels and flash presentation side was not significant (F (1, 2175.18) = 0.264, p = 0.607) (see Figure 2.4). Moreover, we found a main effect of flash presentation side (F (1, 2175.19) = 6.633, p = 0.01) and a main effect of attentional load types (F (1, 1033.18) = 4.499, p = 0.034). Resembling audiovisual integration accuracy results, the main effect of sound-induced flash illusion types was not significant (F (1, 86) = 1.541, p = 0. 218), meaning similar fission and fusion illusion rates.

				flash presentation side			
				left		*right*	
				audiovisual integration stimulus types			
				fission	*fusion*	*fission*	*fusion*
load types	*verbal load*	***load levels***	*low load*	m= 1.349 sd = 1.046	m= 1.407 sd = 1.153	m= 1.284 sd = 1.03	m= 1.362 sd = 1.142
			high load	m= 1.125 sd = 0.989	m= 1.22 sd = 1.141	m= 1.134 sd = 0.994	m= 1.13 sd =1.103
	spatial load	***load levels***	*low load*	m= 1.251 sd = 0.985	m= 1.402 sd = 1.159	m= 1.24 sd = 0.976	m= 1.272 sd = 1.088
			high load	m= 1.15 sd =1.011	m= 1.384 sd = 1.12	m= 1.165 sd = 0.995	m= 1.286 sd = 1.07

Table 2.5. Experiment 1: descriptive statistics for audiovisual integration d'.

Predictors	*Estimates*	*SE*	*CI*
intercept	1.12	0.12	0.88 – 1.35
flash presentation side (right vs left)	-0.07	0.07	-0.21 – 0.08
audiovisual integration illusion (fusion vs fission)	0.02	0.13	-0.24 – 0.28
load type (verbal vs spatial)	-0.19	0.08	-0.35 – -0.04
load level (low vs high)	0.02	0.08	-0.14 – 0.17
flash presentation side (right) X load level (low)	0.04	0.11	-0.17 – 0.24
Marginal R^2 = 0.048; *AIC* = 5528.707			

Table 2.6. Experiment 1: LMM for audiovisual integration d' output.

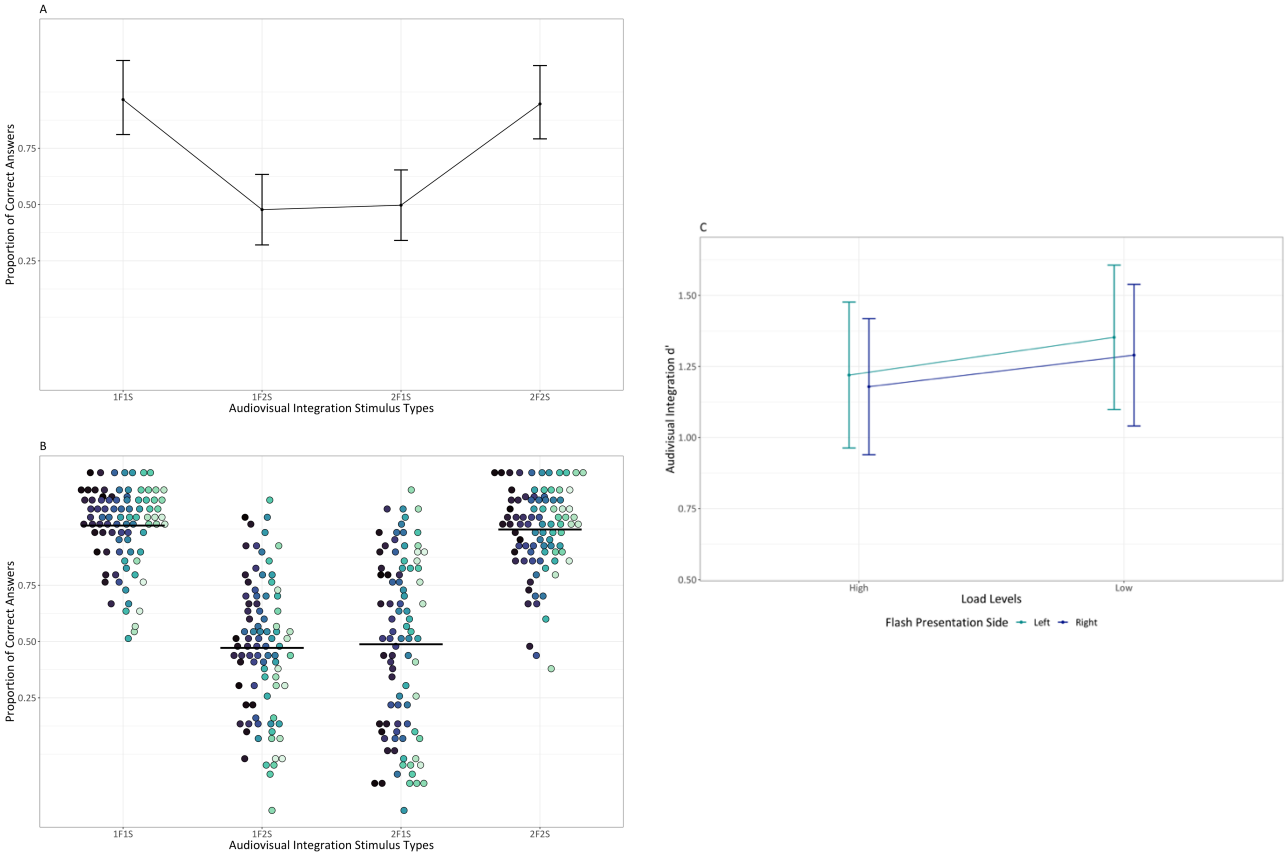

Figure 2.4. Experiment 1.: Panel A *displays averaged proportion of correct answers (i.e., no illusion) for the different audiovisual integration stimulus types. Bars represent 95% confidence intervals, adjusted using the Tryon method as accuracy is a binomial variable. These adjustments were calculated over Anscombe-transformed scores using "superb"* (R Package: superb - v 0.9.7.6, Cousineau et al., 2021)*, and subsequently transformed back into proportions.* ***Panel B*** *displays individual proportion of correct answers (i.e., no illusion) for the different audiovisual integration stimulus types, with each dot corresponding to a different participant. The mean is indicated by a horizontal black line. All the proportions are depicted using a non-linear scale, specifically the "asn_trans()" scale for arcsine.* ***Panel C*** *displays cumulative d' for the different load levels and flash presentation side.*

Experiment 2

Secondary task accuracy

Descriptive statistics for secondary task accuracy (range 0-1) as a function of load levels are summarized in Table 2.7. GLMM for secondary task accuracy is summarized in Table 2.8. Analysis of deviance resulted again in the expected main effect of attentional load levels (X^2 (1) = 527.63, p < .001), with participants being less accurate in the visual discrimination task in case of high load compared to low load (high vs low: $\Delta\hat{\mu}$ = - 2.05, $\Delta\mu$ = - 0.154, SE = 0.089, z = - 22.970, p < .001).

load levels	
high load	*low load*
m= 0.81 sd = 0.392	m= 0.964 sd = 0.185

Table 2.7. Experiment 2: descriptive statistics for secondary task accuracy (range 0-1).

Predictors	*Odds Ratios*	*SE*	*CI*
intercept	5.80	0.65	4.65 – 7.22
load level (low vs high)	7.76	0.69	6.51 – 9.24
Marginal R^2 = 0.187; AIC = 28174.837			

Table 2.8. Experiment 2: GLMM for secondary task accuracy output.

Audiovisual integration accuracy

Descriptive statistics for audiovisual integration accuracy (range 0-1) as a function of flash presentation side, audiovisual integration stimulus types and load types are summarized in Table 2.9. GLMM for audiovisual integration accuracy is summarized in Table 2.10. Analysis of deviance highlighted the expected main effect of audiovisual integration stimulus types (X^2 (3) = 128.656, p < .001). Participants were less accurate with incongruent 1F2S stimuli than with congruent 1F1S stimuli (1F2S vs 1F1S: $\Delta\hat{\mu}$ = - 3.344, $\Delta\mu$ = -0.477, SE = 0.198, z = - 16.858, p < .001) indexing the presence of fission illusion emerged also in this experiment. Additionally, they were less accurate with incongruent 2F1S stimuli than with congruent 2F2S stimuli (2F1S vs 2F2S: $\Delta\hat{\mu}$ = -3.221, $\Delta\mu$ = - 0.469, SE = 0.242, z = - 13.298, p < .001), indexing that also fusion illusion was again reliably detected.

Differently from Experiment 1, there was a significant difference in accuracy between congruent 1F1S stimuli and 2F2S stimuli (1F1S vs 2F2S: $\Delta\hat{\mu}$ = 0.636, $\Delta\mu$ = 0.067, SE = 0.245, z = 2.601, p = 0.011), but not between incongruent 1F2S stimuli and 2F1S stimuli (1F2S vs 2F1S: $\Delta\hat{\mu}$ = 0.513, $\Delta\mu$ = 0.059, SE = 0.271, z = 1.893, p = 0.064) (see Figure 2.5). Moreover, the main effect of flash presentation side was not significant (X^2 (1) = 0.5651, p = 0.452), while there was a main effect of attentional load levels (X^2 (1) = 10.3612, p = .001).

		flash presentation side							
		left				*right*			
		audiovisual integration stimulus types							
		1F1S	*1F2S*	*2F1S*	*2F2S*	*1F1S*	*1F2S*	*2F1S*	*2F2S*
load levels	*low load*	m= 0.918 sd = 0.273	m= 0.443 sd = 0.496	m= 0.403 sd = 0.49	m= 0.871 sd = 0.335	m= 0.921 sd = 0.27	m= 0.431 sd = 0.495	m= 0.381 sd = 0.486	m= 0.857 sd = 0.35
	high load	m= 0.891 sd = 0.311	m= 0.422 sd = 0.494	m= 0.344 sd = 0.47	m= 0.814 sd = 0.389	m= 0.893 sd = 0.309	m= 0.419 sd = 0.493	m= 0.35 sd = 0.477	m= 0.812 sd = 39

Table 2.9. Experiment 2: descriptive statistics for audiovisual integration accuracy range (0-1).

Predictors	*Odds Ratios*	*SE*	*CI*
intercept	13.30	3.21	8.28 – 21.34
flash presentation side (right vs left)	0.91	0.11	0.71 – 1.16
audiovisual integration stimulus types (1F2S vs 1F1S)	0.03	0.01	0.02 – 0.06
audiovisual integration stimulus types (2F1S vs 1F1S)	0.03	0.01	0.01 – 0.07
audiovisual integration stimulus types (2F2S vs 1F1S)	0.67	0.25	0.33 – 1.39
load level (low vs high)	1.63	0.25	1.21 – 2.18
Marginal R^2 = 0.328; *AIC* = 39269.293			

Table 2.10. Experiment 2: GLMM for audiovisual integration accuracy output.

Audiovisual integration d-prime

Descriptive statistics for audiovisual integration d' as a function of flash presentation side, audiovisual integration stimulus types and load types are summarized in Table 2.11. LMM for audiovisual integration d' is summarized in Table 2.12. Analysis of variance highlighted the expected

main effect of attentional load levels (F (1, 193.57) = 34.86, $p < .001$), with participants having higher illusion rates in case of high load compared to low load (high vs low: $\Delta\hat{\mu}$ = -0.231, SE: 0.041, t (194) = -5.619, $p < .001$). Also in this case the interaction between attentional load levels and flash presentation side was not significant (F (1, 870) = 1.908, p = 0.167) (see Figure 2.5). Moreover, the main effect of flash presentation side was not significant (F (1, 870) = 0.699, p = 0. 403). Resembling audiovisual integration accuracy results, the main effect of sound-induced flash illusion types was not significant (F (1, 78) = 0.383, p = 0. 537), meaning similar fission and fusion illusion rates.

		flash presentation side			
		left		*right*	
		audiovisual integration illusion types			
		fission	*fusion*	*fission*	*fusion*
load levels	*low load*	m= 1.07 sd = 0.868	m= 1.094 sd = 1.53	m= 0.980 sd = 0.901	m= 1.057 sd = 1.133
	high load	m= 0.795 sd = 0.713	m= 0.811 sd = 0.917	m= 0.797 sd = 0.755	m= 0.843 sd = 0.885

Table 2.11. Experiment 2: descriptive statistics for audiovisual integration d'.

Predictors	*Estimates*	*SE*	*CI*
intercept	0.65	0.11	0.44 – 0.86
flash presentation side (right vs left)	0.04	0.08	-0.12 – 0.20
audiovisual integration illusion (fusion vs fission)	0.15	0.13	-0.10 – 0.39
load level (low vs high)	0.21	0.09	0.03 – 0.39
flash presentation side (right) X load level (low)	-0.04	0.11	-0.27 – 0.18
Marginal R^2 = 0.032; *AIC* = 2545.206			

Table 2.12. Experiment 2: LMM for audiovisual integration d' output.

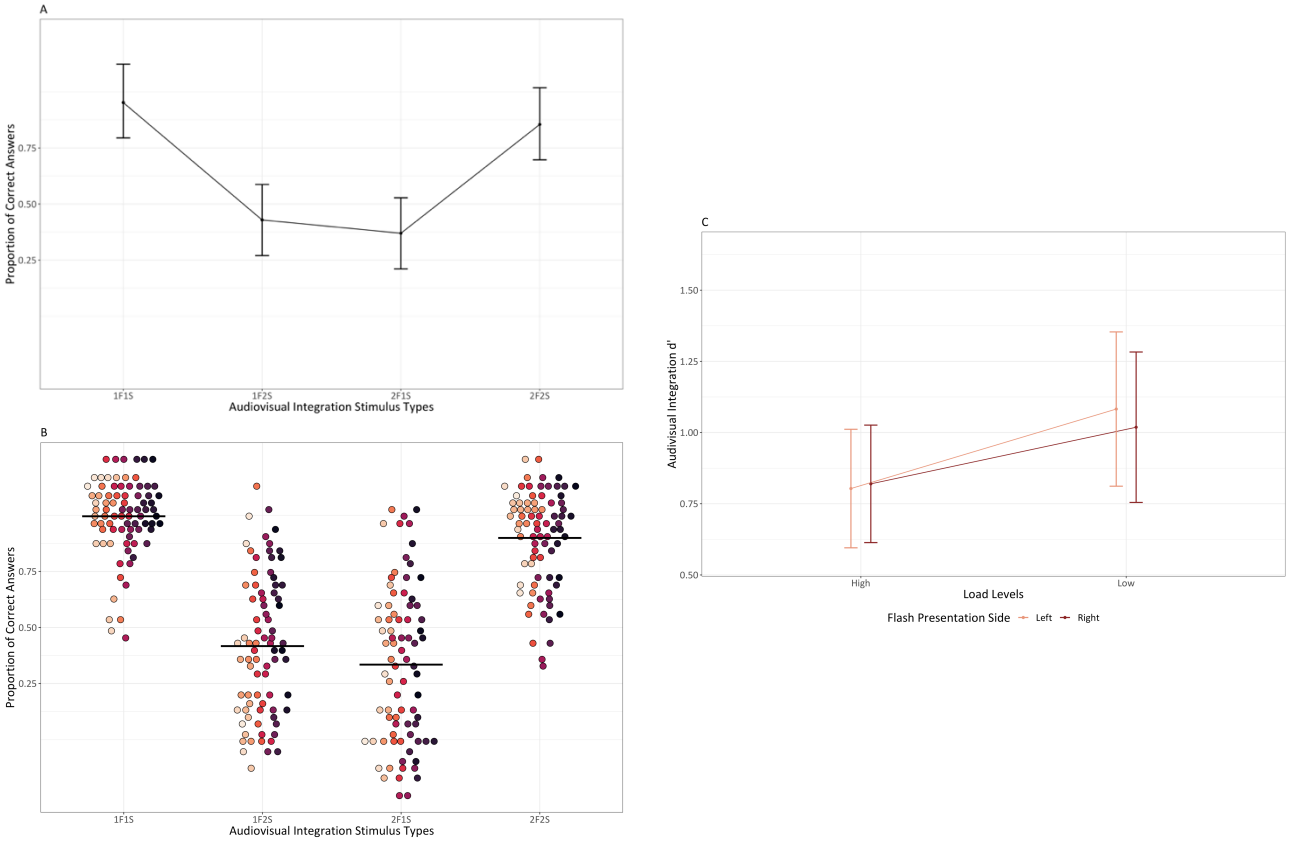

Figure 2.5. Experiment 2: Panel A *displays averaged proportion of correct answers (i.e., no illusion) for the different audiovisual integration stimulus types. Bars represent 95% confidence intervals, adjusted using the Tryon method as accuracy is a binomial variable. These adjustments were calculated over Anscombe-transformed scores using "superb"* (R Package: superb - v 0.9.7.6, Cousineau et al., 2021)*, and subsequently transformed back into proportions.* ***Panel B*** *displays individual proportion of correct answers (i.e., no illusion) for the different audiovisual integration stimulus types, with each dot corresponding to a different participant. The mean is indicated by a horizontal black line. All the proportions are depicted using a non-linear scale, specifically the "asn_trans()" scale for arcsine.* ***Panel C*** *displays cumulative d' for the different load levels and flash presentation side.*

In conclusion, in both experiments, secondary task accuracy was significantly lower under high attentional load compared to low attentional load. Crucially, in both experiments, H1 was confirmed: audiovisual integration accuracy was significantly lower and both fission and fusion illusions emerged in incongruent audiovisual integration stimuli, i.e. 1F2S stimuli and 2F1S stimuli, but not in congruent audiovisual integration stimuli, i.e. 1F1S stimuli and 2F2S stimuli. Moreover, in both experiments, also H2 was verified: the occurrence of SIFI significantly increased under high attentional load. However, H3 was not supported in either experiment: neither of the two different load manipulations revealed that emergence of SIFI under high load was asymmetric across space, being more evident for left-sided flashes.

2.6 Discussion

We conducted two experiments testing healthy adults with a computer-based dual-tasking approach to investigate whether attentional load levels can asymmetrically impact spatial processing in the unimpaired cognitive system during multitasking. In both experiments, we employed a primary audiovisual integration task, characterized by briefly presented stimuli inducing the SIFI on either the left or right side of the screen, along with concurrent secondary tasks that required additional processing. In Experiment 1, the secondary task was a verbal or spatial working memory, that allowed us to manipulate attentional load *offline*, meaning that the stimuli used to vary load were presented before the lateralized audiovisual integration stimuli. In Experiment 2, instead, the secondary task was a visual discrimination task, that enabled us to manipulate attentional load *online*, as the stimuli used to vary the load were presented simultaneously with the lateralized audiovisual integration stimuli. For both experiments, we had the following predictions: (H1) audiovisual integration accuracy would be significantly lower and SIFI would emerge in incongruent audiovisual integration stimuli, namely 1F2S stimuli and 2F1S stimuli, (H2) the emergence of SIFI would significantly increase under high attentional load, (H3) especially in case of left sided flashes.

As a first finding characterizing both experiments, secondary task accuracy was significantly lower when participants were under high attentional load. In Experiment 1, participants exhibited greater accuracy with verbal working memory stimuli compared to spatial working memory stimuli, yet the impact of load was consistently observed in both cases. Therefore, in both experiments it was possible to confirm the effectiveness of secondary tasks in inducing attentional load variations as expected.

In both experiments H1 was clearly confirmed: audiovisual integration accuracy was significantly lower and SIFI emerged in incongruent audiovisual integration stimuli, i.e. 1F2S stimuli and 2F1S stimuli. As expected, 1F2S stimuli successfully triggered the fission illusion: participants were presented with one flash, but due to the presence of two sounds, they were overwhelmed by the illusion and tended to split what was visually perceived, reporting that they had seen two flashes. Differently 2F1S stimuli induced the fusion illusion: in this case, participants were presented with two flashes, but due to the presence of a single sound, they were overwhelmed by the illusion and tended to merge what was visually perceived, reporting that they had seen a single flash. This result

indicates that we were able to successfully replicate SIFI, despite the inherent constraints and drawbacks typically associated with web-based data collections. Since the use of web-based data collections in experimental psychology has exploded in popularity, many effects observed inside the lab have been replicated also in larger samples online (Cipora et al., 2019; Del Popolo Cristaldi, Granziol, et al., 2022; Germine et al., 2012; Hilbig, 2016; Pronk et al., 2022; Schidelko et al., 2021; Semmelmann & Weigelt, 2017), including multisensory integration phenomena such as the ventriloquist aftereffect (Lavan et al., 2022) and the McGurk effect (Magnotti et al., 2018). Our finding contributes to this growing body of evidence, speaking in favour of the reliability of online settings in eliciting effects which are indistinguishable from those obtained in traditional laboratory settings. Additionally, this result indicates that the primary audiovisual integration task was very effective in eliciting to a similar, rather high, extent, not only the ubiquitous fission illusion but also the less commonly reported fusion illusion (for a complete review about differences in fission and fusion illusion rates see: Hirst et al., 2020).

In both experiments, also H2 was verified: the occurrence of SIFI significantly increased under high attentional load. Before delving into the potential explanations for this result, it seems important to highlight the complexity of the multifaceted and situation-dependent interplay between multisensory integration and attentional mechanisms, that leads to the experience of the environment around us (Macaluso et al., 2016; Talsma et al., 2010). Some studies support the idea that the binding of multisensory stimuli might be mediated by top-down attentional mechanisms, (e.g., Fairhall & Macaluso, 2009; Talsma et al., 2006; Talsma & Woldorff, 2005; Van der Stoep et al., 2015). Other studies suggest instead that the binding of multisensory stimuli takes place in an early, automatic, pre-attentive stage thanks to bottom-up information (e.g.: Bertelson et al., 2000; Vroomen et al., 2001). More likely multisensory integration is shaped by a combination of the two, together with several other factors (Choi et al., 2018; Macaluso et al., 2016; Talsma et al., 2010). Within this context, studies that applied dual-tasks to directly investigate how multisensory integration is influenced by attentional load levels yielded different findings. For example, when attentional load was increased during the spatial integration of visuo-tactile stimuli or during the integration of visual cues with emotional valence in songs, there has been no significant modulation of multisensory perception (W. F. Thompson et al., 2008; Zimmer & Macaluso, 2007). Conversely, when attentional load was increased during the processing of audiovisual speech stimuli, illusory multisensory perception was diminished (Alsius et al., 2005, 2007). To round out this picture, and in line with our finding, Michail and colleagues (Michail & Keil, 2018) discovered that when attentional

load was increased during the processing of nonspeech audiovisual stimuli generating SIFI, illusory perception was actually increased (Michail et al., 2021; Michail & Keil, 2018). There are multiple, equally compelling alternative explanations for this finding. While it may be challenging to definitively choose among them, they all offer informative and complementary insights into the mechanisms that contribute to the phenomenon. Firstly, according to Michail and colleagues (Michail & Keil, 2018), one possible explanation for the increased SIFI rates under high attentional load could be related to the concept of the temporal window of integration (TWI), which refers to the maximum temporal asynchrony between two different sensory events that allows their perceptual binding into a singular percept (van Wassenhove et al., 2007). The TWI is known to vary among individuals, and these individual differences can predict susceptibility to SIFI: individuals with narrower TWI can differentiate between audiovisual stimuli that are asynchronous but closely timed and thus are less prone to experience SIFI (Stevenson et al., 2012). As TWI is also influenced by task-specific demands (Mégevand et al., 2013) increased attentional load may have caused its widening, ultimately resulting in enhanced binding of the audiovisual stimuli and increased SIFI rates (Michail & Keil, 2018). Alternatively, according to Michail and colleagues (Michail & Keil, 2018), the increased SIFI rates under high attentional load might be explained according to the “attentional load theory” (Lavie, 2005, 2010). This theory posits that when perception is deeply taxed, distractor processing may be reduced, whereas when high-level cognitive functions are heavily engaged, the processing of task-irrelevant information may be facilitated (Lavie, 2005, 2010). In both Michail and colleagues' design and our own, auditory stimuli were less critical than visual ones, as participants were instructed to report the number of flashes. Consequently, it's possible that, due to high attentional load, auditory stimuli gained a larger sensory influence, potentially resulting in increased SIFI rates (Michail & Keil, 2018). In our view, another explanation for the increased SIFI rates under high attentional load could be linked to a reduced ability to inhibit automatic and task-irrelevant responses. This idea draws insights from research on ageing, where it has been found that older adults frequently display a reduced ability to filter out task-irrelevant responses (Gazzaley et al., 2005; Salthouse & Meinz, 1995), as well as an increased susceptibility to SIFI, that is only in part due to age-related changes in unisensory abilities (Hirst et al., 2019). Notably, the performance in tasks assessing inhibitory control has been found to predict the one in tasks requiring the processing of audiovisual speech stimuli in older but not in younger adults (Dey & Sommers, 2015). Additionally, recent studies proposed that a deficit in inhibitory control may be the mechanism at the base of impairments across both postural stability and the processing of nonspeech audiovisual stimuli

generating SIFI in older adults (O'Dowd et al., 2023; Scurry et al., 2021). Given evidence suggesting that inhibitory control might be reduced when high-level cognitive functions are heavily engaged (Hester & Garavan, 2005; Tiego et al., 2018), it is possible to speculate that the increase in attentional load in our tasks may have mirrored what happen with ageing: a decrease in inhibitory control abilities and, consequently, an increase in SIFI rates. In conclusion, this result indicates that SIFI can be influenced by different levels of attentional load and it challenges the notion of an early, completely automatic and pre-attentive onset of the illusion. Rather, it seems that the emergence of SIFI involves, at some point, the use of domain-general, limited and depletable resources that are taxed by increased attentional load. Therefore, also in this case, similarly to what was concluded for the single-case study detailed in Chapter 1, it is plausible to speculate that different tasks are characterized by the common use of relatively unspecific attentional resources, irrespective of the specific demands of each task. When the attentional load increases, this general yet limited pool of resources is depleted, potentially affecting the perception of audiovisual stimuli, leading to the observed modulation of the SIFI effect. While this explanation may appear simplistic at first glance, it aligns well with the similar effects observed under two very distinct load manipulations: in Experiment 1, participants were tasked with retaining either short or long sequences of verbal or spatial working memory stimuli, while in Experiment 2, they were engaged in the processing of visual discrimination stimuli, subject to both simple and complex instructions.

Finally, H3 was not supported in either experiment, as the emergence of SIFI under high attentional load did not display spatial asymmetry, contrary to the expected increase in SIFI rates for left-sided flashes.

This result is in line with what reported in the studies by Lisi and colleagues (Lisi et al., 2015) and by Dodds and colleagues (Dodds et al., 2008) indicating the absence of load-induced spatial processing asymmetries in healthy participants. The robustness of this null result is further strengthened by its consistent replication across very different load manipulations. This null result cannot be attributed to a floor effect, as the load modulation was clearly present yet manifested itself symmetrically. A more plausible explanation for the lack of lateralization may lie in the absence of an explicit spatial component in the design of the tasks. This idea finds support in previous research that has examined the impact of spatial versus non-spatial task instructions (Cocchini et al., 1999; Vuilleumier & Rafal, 1999). For example, Vuilleumier and Rafal (Vuilleumier & Rafal, 1999), demonstrated that patients with right hemisphere lesions were able to perceive contralesional stimuli when their task involved enumeration, yet they failed to detect the same stimuli when tasked with locating them. Similarly,

Cocchini and colleagues (Cocchini et al., 1999), observed that a patient with right hemisphere lesions exhibited extinction symptoms only when required to perform spatial analysis of the stimuli, rather than when simply detecting them (Cocchini et al., 1999). However, Peers and colleagues (Peers et al., 2006) reported results that challenge this view, not finding a significant difference between dual tasks in which the secondary task involved either spatial or non-spatial instructions in patient and also healthy adult groups. This null result apparently contradicts the findings reported in the study conducted by Eramudugolla and colleagues (Eramudugolla et al., 2011), where they did indeed report load-induced spatial processing asymmetries in the context of processing audiovisual stimuli in healthy participants. However, it is challenging to speculate on the reasons for the difference in results between the two studies. This difficulty arises because, despite both studies employed audiovisual stimuli, the audiovisual illusions generated were inherently different: in the study by Eramudugolla and colleagues the stimuli used produced the ventriloquist aftereffect, in which the visual modality guides perception, while in our study, the stimuli generated the SIFI, in which is the auditory modality to determine what is perceived. Crucially, this finding suggests that the unimpaired cognitive systems and the damaged cognitive systems are not only quantitatively but also qualitatively distinct. Consequently, assessing spatial processing in brain-damaged patients under high attentional load does not exacerbate asymmetries existing in the unimpaired cognitive systems. Instead, it uncovers very subtle (yet potentially hazardous) deficits which are almost exclusively contralesional. In conclusion, in our opinion, the experimental situation of ambiguity characterizing illusions could be an ideal context for facilitating the emergence of subtle asymmetries in spatial processing, which might not be equally prominent under regular perceptual conditions. At the same time, however, it has been suggested that stimuli encompassing audiovisual characteristics are particularly salient (Pluta et al., 2011) and, as such the manipulation we implemented might be not the most sensitive one for exacerbating spatial processing asymmetries. In either case it seems appropriate not to overgeneralize and conclude that while with our manipulations load-induced spatial processing asymmetries were clearly absent, stimuli of a different nature might possibly unveil their existence.

Additionally, there is the possibility that load-induced spatial processing asymmetries, although not apparent in behavioural responses, could be discerned considering other types of informative markers, such as neural responses.

2.7 Supplementary

Model selection for block variable

For each model, a model selection was undertaken to decide how to handle a variable which coded for the block number, independently from the experimental condition characterizing the block.
In all cases we compared Akaike's Information Criterion (AIC) and the Bayesian Information Criterion (BIC) of a model “b0” without the block variable, a model “b” with the block variable coded as fixed effect, a model “b1” with the block variable coded as random intercept and a model “b2” with the block variable coded as random slope nested within participants. In Experiment 1, the “b2” model resulted significatively different from other models for the GLMM analysing secondary task accuracy and the GLMM assessing audiovisual integration accuracy (in all cases $p < .001$), exhibiting the lowest AIC and BIC values. However, when considering the LMM examining audiovisual integration d', none of the models resulted significatively different from the others ($p = 0.097$). Yet, the “b2” models showed the lowest AIC and BIC values In Experiment 2, the “b2” model resulted significatively different from other models for the GLMM analysing secondary task accuracy, the GLMM assessing audiovisual integration accuracy and also the LMM examining audiovisual integration d' (in all cases $p < .001$), exhibiting the lowest AIC and BIC values. Following these results in all cases the block variable was coded as random slope nested within participants. This modelling choice captured the idea that time on task might have different effects at the individual level. Following this modelling choice any possible effect of increased attentional load should not be influenced by the confounding effect of reduced sustained attention over time on task.

Effect of hand-used to respond

In both experiments, in the model with audiovisual integration accuracy and also in the model with audiovisual integration d' as dependent variable, we evaluated the following: 1) presence of a main effect of hand-used to respond, to assess whether there was a facilitation in responding with the dominant hand compared to the non-dominant hand 2) presence of an interaction between hand-used to respond and flash presentation side, to determine whether there was a stimulus-response compatibility effect, i.e. a facilitation in responding to stimuli presented on the right side with the dominant hand (which was consistently the right hand, as all participants were right-handed) and

facilitation in responding to left-sided stimuli with the non-dominant hand (which was consistently the left hand, as all participants were right-handed). In Experiment 1, in the model with audiovisual integration accuracy as dependent variable, analysis of deviance highlighted no effect of hand-used to respond (X^2 (1) = 0.886, p = 0.346) as well as no interaction between hand-used to respond and flash presentation side (X^2 (1) = 1.693, p = 0.193). In Experiment 1, in the model with audiovisual integration d' as dependent variable, analysis of deviance highlighted no effect of hand-used to respond (F (1, 85.21) = 0.017, p = 0. 218) as well as no interaction between hand-used to respond and flash presentation side (F (1, 2175.19) = 0.38, p = 0. 537). In Experiment 2, in the model with audiovisual integration accuracy as dependent variable, analysis of deviance highlighted no effect of hand-used to respond (X^2 (1) = 0.076, p = 0.782) as well as no interaction between hand-used to respond and flash presentation side (X^2 (1) = 1.899, p = 0.168). Experiment 2, in the model with audiovisual integration d' as dependent variable, analysis of deviance highlighted no effect of hand-used to respond (F (1, 77.73) = 0.659, p = 0. 419) as well as no interaction between hand-used to respond and flash presentation side (F (1, 870) = 0.041, p = 0.84).

CHAPTER 3

IMPACT OF ATTENTIONAL LOAD UPON SPATIAL PROCESSING AND MULTISENSORY INTEGRATION: A HIGH-DENSITY EEG INVESTIGATION OF RESTING-STATE AND IN-TASK BRAIN ACTIVITY

3.1 Overview of the chapter

After having examined how spatial processing in the unimpaired cognitive system is influenced by different levels of attentional load during multitasking, as indicated by task performance, we now shift our focus to the neural correlates of these effects. We conducted an experiment using a computer-based dual-task identical to that described in Experiment 2 of Chapter 2 (i.e. involving audiovisual integration stimuli eliciting the sound-induced flash illusion), while recording high-density electroencephalography (EEG) activity during resting-state and simultaneously with the task, to investigate electrophysiological predictors and correlates of task performance. Firstly, we investigated whether "behavioural indexes", particularly task performance with incongruent audiovisual integration stimuli and performance under low or high attentional load, could be predicted using "brain indexes". These brain indexes were average functional connectivity values within specific networks, extracted from EEG recordings during resting-state. Although functional connectivity is typically derived from functional Magnetic Resonance Imaging rather than EEG recordings, we were able to conduct such analysis, using an innovative approach by Liu et al. (2017). Subsequently, we investigated Event-Related Potentials (ERPs) during in-task EEG recordings. Specifically, our focus was on identifying ERP modulations linked to the enhanced perception of sound-induced flash illusions under high attentional load. Additionally, we examined whether these potential ERP modulations differed following left-sided or right-sided flashes. This was aimed at determining whether load-induced spatial processing asymmetries, although not apparent in behavioural responses, could be discerned through ERP responses.

We have uncovered noteworthy correlations between behavioural indexes and functional connectivity, predominantly within networks pertinent to auditory and visual processing, along with the allocation of attentional resources in space. Moreover, we have identified N1, N2, and P3 modulations associated with the presentation of stimuli eliciting the sound-induced flash illusion during different levels of attentional load, with N1 modulations differing depending on the side of the flashes.

3.2 Introduction

Long-range interactions as neural underpinning of spatial processing and multisensory integration

We know considerable information about core brain regions involved in the attention mechanisms that drive spatial processing. These regions extend beyond the early visual areas activated during the processing of relevant stimuli in a specific location in space to encompass parietal, temporal, and frontal regions (for a review see: Somers & Sheremata, 2013). Similarly, we have extensive knowledge about the core brain regions involved in audiovisual integration and specifically in sound-induced flash illusion (SIFI). Also in this context, the implicated regions are not confined to the early visual areas responsible for flashes perception, but also involve other sensory cortices, along with temporal and frontal regions (for a review see: Hirst et al., 2020; Keil, 2020).

In addition to that, it is well known that brain functionality is enhanced by long-range interactions among distant regions. These interactions complement the brain's distributed anatomical and functional organization, allowing for the emergence of coherent behaviour and cognition (Varela et al., 2001). Consequently, a more comprehensive understanding of spatial processing and SIFI may be provided only considering, in addition to core brain regions, their network-level interactions. In this regard, it has been proposed the existence of two broad networks responsible for the allocation of attentional resources in space (Corbetta et al., 2008; Corbetta & Shulman, 2002). The first network is the dorsal attention network (DAN), which facilitates the endogenous, top-down allocation of attention in space, enabling the selective processing of stimuli based on internal goals or expectations. Key nodes of this network comprise the dorsal parietal cortex, particularly the intraparietal sulcus and superior parietal lobule, as well as the dorsal frontal cortex, located near or in the frontal eye fields. The second network is the ventral attention network (VAN), which aids in the exogenous, bottom-up allocation of attention in space, enabling the selective processing of stimuli based on their saliency. Important nodes of this network, which is characterised by a right hemispheric dominance, include the temporoparietal junction, the inferior frontal gyrus, the anterior insula, and the frontal operculum (Corbetta et al., 2008; Corbetta & Shulman, 2002). Recent evidence indicates that the distinction between DAN and VAN does not however align neatly with the initially proposed simple dichotomy of top-down versus bottom-up allocation of attention in space (Tosoni et al., 2023). The DAN is active not only when attention is deliberately oriented toward a stimulus location based on endogenous cues, but also with exogenous cues, suggesting a broader

role in the attention mechanisms that drive spatial processing. On the other hand, the VAN is deactivated during prolonged attention orientation toward a specific location (Anticevic et al., 2010). Still, the VAN is transiently activated, along with the DAN, during shifts of attention and during the detection of salient targets (Tosoni et al., 2023). This evidence implies that neither the DAN nor the VAN controls attention mechanisms in isolation. Instead, the flexible interaction between both systems enables the dynamic control of attention mechanisms in relation to top-down goals and bottom-up stimulation (Vossel et al., 2014). Despite long-range interactions related to SIFI have been studied less systematically compared to the one responsible for the allocation of attention in space, there is evidence suggesting the existence of a widespread network responsible for illusory perception. For example, Keil et al. (2014), found that increased beta band phase synchrony between the left middle temporal gyrus and auditory areas as well as decreased phase synchrony with visual areas, prior to flash onset, predict illusory perception (Keil et al., 2014). In this context, it's important to note that long-range interactions also appear to be crucial for dividing attention between different tasks. For instance, performance impairments observed during dual-tasking have been linked to disruptions in the integrity of the anatomical connections within an extensive network considered responsible for cognitive control (Jiang et al., 2023) and known as the "multiple demand" network (Camilleri et al., 2018). Key nodes of this network comprise: subcortical areas mainly related to sensorimotor processing, pre-supplementary motor area and adjacent middle cingulate cortex, bilateral anterior insula, right middle frontal gyrus extending into the inferior frontal sulcus and a more heterogeneous set of areas recruited based on task demands (Camilleri et al., 2018). Long-range interactions among distant regions can be investigated measuring functional connectivity, which consists in patterns of statistical correlations between signals from two or more spatially separated regions. This idea hinges on the assumption that highly correlated response patterns in two segregated regions indicate that they work together, i.e. they form a network (Friston, 2011). Functional connectivity may be investigated during resting-state activity (i.e. intrinsic functional connectivity). This type of activity is known to be energetically costly and characterized by the activation of specific brain circuits, that are then de-activated during the performance of sensory- or cognitive-demanding tasks. It allows the brain to correctly allocate resources and thus to be ready for internal or external environment changes (van den Heuvel & Hulshoff Pol, 2010). Thus, investigating intrinsic functional connectivity, rather than functional connectivity for example during a specific spatial processing task, might reveal relevant brain features, impacting on multiple different spatial processing tasks.

Intrinsic functional connectivity is known to form several large-scale networks, commonly referred to as resting-state networks (RSNs) (Damoiseaux et al., 2006; Fox & Raichle, 2007), that are usually identified using functional Magnetic Resonance Imaging (fMRI) (Smitha et al., 2017). Nevertheless, there is growing evidence that alternative methods, such as electroencephalography (EEG), can also be effectively employed. EEG offers several advantages over fMRI: it provides high temporal resolution, directly measures postsynaptic neuronal activity, and is more feasible for large-scale studies due to its greater availability and lower invasiveness. While EEG's spatial resolution is undefined in respect to that of fMRI, this limitation becomes less significant in the case of high-density EEG. Indeed, high-density EEG utilizes a large number of electrodes densely distributed across the scalp, allowing for a finer spatial sampling of brain activity (Hedrich et al., 2017). Moreover, functional connectivity from EEG signals can be calculated, not only at the scalp level, but also at the source level (i.e., reconstructing the source space), further mitigating the issue of lower spatial resolution (Lai et al., 2018). This approach has indeed already been successfully validated in studies that used EEG recordings in conjunction with other types of neuroimaging recordings and obtained overlapping results (Mulert et al., 2004). Thus, it has already been exploited in different fields for investigating intrinsic brain organization questions (e.g., Caliandro et al., 2017; Canuet et al., 2011; Hata et al., 2016; Olbrich et al., 2014). Additionally, there is growing evidence that functional connectivity properties of EEG-RSNs can also be used to predict behavioural outcomes (e.g.: Coccaro et al., 2023; Duma et al., 2021; Romeo et al., 2021), as well as, in-task Event-Related Potentials (ERPs) (e.g., Del Popolo Cristaldi et al., 2022; Li et al., 2015; Ma et al., 2023).

Event-Related Potentials associated with spatial processing and multisensory integration

There is a vast body of electrophysiological research exploring ERPs associated with the attention mechanisms that drive spatial processing (for a review see: Somers & Sheremata, 2013). Among these studies, some have also investigated ERP responses indexing load-induced spatial processing asymmetries. However, the findings are nuanced and at times conflicting. This is true especially for want concerns early ERP components that are strongly influenced by the specific characteristics of the manipulation performed. For example, Rauss and colleagues (Rauss et al., 2009, 2012), asked participants to perform a rapid serial visual presentation task, in which they had to perform an easy pop-out detection or a complex conjunction discrimination of centrally presented stimuli. At the same time arrays of distractors were flashed in the periphery. Results showed that distractors

processing was associated to increased C1 amplitude (i.e., the earliest component of the visual evoked potential) with increasing attentional load (Rauss et al., 2009, 2012). Differently, distractors processing was associated to decreased P1 amplitude with increasing attentional load (Handy et al., 2001). However, other studies reported no attentional load modulations on C1 component and/or P1 component (Fu et al., 2008, 2010; Rorden et al., 2008). In addition, attentional load can produce opposite effects depending on whether stimuli are task-relevant or task-irrelevant. For example, Rorden and colleagues (Rorden et al., 2008) asked participants to perform a peripheral gap judgment task, that could be perceptually easy or difficult, while distractor stimuli were centrally presented. Results showed that processing of task-relevant stimuli of the gap judgment task was associated to increased N1 amplitude with increasing attentional load, while processing of task-irrelevant distractors was associated to reduced N1 amplitude with increasing attentional load (Rorden et al., 2008), as predicted by Lavie's load theory (Lavie, 2005, 2010). Similar to our own dual-task approach, O'Connell and colleagues (O'Connell et al., 2011) utilized a dual-task in which the stimuli of both the primary and secondary tasks were task-relevant. They asked participants to perform a visual detection task of left or right lateralized targets. At the same time, they had to respond to an easy or difficult monitoring task, in which they had to detect certain centrally presented stimuli. Results showed that processing of central stimuli was associated to increased P1 and N1 amplitude with increasing attentional load. The processing of peripheral stimuli was associated instead to reduced P2 and P3 amplitude with increasing attentional load. Additionally, it was reported an asymmetric effect induced by the processing of peripheral stimuli on N1 amplitude. More specifically, the typical increased N1 amplitude consequent to the processing of contralateral stimuli (Hopfinger & West, 2006) was reduced with increasing attentional load over occipital and inferior parietal regions of the right hemisphere. The equivalent effect was not seen over left hemisphere (O'Connell et al., 2011). This effect accords well with the studies, described in Chapter 2, which have shown subtle load-induced spatial processing asymmetries, specifically rightward attentional biases, in the behavioural performance of healthy adults during dual-tasking (Naert et al., 2018; Peers et al., 2006; Pérez et al., 2008, 2009). Crucially, this effect was not accompanied by an equivalent behavioural trend, indicating that it is possible to detect load-induced spatial processing asymmetries exclusively through ERP responses (O'Connell et al., 2011). The logic of utilizing a dual-task in which the stimuli of both the primary and secondary tasks were task-relevant was employed also by Bonato and colleagues (Bonato et al., 2015). They asked participants to perform a visual detection task of lateralized (left, right, or bilateral) targets. At the same time, in

the dual-task but not in the single-task condition, participants had to categorize visual or auditory stimuli (see Chapter 1 for further details as this task is similar to the one used with patients in Bonato et al., 2010). Results showed that processing of left peripheral stimuli was associated to decreased posterior P1 and N2 amplitude in the left hemisphere and increased posterior P1 and N2 amplitude in the right hemisphere, while the processing of right peripheral stimuli was associated to similar posterior P1 and N2 amplitudes in both hemispheres. This finding aligns well with Kinsbourne's model of attention mechanisms that drive spatial processing, according to which left sided stimuli are processed mainly by right lateralized processes, while right sided stimuli are processed by both left and right lateralized processes (Kinsbourne, 1987). Additionally, posterior P1 amplitude increased with increasing attentional (visual) load. Crucially, it was also found an interaction between peripheral stimuli position and attentional load condition: the processing of left peripheral stimuli elicited larger posterior N2 amplitude than right peripheral stimuli, but only with increasing attentional (visual) load. Romeo and colleagues (Romeo et al., 2019) employed a similar task and extended the previous findings also to the N1 component: N1 amplitude increased with increasing attentional (visual) load (Romeo et al., 2019).

Electrophysiological research investigating ERPs associated with audiovisual integration and specifically with sound-induced flash illusion confirmed that the illusion is generated by a complex interaction between auditory, visual, and polymodal cortical areas. More specifically, the fission illusion perception (usually generated with 1F2S stimuli, see Chapter 2 for further details) is linked to an early positive ERP component in the visual cortex, which appears 30-60 ms after the second sound onset and to an early negative ERP component in the auditory cortex, emerging even sooner, 20-40 ms after the second sound onset (Mishra et al., 2007). Differently fusion illusion perception (usually generated with 2F1S stimuli, see Chapter 2 for further details) is associated to a slightly later positive ERP component in the superior temporal area, which appears 80–112 ms after the second flash onset (Mishra et al., 2008). Therefore, the illusion types appear to be associated with very distinct spatio-temporal activation patterns (Mishra et al., 2007, 2008). To our knowledge there are no studies focusing on how these ERP components might be modulated with variations of attentional load.

3.3 Aim and hypothesis

In the present study, we examined neural correlates of how spatial processing is influenced by different levels of attentional load during multitasking in the unimpaired cognitive system. To do that we conducted an experiment using a computer-based dual-task identical to that described in Experiment 2 of Chapter 2, while recording high-density EEG activity during resting-state and simultaneously with the task.

Firstly, we analysed dual-task performance. The dual-task included a primary audiovisual integration task that involved presenting stimuli capable of eliciting the SIFI on either the left or right side of the screen. This task not only allowed to investigate audiovisual integration but also indirectly provided an opportunity to investigate spatial processing within a highly complex context. This primary task was combined with a concurrent secondary visual discrimination task that allowed us to manipulate attentional load *online* (i.e., the stimuli used to vary load were presented *simultaneously* with the lateralized audiovisual integration stimuli). This dual-task was selected for the present investigation because it is characterized by the absence of perceptual differences between high and low attentional load conditions. Instead, the variations are exclusively in the instructions, making it suitable for an EEG study and particularly appropriate for ERPs analysis (The Hillyard Principle, see Luck (2014)). Similarly to Experiment 2 of Chapter 2, we expected (H1.1) SIFI to emerge with incongruent stimuli as the result of failed audiovisual integration. Additionally, we expected (H1.2) the emergence of SIFI to be especially pronounced under high attentional load. Finally, we expected (H1.3) the emergence of SIFI to be especially evident for left-sided stimuli compared to right-sided stimuli (i.e., rightward attentional bias). This expectation was based on the premise that if the absence of load-induced spatial processing asymmetries observed in the two experiments of Chapter 2 was due to increased experimental noise related to the online setting, it would manifest differently in the lab setting.

Secondly, we conducted an analysis of EEG recorded during a resting-state period preceding the task. More specifically, we calculated intrinsic functional connectivity building on the state-of-the-art approach of Liu et al. (2017) and thus we extracted EEG-RSNs (see also: Liu et al., 2018; Marino et al., 2019; Samogin et al., 2019, 2020). This approach employs a semi-automatic data cleaning procedure coupled with an automatic analysis pipeline, comprising three steps: “standard head

model creation", "reconstruction of sources" and "ICA-based functional connectivity calculation". Independent Component Analysis (ICA), a technique aimed at dividing data into maximally independent groups, forms a key part of this approach as allows a completely data-driven calculation of functional connectivity. We applied ICA in both its spatial (sICA) and temporal (tICA) variants, where sICA achieves maximum spatial independence and tICA guarantees temporal independence (Calhoun et al., 2001, 2009; Smith et al., 2012). After that, we conducted a correlation analysis, to understand whether "behavioural indexes" could be predicted from "brain indexes". The behavioural indexes considered were the ones emerged as informative from the behavioural analysis: audiovisual integration accuracy across all incongruent 1F2S stimuli, audiovisual integration accuracy across all incongruent 2F1S stimuli, audiovisual integration d-prime across all cases of low attentional load and audiovisual integration d-prime across all cases of high attentional load. These behavioural indexes were correlated with brain indexes, that were mean functional connectivity values of specific EEG-RSNs and of specific Regions Of Interest (ROIs) part of those networks. The EEG-RSNs ROIs were chosen because believed to be potentially involved in SIFI perception under conditions of increased attentional load on the base of the literature (see analysis section for further details about EEG-RSNs and ROIs selection).

We expected (H2) significant correlations to emerge at both the network and region of interest levels. However, given the exploratory nature of our analysis, we did not have specific expectations regarding the exact nature or direction of these correlations. To our knowledge, this is indeed the first study that investigated an association between behavioural indexes derived from a task involving SIFI and brain indices obtained from EEG recordings during a resting-state period.

Thirdly, we conducted an analysis of EEG recorded during dual-task. More specifically, in line with previous studies (Bonato et al., 2015; O'Connell et al., 2011; Romeo et al., 2019) and with the grand average visual inspection, we extracted the following early ERP components: P1 (80-150 ms), N1 (90-140 ms), N2 (140-180 ms), P2 (150-230 ms) and P3 (300-450 ms). Additionally, we calculated a *cost waveform* considering the signal in the high load condition and subtracting the signal in the low load condition (high load – low load) (similar to: Bonato et al., 2015 - cost analysis).

We expected (H3.1) to identify ERP modulations linked to the enhanced perception of SIFI under high attentional load. Additionally, (H3.2) to confirm that spatial processing can be asymmetrically influenced by levels of attentional load during multitasking at the neural level, these potential ERP modulations should differ following left-sided stimuli or right-sided stimuli.

3.4 Methods

Participants and Experimental Protocol

Participants were recruited by word of mouth among the acquaintances of the research laboratory members, were unaware of the aims and hypothesis of the experiments and received no compensation. The inclusion criteria were as follows: age between 18 and 40 years, right-handedness as measured by Edinburgh Handedness Inventory (Oldfield, 1971), no prior participation in the two experiments of Chapter 2, absence of neurological or psychiatric disorders, absence of severe dermatological conditions that would hinder the possibility of applying an electrolytic solution to the scalp to enhance electrodes conductivity, absence of severe vision impairments, severe hearing impairments or any other severe medical condition that would prevent from carrying out tasks on the computer and no substance abuse.

A total of 57 volunteers completed the experiment (mean age: 22.72, age range: 18-31; m: 26). To prevent potential confounding effects related to the hand-used to respond, 28 participants responded to lateralized stimuli with their dominant hand, while the remaining participants used their non-dominant hand.

Before starting the experimental session, participants were asked to sign the informed consent form and complete a set of questions to gather demographic information. Immediately after, they had to fill out three questionnaires to explore emotional aspects, namely the Positive and Negative Affect Schedule (PANAS, Watson et al., 1988), the Beck's Anxiety Inventory (BAI, Beck & Steer, 1993) and the Beck's Depression Inventory (BDI-II, Beck et al., 1996) (not analysed here). Resting-state activity was then recorded using EEG for a period of six minutes. EEG recording continued during the dual-task. Additionally, a second resting-state activity period was recorded after the task (not analysed here). At the end of the experimental session, participants were asked to complete a Likert-scale questionnaire pertaining to their awareness of the illusion (not analysed here). The experimental protocol was approved by the Ethics Committee for Psychological research of the University of Padua (protocol n. 4884) and was conducted according to the principles expressed in the Declaration of Helsinki.

Dual-Task

The dual-task was the same as that in Experiment 2 of Chapter 2. For the sake of clarity, it is described again below. The attentional load manipulation was implemented combining the primary audiovisual integration task with a concurrent secondary visual discrimination task. Participants were required to complete *macro-trials,* which consisted in a combination of the two types of trials. More specifically, these macro-trials were formed by an audiovisual integration trial and a visual discrimination trial integrated together, with all the stimuli displayed simultaneously. After each macro-trial, participants were required to answer firstly to audiovisual integration stimuli and then to visual discrimination stimuli (see Figure 3.1).

Audiovisual integration task. During each audiovisual integration trial, participants firstly were presented with a black fixation cross measuring 0.5° and lasting for 500 ms. This was followed by lateralized flashes and binaural sounds. The lateralized flashes consisted in white discs with diameter measuring 4° and lasting for 16.66 ms (i.e., a refresh rate cycle in the 60 Hz monitor we used). According to the condition, either one flash (1F) or two flashes (2F) were presented on the left or on the right side of the screen with an eccentricity of 8° with a time lag between the first and second flash lasting for 50 ms in case of a double presentation. The binaural sounds consisted in hamming windowed sine waveform tones at the frequency of 3.5 kHz and with a duration of 7 ms. According to the condition, either one sound (1S) or two sounds (2S) were presented, in conjunction with the first flash or in conjunction with both the first and the second flash (see Figure 3.2). Thus, four different audiovisual integration stimulus types were presented with flashes appearing on the left or on the right side of the screen: 1F1S-left (one flash on the left + one sound), 2F2S-left, 1F2S-left, 2F1S-left, 1F1S-right, 2F2S-right, 1F2S-right and 2F1S-right. During each audiovisual integration trial, participants were required to focus their attention on the flashes only, while ignoring sounds. They were asked to report the number of perceived flashes, by pressing the space bar once for one flash and twice for two flashes with the index finger (of the dominant or non-dominant hand, depending on the counterbalancing).

Visual discrimination task. While participants were presented with lateralized flashes and binaural sounds, they were also presented with a central symbol consisting in a blue or red spade or flower shape. These symbols were written with an Arial font of 18 pixels and lasted for 50 ms. The size and

duration of the stimuli were all adjusted based on preliminary data previously collected in pilot studies. During each visual discrimination trial, participants were required to focus their attention either on the colour of the central symbol (i.e., blue vs red), which is an easier task (low attentional load), or on the shape of the central symbol (i.e., spade vs flower), which is a more difficult and resource consuming task (high attentional load). They were asked to report the colour or the shape, by pressing either the “t” or “y” key with any finger of the hand not used during the audiovisual integration task. Thus, exclusively manipulating the instructions (i.e., without any perceptual difference between trials), two attentional load levels were presented: low load and high load.

Dual-task procedure. The dual-task consisted of 4 blocks, formed by 160 macro-trials. Each macro-trial was composed by 1 audiovisual integration trial and by 1 visual discrimination trial, organized as follows: participants firstly were presented with a black fixation cross measuring 0.5° and lasting for 500 ms, followed by audiovisual integration stimuli (i.e., lateralized flashes and binaural sounds) together with visual discrimination stimuli (i.e., central symbol). After the stimuli presentation, participants were required to answer firstly to audiovisual integration stimuli and then to visual discrimination stimuli. As soon as participants provided both their responses, the next macro-trial started. In total, there were 320 trials for each of the two visual discrimination conditions (i.e., low load and high load), presented in random ordered alternated block by block. As for the audiovisual integration trials, there were 80 trials for each of the eight audiovisual integration conditions (i.e., 1F1S-left, 2F2S-left, 1F2S-left, 2F1S-left, 1F1S-right, 2F2S-right, 1F2S-right and 2F1S-right), presented in random order. Before the testing phase it was conducted a practice session that comprised 64 macro-trials, evenly divided with 32 under the low load condition and 32 under the high load condition. All stimuli were presented on a grey background. All responses were collected without time constraints. Instructions were repeated at the start of each block, emphasizing the importance of accuracy over speed. It was also clarified that both tasks were important and that higher scores would only be achieved by correctly answering the visual discrimination task. This was to ensure that participants didn't focus solely on audiovisual integration trials without any attentional load. Participants were allowed to take breaks at the end of each block.

During the entire dual-task procedure, participants were sitting comfortably in a shielded and soundproofed semi-dark room. They were positioned at a viewing distance of 57 cm from a 24-inch monitor with a resolution of 1920x1080 and a refresh rate of 60Hz. The dual-task was programmed using E-Prime Software (v 2.0.8.90; Psychology Software Tools, 2012).

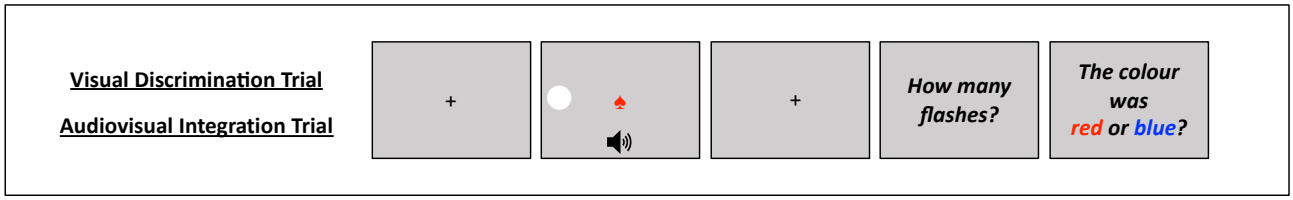

Figure 3.1. Dual-task. *Participants were required to complete macro-trials, which consisted in a combination of the two types of trials. More specifically, these macro-trials were formed by an audiovisual integration trial and a visual discrimination trial integrated together, with all the stimuli displayed simultaneously. After each macro-trial, participants were required to answer firstly to audiovisual integration stimuli and then to visual discrimination stimuli. The figure shows a macro-trial encompassing an audiovisual integration trial from the 1F1S-Left (i.e., one flash on the left + one sound) condition and a visual discrimination trial from the low load (i.e., colour discrimination request) condition.*

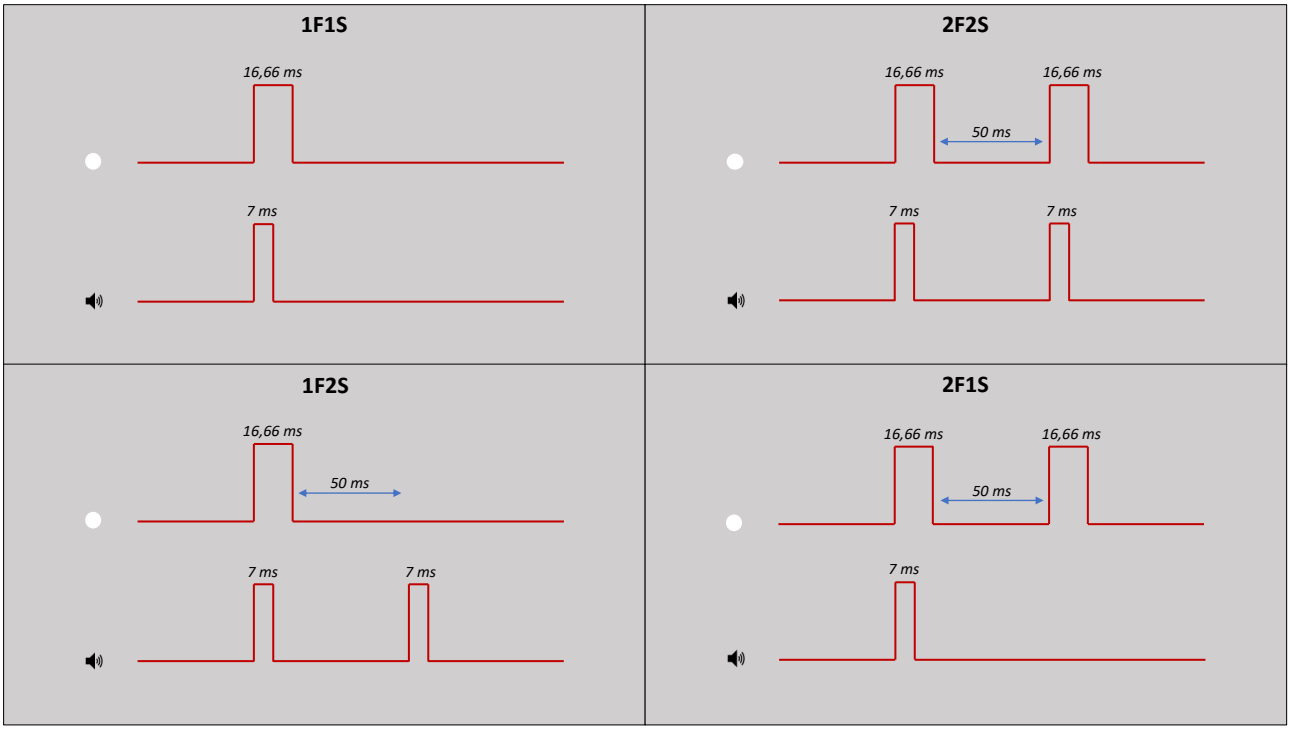

Figure 3.2. Audiovisual integration trial. *In each audiovisual integration trial, participants were concurrently presented with lateralized flashes (lasting 16.66 ms) and binaural sounds (lasting 7 ms). The presentation varied based on the condition: either a single flash (1F) or two successive flashes (2F) were displayed. In the case of the dual flash presentation, there was a 50 ms interval between the first and second flash. Additionally, depending on the condition, either a single sound (1S) or two sounds (2S) were presented in conjunction with the flash(es). In total, four different audiovisual integration stimulus types were possible.*

EEG recordings

For resting-state and in-task EEG recordings we employed a Geodesic hd-EEG System (EGI® Net Amp GES-400) with NetStation EEG Software (v 5.4.2) (Magstim EGI, 2021), utilizing a pre-cabled 256-channel HydroCel Geodesic Sensor Net with electrical referencing to the vertex. The impedance was kept below 50 kΩ. The sampling rate was 1000 Hz, but after the recoding EEG data were down-sampled at 500 Hz to streamline data processing. Resting-state recordings lasted for 6 minutes,

during which participants were instructed to keep their eyes open and refrain from focusing on any specific thoughts. In-task recordings continued until the task was completed.

Analysis - Dual-Task

Dual-Task data preparation and analysis were performed using R Statistical Software (v 4.2.2; R Core Team, 2022).

Data preparation

A data cleaning procedure was implemented to ensure the quality and reliability of dual-task data. Specifically, we excluded participants with individual audiovisual integration accuracy scores deviating in at least one audiovisual integration trial type more than 2 standard deviations from group's average audiovisual integration accuracy. The same threshold was used for audiovisual integration response times and visual discrimination accuracy. The procedure resulted in no exclusions. The adoption of slightly less conservative data cleaning criteria than those used in Experiment 2 of Chapter 2 was allowed by the much higher level of control characterizing the laboratory setting compared to the online setting.

Models fitting and analysis for hypothesis testing

Statistical procedures capitalized on the use of Linear Mixed-effect Models (LMMs) and Generalized Linear Mixed-effect Models (GLMMs) (R Package: lme4 – v 1.1.31, Bates et al., 2015), identical to the one used in Experiment 2 of Chapter 2.

Secondary task accuracy. To assess the efficacy of secondary task (i.e., the visual discrimination of colour/shape) in inducing attentional load modulations we initially performed a GLMM (family: binomial; distribution: logit). The dependent variable was accuracy in the visual discrimination task. The fixed effects included attentional load levels (low, high). Participants entered the model as a random intercept, to account for the inherent variations among their baseline accuracy during the visual discrimination task. Additionally, blocks entered the model as a random slope nested within participants; this modelling choice was based on a model selection (see Supplementary) and it captured the idea that time on task might have different effects at the individual level. We expected

a main effect of attentional load levels: visual discrimination accuracy would be significantly lower in high attentional load (report shape) compared to low attentional load (report colour).

Audiovisual integration accuracy. We then conducted a GLMM (family: binomial; distribution: logit) to investigate H1.1. The dependent variable was audiovisual integration accuracy. The fixed effects included: audiovisual integration stimulus types (1F1S, 2F2S, 1F2S, 2F1S), flash presentation side (left, right), attentional load levels (low, high) and hand-used to respond (dominant, non-dominant). Random effects included also in this case participants as a random intercept and blocks as a random slope nested within participants. Additionally, random effects included audiovisual integration stimulus types as random slope nested within participants; also this modelling choice aimed at capturing the previously reported individual variability in audiovisual integration accuracy when considering stimuli generating fission and fusion illusions (Hirst et al., 2020). We expected (H1.1) a main effect of audiovisual integration stimulus types: audiovisual integration accuracy would be significantly lower and SIFI would emerge in incongruent audiovisual integration stimuli, i.e. 1F2S stimuli and 2F1S stimuli, compared to congruent audiovisual integration stimuli, i.e. 1F1S stimuli and 2F2S stimuli.

Audiovisual integration d-prime. Finally, we implemented a LMM to investigate H1.2 and H1.3. In this case the dependent variable audiovisual integration accuracy was transformed using signal detection theory principles (similar to: Watkins et al., 2006; Whittingham et al., 2014), which is a standard approach to investigate sound-induced flash illusion (Keil, 2020). We aggregated audiovisual integration accuracy values from different congruent and incongruent audiovisual integration stimuli to calculate d-prime (d'). A lower d' value indicates poorer discrimination ability, and in the present context it indexes a greater susceptibility to illusions. Congruent 2F2S stimuli and incongruent 1F2S stimuli were used to calculate d' related to fission illusion. In 2F2S the correct response “2” was considered a hit, while the wrong response “1” was considered a miss. In 1F2S stimuli the illusory response “2” was considered a false alarm, while the correct response “1” was considered a correct rejection. Congruent 1F1S stimuli and incongruent 2F1S stimuli were instead used to calculate d' related to fusion illusion. In 1F1S stimuli the correct response “1” was considered a hit, while the wrong response “2” was considered a miss. In 2F1S stimuli the illusory response “1” was considered a false alarm, while the correct response “2” was considered a correct rejection. From these values, d' was computed as Z value of the hit rate minus that of the false alarm rate,

adjusting for extreme values with the log-linear rule recommended by Hautus (Hautus, 1995) (R Package: psycho - v 0.6.1, Makowski, 2018). The so-calculated audiovisual integration d' entered the LMM as the dependent variable. The fixed effects included: sound-induced flash illusion types (fission, fusion), flash presentation side (left, right), attentional load levels (low, high) and hand-used to respond (dominant, non-dominant). Random effects included also in this case participants as a random intercept and blocks as a random slope nested within participants. Additionally, random effects included audiovisual integration illusion types as a random slope nested within participants, following the same rationale as the inclusion of audiovisual integration stimulus types as random slope nested within participants in the previous model. We expected (H1.2) a main effect of attentional load levels: the emergence of SIFI would be significantly higher with high attentional load compared to low attentional load. Additionally, we expected (H1.3) an interaction between attentional load levels and flash presentation side: the emergence of SIFI would be significantly higher with high attentional load, especially in case of left sided flashes.

For all the models, we performed model assumption checks using “DHARMa”(R Package: DHARMa - v 0.4.6, Hartig, 2022), which employs a simulation-based approach to analyse residuals for fitted LMMs and GLMMs. The analysis indicated small deviations from expected residuals with no evident pattern. None of the models exhibited evident overdispersion, underdispersion, or heteroscedasticity.

To conduct hypothesis tests, LMMs were assessed through Analysis of Variance (Type III) with Satterthwaite’s method for computing degrees of freedom and F statistics (R Package: lmerTest – v 3.1.3, Kuznetsova et al., 2017), while GLMMs were assessed through Analysis of Deviance with Type III Wald test for computing Chi-square statistics (R Package: car - v 3.1.1, Fox J. & Weisberg S., 2019). Post-hoc pairwise comparisons between the levels of fixed factors were tested for main effects and interactions of interest when significant, computing estimated marginal means contrasts (R package: emmeans - v 1.8.3, Russell V. L., 2022) and adjusting for multiple comparisons with the false discovery rate method (Glickman et al., 2014).

Analysis - EEG during Resting-State

EEG data pre-processing and analysis were performed using Matlab Software (v 9.1.0; The MathWorks Inc, 2016) with NET toolbox (Taberna et al., Under Review) and R Statistical Software (v 4.2.2; R Core Team, 2022).

Data pre-processing

We implemented a semi-automatic data cleaning procedure, developed and validated in previous studies (Liu et al., 2017, 2018; Marino et al., 2019; Samogin et al., 2019, 2020).
Initially, channels with poor signal quality were identified combining information from two different parameters: 1) minimum Pearson correlation between the signal of each channel and the signal of all other channels, in the band 1-80 Hz; 2) signal noise variance of each channel, in the 200-250 Hz band, where the contribution of brain activity can be considered negligible. The channels marked as bad were those for which at least one of the two channel-specific parameters was an outlier with respect to the total distribution of values. Additionally, it was conducted a visual inspection for further confirmation. The identified bad channels were reconstructed, interpolating their respective time courses with the neighbouring channels. Subjects in which more than 12% of the channels (i.e. 30 channels) had to be reconstructed were excluded from the sample (n excluded: 2) (for further details see: Liu et al., 2017; Samogin et al., 2020). After that, the EEG data were band-pass filtered in the frequency band 1-80 Hz. Next, biological artifacts (i.e., movement artifacts, ocular artifacts, myogenic artifacts and cardiac artifacts) were identified using ICA. Independent Components (ICs), as well as the weights with which the ICs were mixed in the signal, were estimated with a fast fixed-point ICA (FastICA) algorithm, based on a deflation approach and hyperbolic tangent as contrast function (Mantini et al., 2008). An automated classification of the ICs was done according to three parameters: 1) correlation between the power of the IC with vertical electrooculogram, horizontal electrooculogram, and electromyogram; 2) coefficient of determination obtained by fitting the IC power spectrum with the $1/f$ function; 3) IC kurtosis. An IC was classified as artifactual if at least one of the above parameters surpassed a given threshold, which was set in accordance with previous studies (de Pasquale et al., 2010; Mantini et al., 2009). The time courses of the ICs classified as bad were reconstructed at the channel level and then subtracted from the EEG data (for further details see: Liu et al., 2017; Samogin et al., 2020). At this point, the EEG data were re-referenced with an optimized version of the Reference Electrode Standardization Technique (for further details

see: Liu et al., 2017; Samogin et al., 2020). The procedure resulted in a final sample consisting of 55 participants (mean age: 22.78, age range: 18-31; number of males: 30, number of responders with dominant hand: 28).

Functional connectivity calculation

An automated analysis pipeline, developed and validated in previous studies (Liu et al., 2017, 2018; Marino et al., 2019; Samogin et al., 2019, 2020) was used for calculating intrinsic functional connectivity. This analysis pipeline comprised three steps: "standard head model creation", "reconstruction of sources" and "ICA-based functional connectivity calculation."

Step 1: standard head model creation. This step was performed to obtain a head model based on a standard magnetic resonance (MR) image based on the Montreal Neurological Institute (MNI) template and template electrode positions associated with the specific EEG system used for this study. Firstly, a segmentation of the head was performed in the standard MR image using 12 different compartments: skin, eyes, muscle, fat, spongy bone, compact bone, cortical grey matter, cerebellar grey matter, cortical white matter, cerebellar white matter, cerebrospinal fluid and brain stem (for further details see: Liu et al., 2017; Samogin et al., 2020). A co-registration of the electrode's positions to the head contour (i.e. outer layer of the skin compartment) was then performed (for further details see: Liu et al., 2017; Samogin et al., 2020). For each compartment, a specific conductivity value was set based on previous literature (Haueisen et al., 1997). In the compartments corresponding to cortical, subcortical, and cerebellar grey matter, it was used a regular 3D 6 mm grid in order to define all the possible dipole sources. Next, SimBio (Wolters et al., 2004; Ziegler et al., 2014) was used to generate the whole-head finite element standard head model (for further details see: Liu et al., 2017; Samogin et al., 2020).

Step 2: reconstruction of sources. This step was done to estimate, based on the standard head model and the pre-processed EEG data, the spatial distribution of sources that most likely generates the signal measured over the scalp. It was employed the exact low-resolution brain electromagnetic tomography (eLORETA) algorithm (Pascual-Marqui et al., 2011), providing as input the standard head model and the pre-processed EEG data. The result was the computation of the three-dimensional distribution of neural activity in the source space, in a 6 mm homogeneous grid constrained to the grey matter (for further details see: Liu et al., 2017; Samogin et al., 2020).

Step 3. ICA-based functional connectivity calculation. This step was performed to obtain maps showing segregated regions that have a highly correlated response pattern, and are therefore

functionally connected, forming EEG-RSNs. First, it was performed a time-frequency decomposition of the reconstructed distribution of neural activity in the source space using the spectrogram method, which yielded power time-courses for the classical frequency bands, namely delta (1-4 Hz), theta (4-8 Hz), alpha (8-13 Hz), beta (13-30 Hz), and gamma (30-80 Hz). Then, it was employed ICA, in both its spatial (sICA) and temporal (tICA) variants (Calhoun et al., 2001, 2009; Smith et al., 2012). Typically, sICA is considered the gold standard for analysing fMRI data, where the number of time points is always significantly smaller than the number of voxels. Differently, tICA has been suggested to be more informative for EEG data, as it may be better equipped to capture the nonlinear and nonstationary nature of neurophysiological signals (Brookes et al., 2011; Yuan et al., 2016). However, the situation is not so clear-cut, and numerous EEG studies prefer to use sICA (e.g., Marino et al., 2019; Sockeel et al., 2016; Yi et al., 2020). Note that specific differences between RSNs obtained by sICA and tICA exist. In particular, RSNs with more widespread, sometimes overlapping regions can be observed when reconstructing them with tICA, whereas RSNs reconstructed by sICA show more selective spatial patterns and cover more limited portions of the cortical space (Liu et al., 2017). The ICA computation resulted in a number of ICs, each of which consists of a spatial map and an associated time-course. The spatial map reveals segregated regions that have a highly correlated response pattern, and are therefore functionally connected (Brookes et al., 2011; Mantini et al., 2007) (for further details see: Liu et al., 2017). At this point, EEG-RSNs of interest were selected using a template-matching procedure based on the similarity between extracted ICs and RSNs templates derived from fMRI data in a previous study (Mantini et al., 2013). These fMRI-RSN templates encompassed 14 distinct networks: default mode network (DMN), dorsal attention network (DAN), ventral attention network (VAN), right fronto-parietal network (rFPN), left fronto-parietal network (lFPN), language network (LN), cingulo-opercular network (CON), auditory network (AN), ventral somatomotor network (VSN), dorsal somatomotor network (DSN), visual foveal network (VFN), visual peripheral network (VPN), medial prefrontal network (MPN), and lateral prefrontal network (LPN). The best IC match for each template was extracted iteratively, labelled as a specific EEG-RSN, and removed from the pool of the remaining ICs. Accordingly, the same IC could not be associated with two different templates (for further details see: Liu et al., 2017). In conclusion, the final outcome of this procedure consisted of individual spatial maps for each subject, separately for sICA and tICA functional connectivity, for each of the fourteen EEG-RSN and for each of the five classical frequency bands.

Correlation analysis

To investigate H2, for both sICA and tICA functional connectivity, a specific subsample of EEG-RSNs of interest was selected a priori for the correlation analysis. This subsample comprised EEG-RSNs thought to be potentially engaged in SIFI perception during increased attentional load. These included: AN, VFN, VPN, DMN, DAN, and VAN, for each of the classic frequency bands (delta, theta, alpha, beta and gamma). More precisely, the AN was choosen because it includes areas dedicated to auditory processing (Mantini et al., 2007, 2013), while VFN and VPN were selected because they include areas dedicated to visual processing (Damoiseaux et al., 2006; Mantini et al., 2007, 2013), that are all crucial in SIFI perception (Mishra et al., 2007; Watkins et al., 2006, 2007). The DMN was chosen because it includes areas that are usually more active at rest than during task performance and mediate processes that are important for the resting-state (Fox & Raichle, 2007; Mantini et al., 2007, 2013). The DAN and VAN were chosen because they are known to be responsible for the allocation of attentional resources in space (Corbetta et al., 2008; Corbetta & Shulman, 2002). In total, both the sICA and tICA sub-samples were composed by 30 individual spatial maps for each subject.

Correlations between behavioural indexes and functional connectivity within specific networks. Firstly, for each of these individual spatial maps we computed an individual mean functional connectivity value. Subsequently, it was computed a Pearson correlation between various individual task accuracy indexes (i.e., mean audiovisual integration accuracy across all incongruent 1F2S stimuli, mean audiovisual integration accuracy across all incongruent 2F1S stimuli, mean audiovisual integration d-prime across all cases of low attentional load and mean audiovisual integration d-prime across all cases of high attentional load) and the individual mean functional connectivity values. All correlations underwent adjustment for multiple comparisons with the false discovery rate method (Glickman et al., 2014).

Correlations between behavioural indexes and functional connectivity within specific ROIs. When significant correlations were found at the network level, the analysis proceeded further. More specifically, correlations were explored calculating individual mean functional connectivity values, not within specific individual spatial maps but within specific ROIs part of such maps.

Wide areas of interest were chosen a-priori, based on previous studies indicating their involvement in SIFI perception during increased attentional load and were the following: primary visual cortex

(Watkins et al., 2006, 2007), primary auditory cortex (Mishra et al., 2007), superior temporal gyrus (Watkins et al., 2006, 2007), middle temporal gyrus (Keil et al., 2014), angular gyrus (Hamilton et al., 2013; Kamke et al., 2012), inferior frontal gyrus (Mishra et al., 2007), middle frontal gyrus (Keil et al., 2014), middle and anterior cingulate cortex (Keil et al., 2014; Michail et al., 2021). These areas were associated with the corresponding Brodmann areas and the relative MNI coordinates were extracted using the Yale BioImage Suite Package web application (Lacadie et al., 2008). ROIs were defined applying in each spatial map a 6 mm radius spherical mask centred on ROIs' MNI coordinates (see Table 3.1). Only certain ROIs were defined for each spatial map (e.g., for spatial maps associated with the VFN it was calculated the ROI relative to the primary visual cortex but not the one relative to the cingulate cortex, for spatial maps associated to the VAN were calculated only right lateralized ROIs as the VAN is characterised by a right hemispheric dominance (Tosoni et al., 2023). At this point, for each of these ROIs we computed an individual mean functional connectivity value. Subsequently, it was computed a Pearson correlation between the various task accuracy indexes and individual mean functional connectivity values. All correlations underwent adjustment for multiple comparisons with the false discovery rate method (Glickman et al., 2014).

We expected (H2) significant correlations to emerge at both the network and region of interest levels.

ROI Number		*Brodman Area*	*MNI Coordinates [x y z] for Left Hemisphere*	*MNI Coordinates [x y z] for Right Hemisphere*
1	primary visual cortex	17	-11 -81 7	11 -78 9
2	primary auditory cortex	41	-52 -19 7	50 -21 7
3	superior temporal gyrus	22	-57 -20 1	54 -19 1
4	middle temporal gyrus	21	-59 -25 -13	60 -27 9
5	angular gyrus	39	-46 -60 33	46 -59 31
6	inferior frontal gyrus	44	-48 13 17	49 12 17
7		45	-47 27 6	46 26 7
8		47	-40 31 -13	38 30 -12
9	middle frontal gyrus	9	-39 34 37	35 39 31
10	cingulate cortex (middle and anterior)	32	-5 39 20	6 33 16
11		24	-5 1 32	5 5 31

Table 3.1. Areas of interest, corresponding Brodmann Areas and MNI coordinates.

Analysis - EEG during Dual-Task

EEG data pre-processing and analysis were performed using Matlab Software (v 9.14.0; The MathWorks Inc, 2023) with EEGLAB toolbox (v 2023.1 Delorme A. & Makeig S., 2004) and R Statistical Software (v 4.2.2; R Core Team, 2022).

Data pre-processing

Firstly, EEG data were down-sampled at 250 Hz, again to streamline data processing. Next, EEG data were cleaned from line noise (50 Hz), using ZapLine method from NoiseTools (de Cheveigné, 2020), and high-pass filtered at 0.1 Hz. Additionally, EEG data were cleaned from channels with poor signal quality. Specifically, a channel was marked as bad and excluded if either one of the following conditions was met: 1) a channel recorded a flat-line for at least 5 seconds; 2) a channel contained predominantly line noise for more than 4 noise standard deviations; 3) A channel was poorly correlated with its neighbours (correlation threshold < 0.8). Then, EEG data were divided in large epochs between -1500 and +1500 ms from first flash onset and epochs with gross movement artifacts (i.e., channels showing a differential average amplitude of +/-500 μV) were excluded. Artifact-reduced EEG data were then subjected to ICA using the Infomax algorithm (Bell & Sejnowski, 1995) implemented in EEGLab, obtaining 40 independent components (ICs). The resulting independent ICs were visually inspected in topography and time-series, and those clearly related to ocular artifacts, movement artifacts, myogenic artifacts and cardiac artifacts were discarded. The remaining components were then projected back to the electrode space to obtain cleaner epochs. Then, EEG data were re-epoched between -100 and +1000 ms from first flash onset. All the epochs were digitally inspected through the TBT plugin implemented in EEGLAB, which performs an automatic rejection of channels and epochs on an epoch-by-epoch basis. Specifically, a channel that exceeded a differential average amplitude of +/-100 μV on more than 30% of all epochs was marked as bad and excluded. Epochs having more than 10 bad channels were also excluded. Channels marked as bad through the various steps were reconstructed with the spherical spline interpolation method (Ferree, 2006; Perrin et al., 1989). At this point, EEG data were low-pass filtered at 30 Hz. Finally, EEG data were re-referenced to the average of all electrodes. Subjects in which more than 15% of epochs had to be excluded were excluded from the sample (n excluded: 8). Additionally, one more subject was excluded due to issues during recording related to trigger labelling. The procedure resulted in a final sample consisting of 48 participants (mean age: 22.54, age range: 18-31; number

of males: 23, number of responders with dominant hand: 24). Individual average and grand average ERPs were computed for all experimental conditions, applying a weighted average in order to control for any potential unbalanced number of epochs per condition (Kotowski et al., 2019; Leski, 2002).

ERP components calculation

In line with previous studies (Bonato et al., 2015; O'Connell et al., 2011; Romeo et al., 2019) and with the grand average visual inspection, we extracted the following ERP components as the mean voltage amplitude in specific time windows: P1 (80-150 ms), N1 (90-140 ms), N2 (140-180 ms), P2 (150-230 ms) and P3 (300-450 ms). Each ERP component was investigated by averaging the signal within specific electrode clusters of interest (see Figure 3.3): Frontal-Left Cluster (electrodes 40, 41, 42, 49 and 50), Frontal-Right Cluster (electrodes 205, 206, 213, 214 and 223), Frontal-Central Cluster (electrodes 6, 7, 14, 15, 16, 22 and 23), Central-Left Cluster (electrodes 51, 52, 58, 59, 60, 65 and 66), Central-Right Cluster (electrodes 155, 164, 182, 183, 184, 195 and 196), Parietal-Left Cluster (electrodes 76, 77, 85, 86, 87, 97 and 98), Parietal-Right Cluster (electrodes 152, 153, 161, 162, 163, 171 and 172), Parietal-Central Cluster (electrodes 100, 101, 110, 119, 126, 128 and 129), Occipital-Left Cluster (electrodes 115, 123, 124 and 135), Occipital-Right Cluster (electrodes 149, 157, 158 and 159) and Occipital-Central Cluster (electrodes 125, 137 and 138).
More specifically: P1 was investigated in Occipital-Left Cluster, Occipital-Right Cluster, Occipital-Central Cluster, Parietal-Left Cluster, Parietal-Right Cluster and Parietal-Central Cluster; N1 was investigated in Central-Left Cluster, Central-Right Cluster, Frontal-Left Cluster, Frontal-Right Cluster and Frontal-Central Cluster; N2 was investigated in Occipital-Left Cluster, Occipital-Right Cluster, Occipital-Central Cluster, Parietal-Left Cluster, Parietal-Right Cluster and Parietal-Central Cluster; P2 was investigated in Parietal-Left Cluster, Parietal-Right Cluster and Parietal-Central Cluster; P3 was investigated in Parietal-Left Cluster, Parietal-Right Cluster and Parietal-Central Cluster.

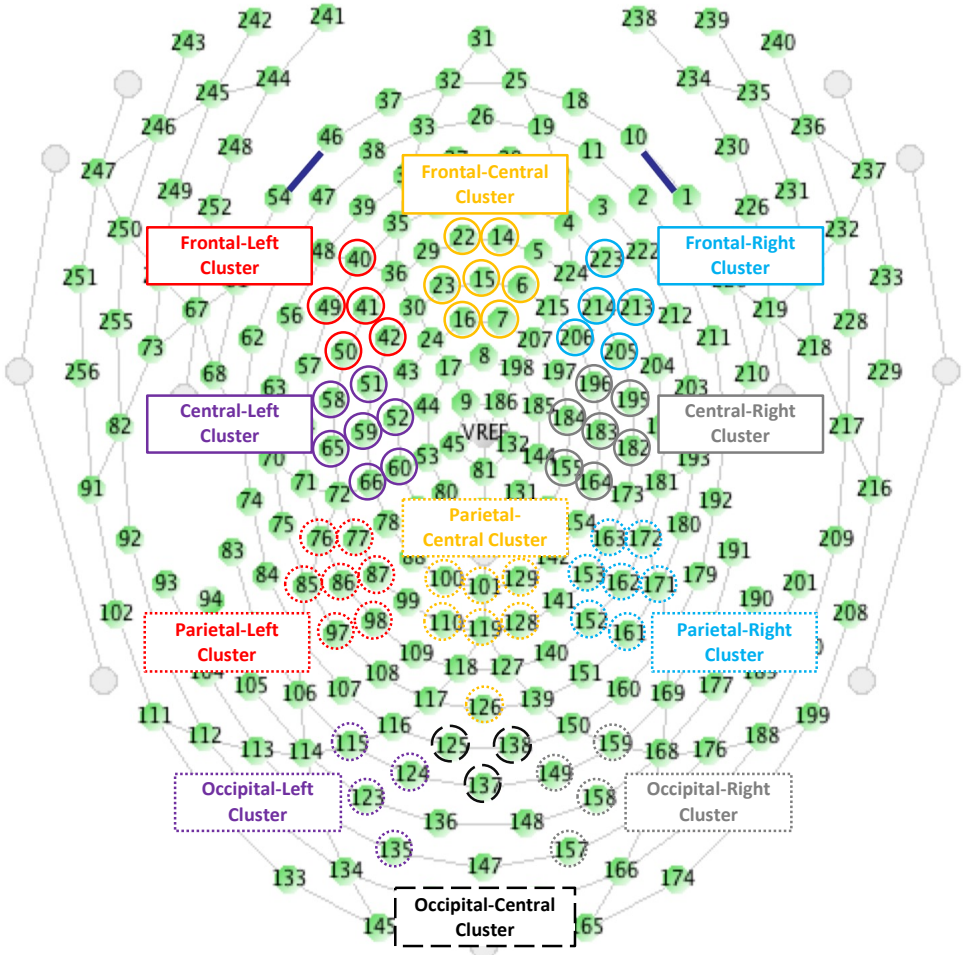

Figure 3.3. Sensor layout for 256-channel HydroCel Geodesic Sensor Net. *The orientation of sensor layout is top-down, with the nose at the top of the page.*

Models fitting and analysis for hypothesis testing

Statistical procedures capitalized on the use of Linear Mixed-effect Models (LMMs) (R Package: lme4 – v 1.1.31, Bates et al., 2015).

To investigate H3.1 and H3.2 we initially performed various LMMs. In each model, the dependent variable was one the extracted ERP components. The fixed effects included: audiovisual integration stimulus types (1F1S, 2F2S, 1F2S, 2F1S), flash presentation side (left, right), attentional load levels (low, high) and electrode clusters (note that the levels of this predictor varied depending on the ERP component being investigated, since each ERP component was examined in different clusters, as outlined in the preceding section). Participants entered the model as a random intercept, to account for the inherent variations among individual signal. However, all models exhibited issues with multicollinearity: most predictors in each model had a Variance Inflation Factor (VIF) exceeding 10.

A VIF above 10 is generally considered an index of high collinearity among predictors, leading to inflated standard errors for the coefficients and potentially reducing the reliability of the model's estimates (Kalnins, 2018; C. G. Thompson et al., 2017). To mitigate multicollinearity, the recommended solution is to simplify the models. To do that we adopted the following procedure:

1) First, to identify the cluster where the investigated ERP component exhibited the largest signal amplitude, we ran a LMM defined as follows: the dependent variable was the signal of the investigated ERP component, the fixed effects included exclusively electrode clusters and participants entered the model as a random intercept. The signal in the cluster with the largest signal amplitude was considered as dependent variable for the following step.
2) Next, to ensure that there was an effect of attentional load levels, we ran another LMM, defined as follows: the dependent variable was the signal of the investigated ERP component in the cluster selected during step 1, the fixed effects included exclusively attentional load levels (low, high) and participants entered the model as a random intercept. If the effect of attentional load levels was significant, we calculated a *cost waveform* considering the signal in the high load condition and subtracting the signal in the low load condition (high load – low load) (similar to: Bonato et al., 2015 - cost analysis). Note that for positive ERP components, when the signal amplitude during high attentional load is larger than during low attentional load (high load > low load), the subtraction yields a *positive cost signal* (high load – low load > 0). Conversely, if the signal amplitude during high attentional load is smaller than during low attentional load (high load < low load), the subtraction results in a *negative cost signal* (high load – low load < 0). For negative ERP components the subtraction leads to opposite values and therefore when when the signal amplitude during high attentional load is larger than during low attentional load (high load > low load), the subtraction yields a *negative cost signal* (high load – low load < 0). Conversely, if the signal amplitude during high attentional load is smaller than during low attentional load (high load < low load), the subtraction results in a *positive cost signal* (high load – low load > 0). In addition to this operation, we combined together the signal of the two congruent and the two incongruent audiovisual integration stimulus types.
3) Finally, we ran the last simplified LMM, defined as follows: the dependent variable was the cost waveform of the investigated ERP component, the fixed effects included congruency (congruent, incongruent) and flash presentation side (left, right), and participants entered the model as a random intercept.

In all the simplified models derived from step 3, VIF was below 5 for all the predictors. Moreover, for these simplified models, we performed model assumption checks using "DHARMa"(R Package: DHARMa - v 0.4.6, Hartig, 2022), which employs a simulation-based approach to analyse residuals for fitted LMMs. The analysis indicated small deviations from expected residuals with no evident pattern. None of the simplified models exhibited evident overdispersion, underdispersion, or heteroscedasticity.

In the simplified models we expected (H3.1) a main effect of congruency: the cost waveform would be significantly different for congruent stimuli and incongruent stimuli (i.e., the ones in which SIFI is usually generated). Additionally, we expected (H3.2) an interaction between congruency and flash presentation side: the cost waveform would vary significantly in incongruent stimuli (i.e., the ones in which SIFI is usually generated) following left-sided stimuli or right-sided stimuli.

To conduct hypothesis tests, LMMs were assessed through Analysis of Variance (Type III) with Satterthwaite's method for computing degrees of freedom and F statistics (R Package: lmerTest – v 3.1.3, Kuznetsova et al., 2017). Post-hoc pairwise comparisons between the levels of fixed factors were tested for main effects and interactions of interest when significant, computing estimated marginal means contrasts (R package: emmeans - v 1.8.3, Russell V. L., 2022) and adjusting for multiple comparisons with the false discovery rate method (Glickman et al., 2014).

3.5 Results

Dual-Task

We present below the results pertaining to secondary task accuracy, audiovisual integration accuracy, and audiovisual integration d'. We provide details on all the main effects, while we include exclusively those interactions highlighted in the analysis section as relevant for addressing our hypothesis. For each of these main effect and interaction, for what concerns analysis of variance (for LMMs) or analysis of deviance (for GLMMs), we have reported either the Chi-square (for GLMMs) or F value (for LMMs). For post-hoc pairwise comparisons, we have then reported: the difference between estimated means ($\Delta\hat{\mu}$, in log odds ratio scale for GLMMs and in response scale for LMMs), as well as, exclusively for GLMMS, the difference between observed means ($\Delta\mu$ in response scale), the standard error (SE) and associated statistics (*z* test for GLMMs and *t* test for LMMs). Note that odds ratios are the ratios between the frequency with which a correct response

occurs in a certain condition and the frequency with which a correct response occurs in another condition.

Secondary task accuracy

Descriptive statistics for secondary task accuracy (range 0-1) as a function of load levels are summarized in Table 3.2. GLMM for secondary task accuracy is summarized in Table 3.3. Analysis of deviance resulted in the expected main effect of attentional load levels (X^2 (1) = 614.43, p < .001), with participants being less accurate in the visual discrimination task in case of high load compared to low load (high vs low: $\Delta\hat{\mu}$ = - 2.15, $\Delta\mu$ = - 0.128, SE = 0.087, z = -24.788, p < .001).

load levels	
high load	*low load*
m= 0.853 sd = 0.354	m= 0.981 sd = 0.135

Table 3.2. Dual-Task: descriptive statistics for secondary task accuracy (range 0-1).

Predictors	*Odds Ratios*	*SE*	*CI*
intercept	7.18	0.67	5.98 – 8.63
load level (low vs high)	8.60	0.75	7.26 – 10.20
Marginal R^2 = 0.227; AIC = 17432.500			

Table 3.3. Dual-Task: GLMM for secondary task accuracy output.

Audiovisual integration accuracy

Descriptive statistics for audiovisual integration accuracy (range 0-1) as a function of flash presentation side, audiovisual integration stimulus types and load types are summarized in Table 3.4. GLMM for audiovisual integration accuracy is summarized in Table 3.5. Analysis of deviance highlighted the expected main effect of audiovisual integration stimulus types (X^2 (3) = 121.436, p < .001). Participants were less accurate with incongruent 1F2S stimuli than with congruent 1F1S stimuli (1F2S vs 1F1S: $\Delta\hat{\mu}$ = -3.765, $\Delta\mu$ = -0.455, SE = 0.226, z = -16.669, p < .001) replicating the presence of fission illusion also in the lab setting. Additionally, they were less accurate with incongruent 2F1S stimuli than with congruent 2F2S stimuli (2F1S vs 2F2S: $\Delta\hat{\mu}$ = -4.220, $\Delta\mu$ = -0.582,

SE = 0.305, z = -13.832, p < .001), indexing that also fusion illusion was replicated in the lab setting. There was a significant difference in accuracy between congruent 1F1S stimuli and 2F2S stimuli (1F1S vs 2F2S: $\Delta\hat{\mu}$ = 0.831, $\Delta\mu$ = 0.039, SE = 0.369, z = 2.250, p = 0.024), and also between incongruent 1F2S stimuli and 2F1S stimuli (1F2S vs 2F1S: $\Delta\hat{\mu}$ = 1.285, $\Delta\mu$ = 0.166, SE = 0.395, z = 3.256, p = 0.0014) (see Figure 3.4). Moreover, the main effect of flash presentation side was not significant (X^2 (1) = 0.102, p = 0.749) and also the main effect of attentional load levels was not significant (X^2 (1) = 2.232, p = 0.135).

		flash presentation side							
		left				*right*			
		audiovisual integration stimulus types							
		1F1S	*1F2S*	*2F1S*	*2F2S*	*1F1S*	*1F2S*	*2F1S*	*2F2S*
load levels	*low load*	m= 0.923 sd = 0.267	m= 0.491 sd = 0.5	m= 0.325 sd = 0.468	m= 0.914 sd = 0.281	m= 0.938 sd = 0.242	m= 0.482 sd = 0.5	m= 0.296 sd = 0.457	m= 0.889 sd = 0.315
	high load	m= 0.906 sd = 0.292	m= 0.435 sd = 0.496	m= 0.299 sd = 0.458	m= 0.864 sd = 0.343	m= 0.91 sd = 0.285	m= 0.449 sd = 0.497	m= 0.27 sd = 0.444	m= 0.853 sd = 0.354

Table 3.4. Dual-Task: descriptive statistics for audiovisual integration accuracy range (0-1).

Predictors	*Odds Ratios*	*SE*	*CI*
intercept	38.43	15.04	17.85 – 82.78
flash presentation side (right vs left)	1.07	0.23	0.70 – 1.63
audiovisual integration stimulus types (1F2S vs 1F1S)	0.02	0.01	0.01 – 0.04
audiovisual integration stimulus types (2F1S vs 1F1S)	0.01	0.00	0.00 – 0.03
audiovisual integration stimulus types (2F2S vs 1F1S)	0.25	0.14	0.09 – 0.73
load level (low vs high)	1.41	0.33	0.90 – 2.22
Marginal R^2 = 0.574; AIC = 25615.415			

Table 3.5. Dual-Task: GLMM for audiovisual integration accuracy output.

Audiovisual integration d-prime

Descriptive statistics for audiovisual integration d' as a function of flash presentation side, audiovisual integration stimulus types and load types are summarized in Table 3.6. LMM for

audiovisual integration d' is summarized in Table 3.7. Analysis of variance highlighted the expected main effect of attentional load levels (F (1, 232.29) = 64.7527, $p < .001$), replicating in the lab setting the finding of significantly higher illusion rates in case of high load compared to low load (high vs low: $\Delta\hat{\mu}$ = -0.27, SE: 0.036, t (152) = -7.483, $p < .001$). Additionally, it was also replicated the non-significant interaction between attentional load levels and flash presentation side which already emerged in the online setting during the two experiments of Chapter 2 (F (1, 669.56) = 0.274, p = 0.601) (see Figure 3.4). Moreover, we found a main effect of flash presentation side (F (1, 669.56) = 5.5918, p = 0.018). Resembling audiovisual integration accuracy results, the main effect of sound-induced flash illusion types was significant (F (1, 55) = 13.0386, $p < .001$) indicating different fission and fusion illusion rates.

		flash presentation side			
		left		*right*	
		audiovisual integration illusion types			
		fission	*fusion*	*fission*	*fusion*
load levels	*low load*	m= 0.932 sd = 1.406	m= 0.93 sd = 1.03	m= 1.29 sd = 0.887	m= 0.876 sd = 1.139
	high load	m= 1.02 sd = 0.77	m= 0.785 sd = 1.012	m= 1.036 sd = 0.885	m= 0.659 sd = 1.017

Table 3.6. Dual-Task: descriptive statistics for audiovisual integration d'.

Predictors	*Estimates*	*SE*	*CI*
intercept	0.90	0.13	0.64 – 1.15
flash presentation side (right vs left)	0.11	0.08	-0.06 – 0.27
audiovisual integration illusion (fusion vs fission)	-0.10	0.17	-0.43 – 0.22
load level (low vs high)	0.43	0.09	0.26 – 0.60
flash presentation side (right) X load level (low)	-0.26	0.12	-0.50 – -0.03
Marginal R^2 = 0.251; AIC = 1623.041			

Table 3.7. Dual-Task: LMM for audiovisual integration d' output.

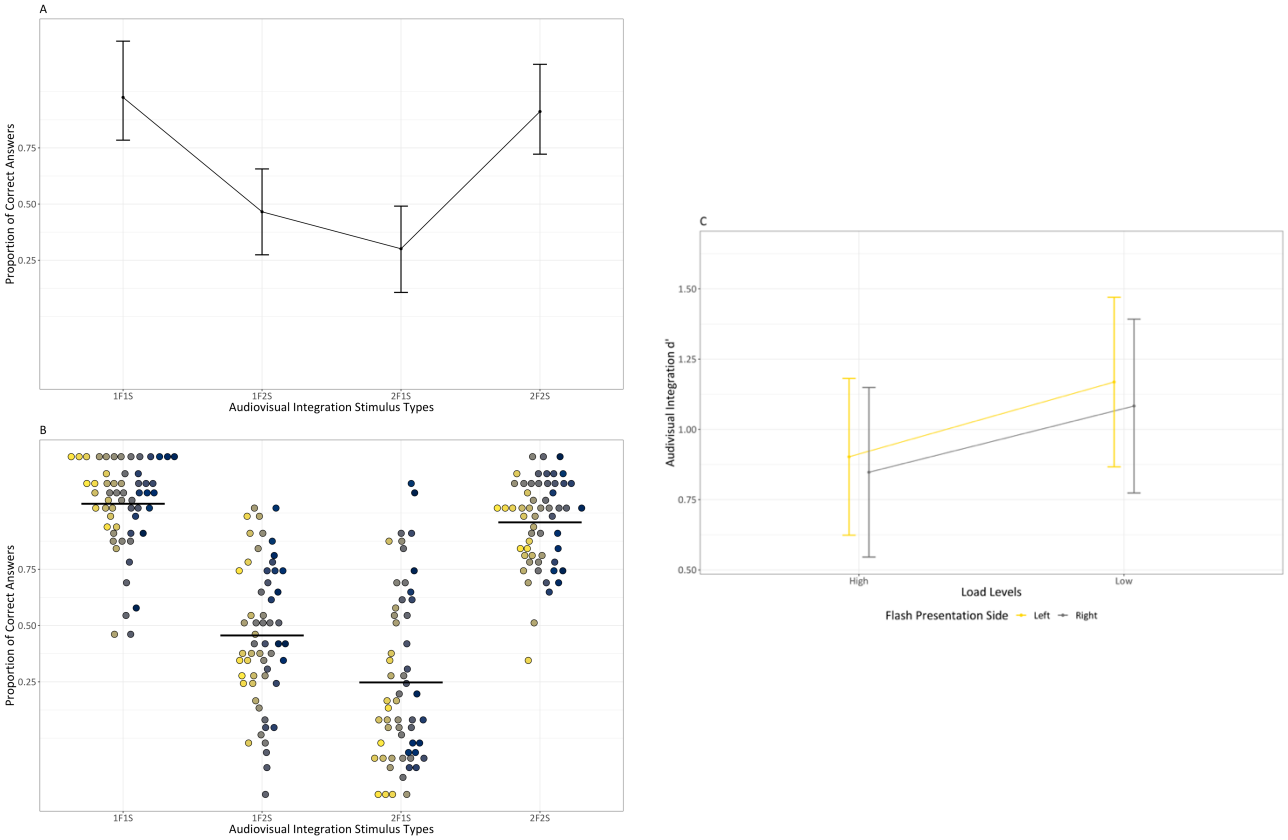

Figure 3.4. Dual-Task: Panel A *displays averaged proportion of correct answers (i.e., no illusion) for the different audiovisual integration stimulus types. Bars represent 95% confidence intervals, adjusted using the Tryon method as accuracy is a binomial variable. These adjustments were calculated over Anscombe-transformed scores using "superb"* (R Package: superb - v 0.9.7.6, Cousineau et al., 2021)*, and subsequently transformed back into proportions.* ***Panel B*** *displays individual proportion of correct answers (i.e., no illusion) for the different audiovisual integration stimulus types, with each dot corresponding to a different participant. The mean is indicated by a horizontal black line. All the proportions are depicted using a non-linear scale, specifically the "asn_trans()" scale for arcsine.* ***Panel C*** *displays cumulative d' for the different load levels and flash presentation side.*

In conclusion, secondary task accuracy was significantly lower under high attentional load compared to low attentional load. Crucially, H1.1 was confirmed in the lab setting: audiovisual integration accuracy was significantly lower and both fission and fusion illusions emerged in incongruent audiovisual integration stimuli, i.e. 1F2S stimuli and 2F1S stimuli, but not in congruent audiovisual integration stimuli, i.e. 1F1S stimuli and 2F2S stimuli. Moreover, also H1.2 was verified in the lab setting: the occurrence of SIFI significantly increased under high attentional load. However, H1.3 was not supported in the lab setting, just as in the online setting: the load manipulations did not reveal that emergence of SIFI under high load was asymmetric across space, being more evident for left-sided flashes.

EEG during Resting-State

Correlations between behavioural indexes and functional connectivity within specific networks.

For sICA (individual) functional connectivity six significant correlations emerged. First of all, audiovisual integration accuracy in 1F2S stimuli negatively correlated with functional connectivity in VAN (theta) (r= -0.293, p = 0.03[2]) and positively in AN (gamma) (r= 0.294, p = 0.03), while audiovisual integration accuracy in 2F1S positively correlated with functional connectivity in VAN (alpha) (r= 0.325, p = 0.03) (see Figure 3.5). Additionally, audiovisual integration d-prime in case of low load negatively correlated with functional connectivity in DAN (alpha) (r= -0.305, p = 0.03). Differently, audiovisual integration d-prime in case of high load positively correlated with functional connectivity in DMN (beta) (r= 0.298, p = 0.03) and in VPN (gamma) (r= 0.341, p = 0.03). These correlations are summarized in Table 3.8.

For tICA (individual) functional connectivity four significant correlations emerged. First of all, audiovisual integration accuracy in 1F2S stimuli positively correlated with functional connectivity in VFN (gamma) (r= 0.281, p = 0.038). Audiovisual integration accuracy in 2F1S positively correlated with functional connectivity in DMN (gamma) (r= 0.320, p = 0.035). Additionally, audiovisual integration d-prime in case of low load negatively correlated with functional connectivity in DAN (alpha) (r= -0.323, p = 0.035). Differently, audiovisual integration d-prime in case of high load positively correlated with functional connectivity in VAN (alpha) (r= 0.288, p = 0.038). These correlations are summarized in Table 3.9.

Behavioural indexes	***Networks***	***Correlation Value***	***p-value (adjusted)***
accuracy in 1F2S stimuli	VAN (theta)	-0,293	0,03
accuracy in 1F2S stimuli	AN (gamma)	0,294	0,03
accuracy in 2F1S stimuli	VAN (alpha)	0,325	0,03
d-prime in low load	DAN (alpha)	-0,305	0,03
d-prime in high load	DMN (beta)	0,298	0,03
d-prime high load	VPN (gamma)	0,341	0,03

Table 3.8. EEG during Resting-State: significant correlations between behavioural indexes and sICA functional connectivity calculated as mean connectivity value within specific networks.

[2] The reported p-values are corrected for multiple comparisons using the false discovery rate method (Glickman et al., 2014). This method employs a step-up approach. It takes the smallest raw p-value and multiplies it by n, the number of comparisons, to get a temporary adjusted p-value. Then it takes the second smallest raw p-value and multiplies it by n-1 and so on. Whenever a higher-ranking temporary p-value is lower than the ones below it, it replaces all lower-ranking p-values. It follows that it is possible to have uniform adjusted p-values after the correction.

Behavioural indexes	*Networks*	*Correlation Value*	*p-value (adjusted)*
accuracy in 1F2S stimuli	VFN (gamma)	0,281	0,038
accuracy in 2F1S stimuli	DMN (gamma)	0,320	0,035
d-prime in low load	DAN (alpha)	-0,323	0,035
d-prime in high load	VAN (alpha)	0,288	0,038

Table 3.9. EEG during Resting-State: significant correlations between behavioural indexes and tICA functional connectivity calculated as mean connectivity value within specific networks.

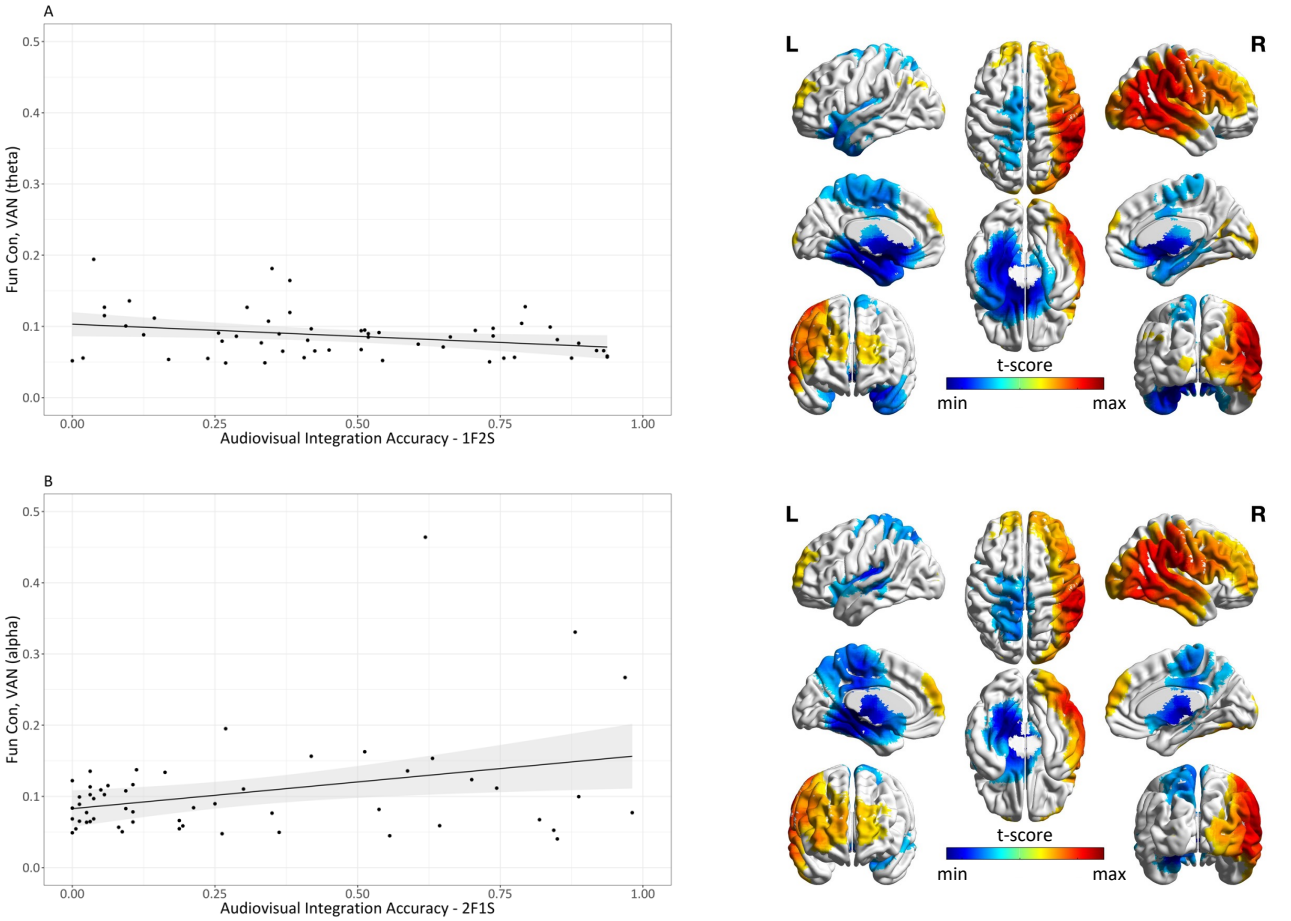

***Figure 3.5. EEG during Resting-State: Panel A** displays on the left the negative correlation between audiovisual integration accuracy in 1F2S stimuli and sICA functional connectivity in VAN (theta). On the right is presented the group level spatial map of functional connectivity in VAN (theta). **Panel B** displays on the left the positive correlation of audiovisual integration accuracy in 2F1S and sICA functional connectivity in VAN (alpha). On the right is presented the group level spatial map of functional connectivity in VAN (alpha). For visualization purposes, spatial maps were plotted as t-scores maps, thresholded at $p < 0.05$ and adjusted with fdr.*

Correlations between behavioural indexes and functional connectivity within specific ROIs

At this point, we defined specific ROIs exclusively within spatial maps of networks and frequencies that showed significant correlation with behavioural indexes.

For sICA functional connectivity in the VPN (gamma) spatial map we defined two ROIs within the primary visual cortex (ROI1-LeftHemi, ROI1-RightHemi). In the AN (gamma) spatial map we defined two ROIs within each primary auditory cortex (ROI2-LeftHemi, ROI2-RightHemi). In the VAN (theta) and in the VAN (alpha) spatial maps we defined one ROI within the angular gyrus (ROI5-RightHemi), three ROIs within the inferior frontal gyrus (ROI6- RightHemi, ROI7- RightHemi, ROI8- RightHemi), one ROI within the middle frontal gyrus (ROI9-RightHemi) and two ROIs within the cingulate cortex (ROI10-RightHemi, ROI11-RightHemi). In the DAN (alpha) spatial map we defined two ROIs within the middle temporal gyrus (ROI4-LeftHemi, ROI4-RightHemi). Finally, in the DMN (beta) spatial map we defined two ROIs within the angular gyrus (ROI5-LeftHemi, ROI5-RightHemi). Seven significant correlations emerged. First of all, audiovisual integration accuracy in 2F1S trials positively correlated with functional connectivity in ROI1-RightHemi within primary visual cortex and defined within the VPN (gamma) (r= 0.342, p = 0.03). Accuracy in 2F1S trials positively correlated also with functional connectivity in ROI5-LeftHemi within angular gyrus and defined within the DMN (beta) (r= 0.276, p = 0.045) and negatively correlated with functional connectivity in ROI10-RightHemi within cingulate cortex and defined within the VAN (theta) (r= -0.271, p = 0.045). Additionally, audiovisual integration d-prime in case of low load positively correlated with functional connectivity in ROI1-RightHemi within primary visual cortex and defined within the VPN (gamma) (r= 0.333, p = 0.030) and negatively correlated with functional connectivity in ROI9-RightHemi within middle frontal gyrus and defined within the VAN (alpha) (r= -0.306, p = 0.036). Finally, audiovisual integration d-prime in case of high load positively correlated with functional connectivity in ROI1-RightHemi and also ROI1-LeftHemi within primary visual cortex and defined within the VPN (gamma) (respectively: r= 0.470, p = 0.002; r= 0.301, p = 0.036). These correlations are summarized in Table 3.10.

For tICA functional connectivity in the VFN (gamma) spatial map we defined the ROIs within the primary visual cortex (ROI1-LeftHemi, ROI1-RightHemi). In the VAN (alpha) spatial map we defined one ROI within the angular gyrus (ROI5-RightHemi), three ROIs within the inferior frontal gyrus (ROI6- RightHemi, ROI7- RightHemi, ROI8- RightHemi), one ROI within the middle frontal gyrus (ROI9-RightHemi) and two ROIs within the cingulate cortex (ROI10-RightHemi, ROI11-RightHemi). In the DAN (alpha) spatial map we defined two ROIs within the middle temporal gyrus (ROI4-LeftHemi, ROI4-RightHemi). Finally, in the DMN (gamma) spatial map we defined two ROIs within the angular gyrus (ROI5-LeftHemi, ROI5-RightHemi). Two significant correlations emerged. Specifically, audiovisual integration accuracy in 2F1S stimuli negatively correlated with functional connectivity in two ROIs defined within the the VAN (alpha) spatial map and specifically the ones within the

cingulate cortex: ROI10-RightHemi (r= -0,282, *p* = 0.041), ROI11-RightHemi (r= -0.277, *p* = 0.040). These correlations are summarized in Table 3.11.

Behavioural indexes	*ROIs*	*Correlation Value*	*p-value (adjusted)*
accuracy in 2F1S stimuli	ROI1-RightHemi (i.e., a ROI within primary visual cortex in right hemisphere) defined within the VPN (gamma) spatial map	0,342	0,030
accuracy in 2F1S stimuli	ROI5-LeftHemi (i.e., a ROI within angular gyrus in left hemisphere) defined within the DMN (beta) spatial map	0,276	0,045
accuracy in 2F1S stimuli	ROI10-RightHemi (i.e., a ROI within cingulate cortex in right hemisphere) defined within the VAN (theta) spatial map	-0,271	0,045
d-prime low load	ROI1-RightHemi (i.e., a ROI within primary visual cortex in right hemisphere) defined within the VPN (gamma) spatial map	0,333	0,030
d-prime low load	ROI9-RightHemi (i.e., a ROI within middle frontal gyrus in right hemisphere) defined within the VAN (alpha) spatial map	-0,306	0,036
d-prime high load	ROI1-RightHemi (i.e., a ROI within primary visual cortex in right hemisphere) defined within the VPN (gamma) spatial map	0,470	0,002
d-prime high load	ROI1-LeftHemis (i.e., a ROI within primary visual cortex in left hemisphere) defined within the VPN (gamma) spatial map	0,301	0,036

Table 3.10. EEG during Resting-State: significant correlations between behavioural indexes and sICA functional connectivity calculated as mean connectivity value within specific ROIs.

Behavioural indexes	*"Brain" Variable: functional connectivity in..*	*Correlation Value*	*p-value (adjusted)*
accuracy in 2F1S stimuli	ROI10-RightHemi (i.e., a ROI within cingulate cortex in right hemisphere) defined within the VAN (alpha) spatial map,	-0,282	0,041
accuracy in 2F1S stimuli	ROI11-RightHemi (i.e., a ROI within cingulate cortex in right hemisphere) defined within the VAN (alpha) spatial map	-0,277	0,040

Table 3.11. EEG during Resting-State: significant correlations between behavioural indexes and tICA functional connectivity calculated as mean connectivity value within specific ROIs.

EEG during Dual-Task

We present below the results pertaining to P1, N1, N2, P2 and P3 components. We provide details on all the main effects, while we include exclusively those interactions highlighted in the analysis section as relevant for addressing our hypothesis. For each of these main effect and interaction, for what concerns analysis of variance, we have reported the F value. For post-hoc pairwise comparisons, we have then reported: the difference between estimated means (in response scale), the standard error (SE) and associated statistics (*t* test).

P1

For P1 component, analysis of variance of the LMM aiming at finding the electrode cluster with the largest signal amplitude showed a main effect of electrode clusters (F (5, 4555) = 254.76, $p < .001$). Specifically, both the Occipital-Central Cluster and the Occipital-Right Cluster exhibited the largest positive signal amplitudes and were not significantly different from each other (Occipital-Central Cluster vs Occipital-Right Cluster: $\Delta\hat{\mu} = 0.039$, SE: 0.043, t (4555) = 0.924, $p = 0.356$; Occipital-Central Cluster vs Occipital-Left Cluster: $\Delta\hat{\mu} = 0.17$, SE: 0.043, t (4555) = 3.989, $p < .001$) (see Figure 3.6A). Consequently, the signal in Occipital-Central Cluster and Occipital-Right Cluster was averaged and considered as dependent variable for the following step.

Analysis of variance of the second LMM revealed the effect of attentional load levels (F (1, 719) = 20.106, $p < .001$), with larger signal amplitude during high than during low attentional load (high vs low: $\Delta\hat{\mu} = 0.252$, SE: 0.056, t (719) = 4.484, $p < .001$) (see Figure 3.6B). Consequently, the cost waveform, defined considering the signal in the high load condition and subtracting the signal in the low load condition (high load – low load), was considered as dependent variable for the following step. Note that in this case the ERP component is positive and, because signal amplitude during high attentional load was larger than during low attentional load (high load > low load), the cost signal is expected to be positive at the group level (high load – low load>0).

Analysis of variance of the last simplified LMM not show any significant effect. The main effect of congruency was non-significant, (F (1, 333) = 1.198, $p = 0.274$), the main effect of flash presentation side was non-significant (F (1, 333) = 2.069, $p = 0.151$), as well as no interaction emerged between congruency and flash presentation side (F (1, 333) = 0.021, $p = 0.884$) (see Figure 3.6C and 3.6D). This simplified LMM is summarized in Table 3.12.

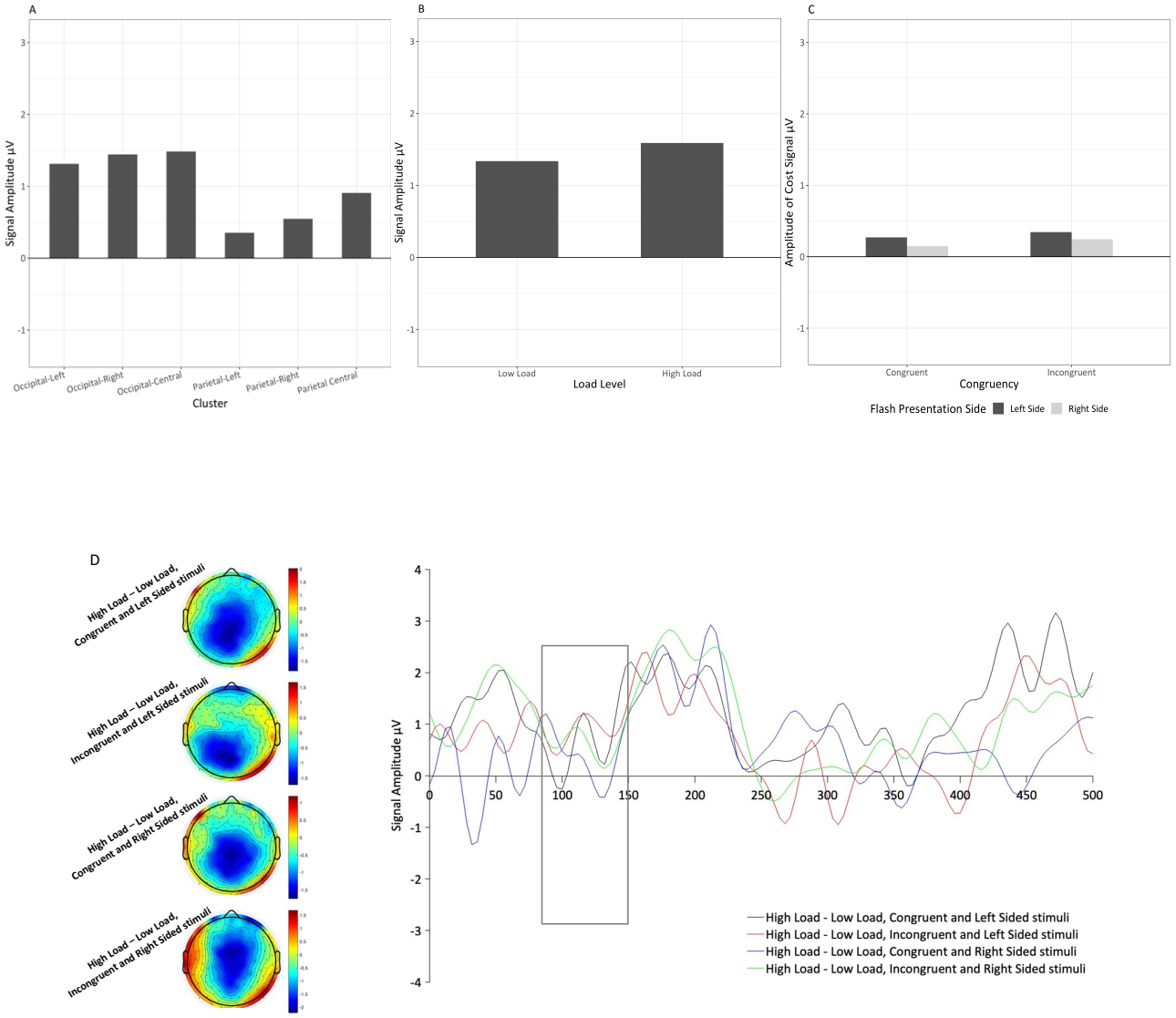

Figure 3.6. EEG during Dual-Task, P1 component: Panel A *displays signal amplitude, as a function of electrode clusters.* ***Panel B*** *displays signal amplitude in the selected cluster, as a function of load levels.* ***Panel C*** *displays amplitude of cost signal, as a function of congruency and flash presentation side.* ***Panel D*** *displays grand average waveforms and scalp maps in the following conditions: High Load – Low Load in Congruent and Left Sided Stimuli, High Load – Low Load in Incongruent and Left Sided Stimuli, High Load – Low Load in Congruent and Right Sided Stimuli, High Load – Low Load in Incongruent and Right Sided Stimuli. Grand average waveforms are derived by plotting the average signal from electrode 137 (part of Occipital-Central Cluster) and electrode 158 (part of Occipital-Right Cluster). Scalp maps are derived by plotting average signal from all electrodes in the time window of P1 component, i.e. 80-150 msec.*

Predictors	*Estimates*	*SE*	*CI*
intercept	0.27	0.10	0.07 – 0.47
congruency (incongruent vs congruent)	0.07	0.11	-0.14 – 0.29
flash presentation side (right vs left)	-0.12	0.11	-0.34 – 0.09
congruency (incongruent) X flash presentation side (right)	0.02	0.16	-0.29 – 0.33
Marginal R^2 = 0.006; AIC = 969.509			

Table 3.12. EEG during Dual-Task: Simplified LMM for P1 component output.

N1

For N1 component, analysis of variance of the LMM aiming at finding the electrode cluster with the largest signal amplitude showed a main effect of electrode clusters (F (4, 3788) = 151.78, $p < .001$). Specifically, the Frontal-Right Cluster exhibited the largest negative signal amplitude (Frontal-Right Cluster vs Frontal-Left Cluster: $\Delta\hat{\mu}$ = -0.112, SE: 0.041, t (3788) = -2,736, p = 0.006; Frontal-Right Cluster vs Frontal-Central Cluster: $\Delta\hat{\mu}$ = -0.136, SE: 0.041, t (3788) = -3.319, p = 0.001) (see Figure 3.7A). Consequently, the signal in Frontal-Right Cluster was considered as dependent variable for the following step.

Analysis of variance of the second LMM revealed the effect of attentional load levels (F (1, 719) = 14,465, $p < .001$), with larger signal amplitude during high attentional load than during low attentional load (high vs low: $\Delta\hat{\mu}$ = -0.228, SE: 0.06, t (719) = - 3.803, $p < .001$) (see Figure 3.7B). Consequently, the cost waveform, defined considering the signal in the high load condition and subtracting the signal in the low load condition (high load – low load), was considered as dependent variable for the following step. Note that in this case the ERP component is negative and, because signal amplitude during high attentional load was larger than during low attentional load (high load > low load), the cost signal is expected to be negative at the group level (high load – low load<0).

Analysis of variance of the last simplified LMM showed a non-significant main effect of congruency, (F (1, 333) = 0.278, p = 0.598). Additionally, there was a significant main effect of flash presentation side (F (1, 333) = 9.825, $p < .001$), as well as an interaction between congruency and flash presentation side (F (1, 333) = 12.644, $p < .001$). More specifically the amplitude of the cost signal related to left sided flashes was smaller than the one related to right sided flashes in case of incongruent (left vs right: $\Delta\hat{\mu}$ = 0.591, SE: 0.125, t (333) = 4.731, $p < .001$) but not in the case of congruent stimuli (left vs right: $\Delta\hat{\mu}$ = -0.037, SE: 0.125, t (333) = -0.298, p = 0.766) (see Figure 3.7C and 7D). This simplified LMM is summarized in Table 3.13.

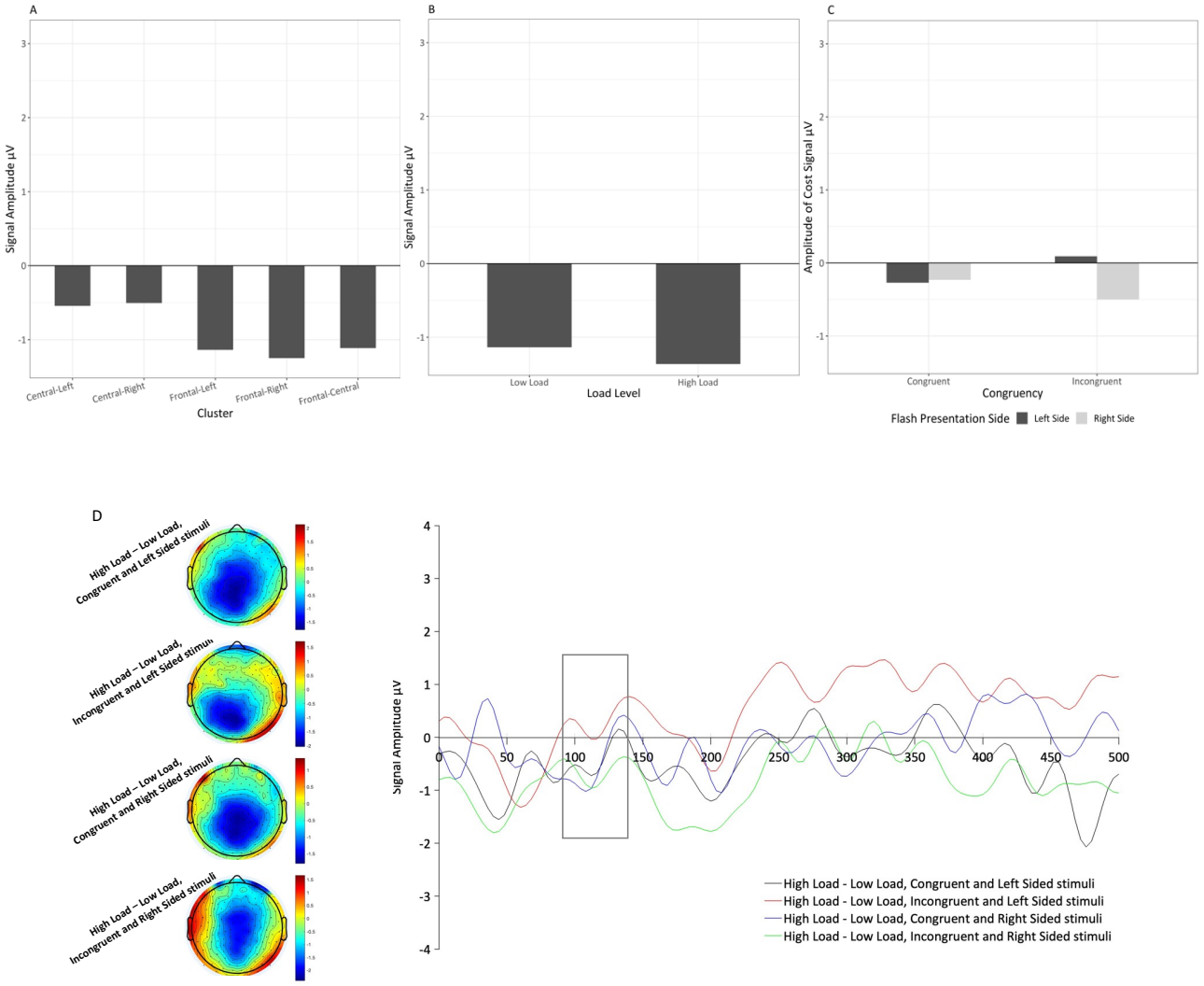

Figure 3.7. EEG during Dual-Task, N1 component: Panel A *displays signal amplitude, as a function of electrode clusters.* ***Panel B*** *displays signal amplitude in the selected cluster, as a function of load levels.* ***Panel C*** *displays amplitude of cost signal, as a function of congruency and flash presentation side.* ***Panel D*** *displays grand average waveforms and scalp maps in the following conditions: High Load – Low Load in Congruent and Left Sided Stimuli, High Load – Low Load in Incongruent and Left Sided Stimuli, High Load – Low Load in Congruent and Right Sided Stimuli, High Load – Low Load in Incongruent and Right Sided Stimuli. Grand average waveforms are derived by plotting the signal from electrode 213 (part of Frontal-Right Cluster). Scalp maps are derived by plotting average signal from all electrodes in the time window of N1 component, i.e. 90-140 msec.*

Predictors	*Estimates*	*SE*	*CI*
intercept	-0.27	0.10	-0.46 – -0.08
congruency (incongruent vs congruent)	0.36	0.12	0.12 – 0.61
flash presentation side (right vs left)	0.04	0.12	-0.21 – 0.28
congruency (incongruent) X flash presentation side (right)	-0.63	0.18	-0.98 – -0.28
Marginal R^2 = 0.052; AIC = 1023.418			

Table 3.13. EEG during Dual-Task: Simplified LMM for N1 component output.

N2

For N2 component, analysis of variance of the LMM aiming at finding the electrode cluster with the largest signal amplitude showed a main effect of electrode clusters (F (5, 4555) = 32.172, $p < .001$). Specifically, both the Parietal-Left Cluster and the Parietal-Right Cluster exhibited the largest negative signal amplitudes and were not significantly different from each other (Parietal-Left Cluster vs Parietal-Right Cluster: $\Delta\hat{\mu}$ = -0.055, SE: 0.057, *t* (4555) = -0.978, $p = 0.328$; Parietal-Left Cluster vs Occipital-Central Cluster: $\Delta\hat{\mu}$ = -0.334, SE: 0.057, *t* (4555) = -5.883, $p < .001$) (see Figure 3.8A). Consequently, the signal in Parietal-Left Cluster and the Parietal-Right Cluster was averaged and considered as dependent variable for the following step.

Analysis of variance of the second LMM revealed the effect of attentional load levels (F (1, 719) = 27.352, $p < .001$), with larger signal amplitude during high attentional load than during low attentional load (high vs low: $\Delta\hat{\mu}$ = -0.167, SE: 0.032, *t* (719) = -5.230, $p < .001$) (see Figure 3.8B). Consequently, the cost waveform, considering the signal in the high load condition and subtracting the signal in the low load condition (high load – low load), was considered as dependent variable for the following step. Note that in this case the ERP component is negative and, because signal amplitude during high attentional load was larger than during low attentional load (high load > low load), the cost signal is expected to be negative at the group level (high load – low load<0).

Analysis of variance of the last simplified LMM showed a significant main effect of congruency (F (1, 333) = 22.696, $p < .001$) with amplitude of cost signal during congruent stimuli being larger than during incongruent stimuli (congruent vs incongruent: $\Delta\hat{\mu}$ = -0.27, SE: 0.057, *t* (333) = -4.764, $p < .001$). Additionally, there was a non-significant main effect of flash presentation side (F (1, 333) = 0.001, $p = 0.975$) and a significant interaction between congruency and flash presentation side (F (1, 333) = 4.805, $p = 0.029$). However post-hoc comparisons revealed that the amplitude of cost signal related to left sided flashes was not different from the one related to right sided flashes in case of congruent (left vs right: $\Delta\hat{\mu}$ = 0.126, SE: 0.08, *t* (333) = 1.572, $p = 0.127$), as well as in the case of incongruent stimuli (left vs right: $\Delta\hat{\mu}$ = -0.123, SE: 0.08, *t* (333) = -1.528, $p = 0.127$) (see Figure 3.8C and 8D). This simplified LMM is summarized in Table 3.14.

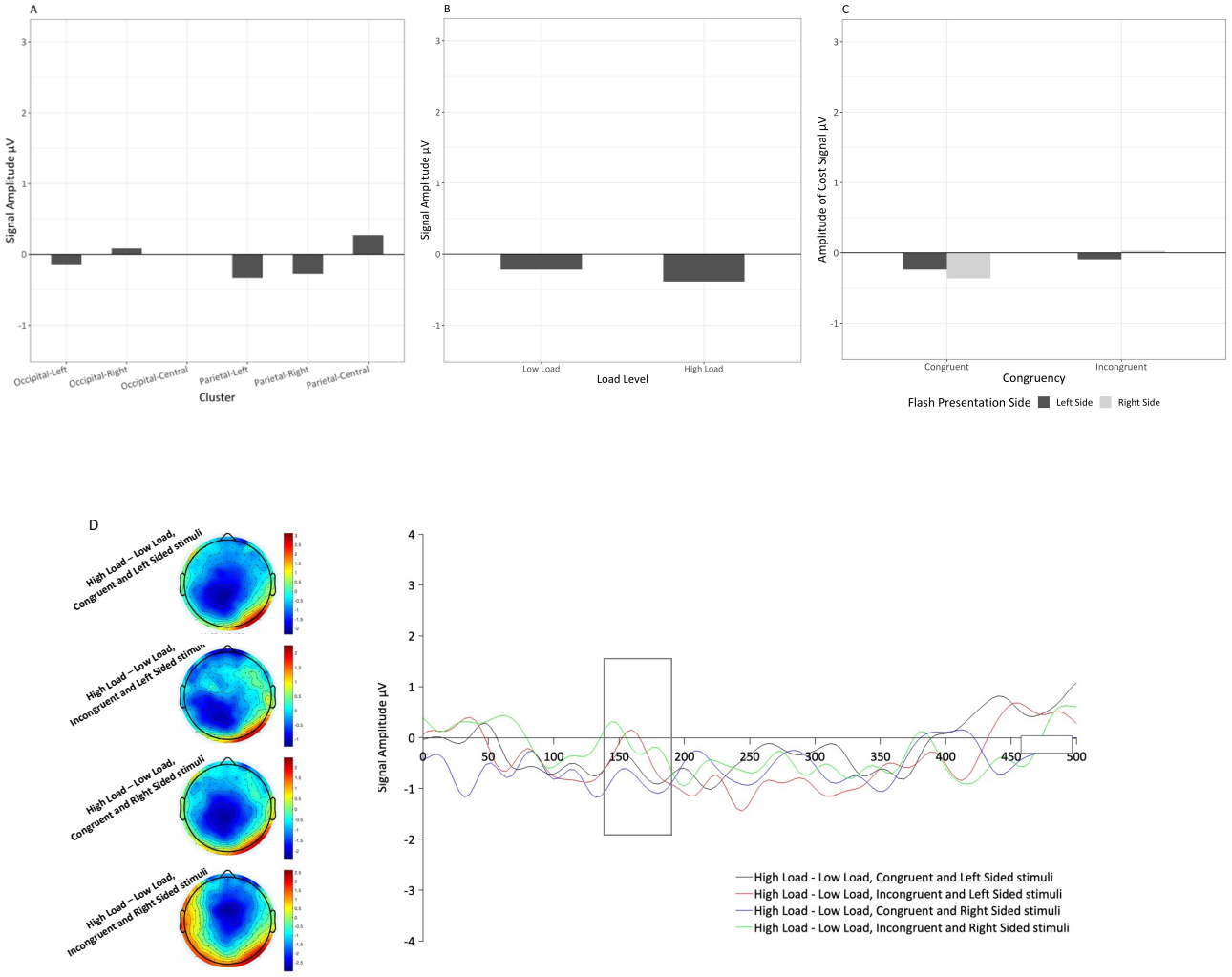

Figure 3.8. EEG during Dual-Task, N2 component: Panel A *displays signal amplitude, as a function of electrode clusters.* ***Panel B*** *displays signal amplitude in the selected cluster, as a function of load levels.* ***Panel C*** *displays amplitude of cost signal, as a function of congruency and flash presentation side.* ***Panel D*** *displays grand average waveforms and scalp maps in the following conditions: High Load – Low Load in Congruent and Left Sided Stimuli, High Load – Low Load in Incongruent and Left Sided Stimuli, High Load – Low Load in Congruent and Right Sided Stimuli, High Load – Low Load in Incongruent and Right Sided Stimuli. Grand average waveforms are derived by plotting the average signal from electrode 86 (part of Parietal-Left Cluster) and electrode 162 (part of Parietal-Left Cluster). Scalp maps are derived by plotting average signal from all electrodes in the time window of N2 component, i.e. 140-180 msec.*

Predictors	*Estimates*	*SE*	*CI*
intercept	-0.24	0.07	-0.37 – -0.10
congruency (incongruent vs congruent)	0.15	0.08	-0.01 – 0.3
flash presentation side (right vs left)	-0.13	0.08	-0.28 – 0.03
congruency (incongruent) X flash presentation side (right)	0.25	0.11	0.03 – 0.47
Marginal R^2 = 0.055; AIC = 711.698			

Table 3.14. EEG during Dual-Task: Simplified LMM for N2 component output.

P2

For P2 component, analysis of variance of the LMM aiming at finding the electrode cluster with the largest signal amplitude showed a main effect of electrode clusters (F (2, 2254) = 176.94, $p < .001$). Specifically, the Parietal-Central Cluster exhibited the largest positive signal amplitude (Parietal-Central Cluster vs Parietal-Left Cluster: $\Delta\hat{\mu} = 0.575$, SE: 0.043, t (2254) = 13.404, $p < .001$; Parietal-Central Cluster vs Parietal-Right Cluster: $\Delta\hat{\mu} = 0.778$, SE: 0.043, t (2254) = 18.133, $p < .001$) (see Figure 3.9A). Consequently, the signal in Parietal-Central Cluster was considered as dependent variable for the following step.

Analysis of variance of the second LMM revealed the effect of attentional load levels (F (1, 719) = 172.18, $p < .001$), with smaller signal amplitude during high attentional load than during low attentional load (high vs low: $\Delta\hat{\mu} = -0.655$, SE: 0.05, t (719) = -13.122, $p < .001$) (see Figure 3.9B). Consequently, the cost waveform, defined considering the signal in the high load condition and subtracting the signal in the low load condition (high load – low load), was considered as dependent variable for the following step. Note that in this case the ERP component is positive and, because signal amplitude during high attentional load was smaller than during low attentional load (high load < low load), the cost signal is expected to be negative at the group level (high load – low load<0).

Analysis of variance of the last simplified LMM not show any significant effect. The main effect of congruency was non-significant main effect of congruency (F (1, 333) = 0.506, $p = 0.477$), the main effect of flash presentation side was non-significant (F (1, 333) = 0.175, $p = 0.676$), as well as no interaction emerged between congruency and flash presentation side (F (1, 333) = 1.462, $p = 0.2275$ (see Figure 3.9C and 3.9D). This simplified LMM is summarized in Table 3.15.

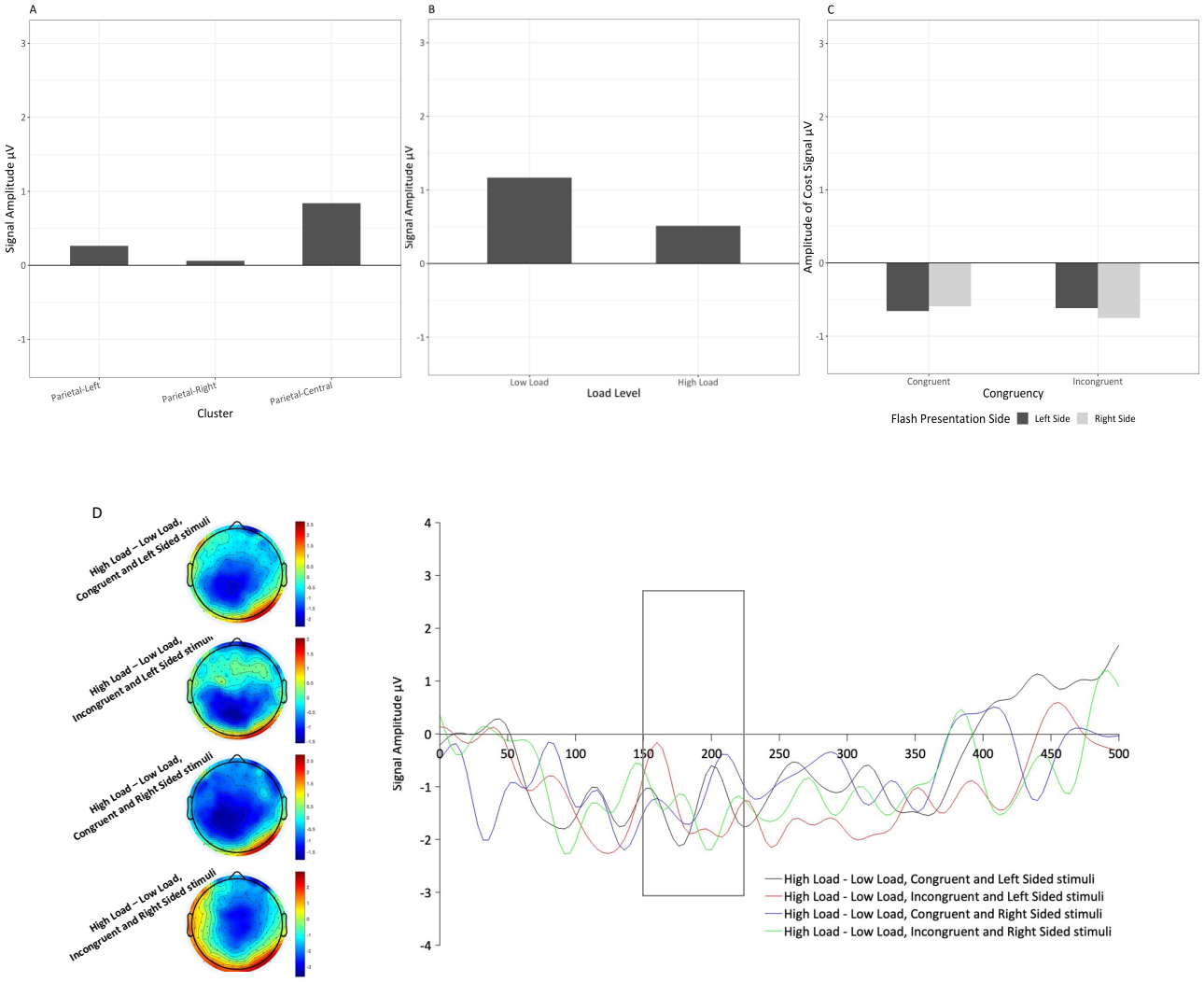

Figure 3.9. EEG during Dual-Task, P2 component: Panel A *displays signal amplitude, as a function of electrode clusters.* ***Panel B*** *displays signal amplitude in the selected cluster, as a function of load levels.* ***Panel C*** *displays amplitude of cost signal, as a function of congruency and flash presentation side.* ***Panel D*** *displays grand average waveforms and scalp maps in the following conditions: High Load – Low Load in Congruent and Left Sided Stimuli, High Load – Low Load in Incongruent and Left Sided Stimuli, High Load – Low Load in Congruent and Right Sided Stimuli, High Load – Low Load in Incongruent and Right Sided Stimuli. Grand average waveforms are derived by plotting the signal from electrode 119 (part of Parietal-Central Cluster). Scalp maps are derived by plotting average signal from all electrodes in the time window of P2 component, i.e. 150-230 msec.*

Predictors	*Estimates*	*SE*	*CI*
intercept	-0.66	0.13	-0.91 – -0.40
congruency (incongruent vs congruent)	0.04	0.12	-0.19 – 0.27
flash presentation side (right vs left)	0.07	0.12	-0.17 – 0.30
congruency (incongruent) X flash presentation side (right)	-0.20	0.17	-0.53 – 0.13
Marginal R^2 = 0.003; AIC = 1046.928			

Table 3.15. EEG during Dual-Task: Simplified LMM for P2 component output.

P3

For P3 component, analysis of variance of the LMM aiming at finding the electrode cluster with the largest signal amplitude showed a main effect of electrode clusters (F (2, 2254) = 400.71, $p < .001$). Specifically, the Parietal-Central Cluster exhibited the largest positive signal amplitude (Parietal-Central Cluster vs Parietal-Right Cluster: $\Delta\hat{\mu}$ = 0.980, SE: 0.043, t (2254) = 23.038, $p < .001$; Parietal-Central Cluster vs Parietal-Left Cluster: $\Delta\hat{\mu}$ = 1.097, SE: 0.043, t (2254) = 25.767, $p < .001$) (see Figure 3.10A). Consequently, the signal in Parietal-Central Cluster was considered as dependent variable for the following step.

Analysis of variance of the second LMM revealed the effect of attentional load levels (F (1, 719) = 44.929, $p < .001$), with smaller signal amplitude during high attentional load than during low attentional load (high vs low: $\Delta\hat{\mu}$ = -0.367, SE: 0.055, t (719) = -6.703, $p < .001$) (see Figure 3.10B). Consequently, the cost waveform, defined considering the signal in the high load condition and subtracting the signal in the low load condition (high load – low load) was considered as dependent variable for the following step. Note that in this case the ERP component is positive and, because signal amplitude during high attentional load was smaller than during low attentional load (high load < low load), the cost signal is expected to be negative at the group level (high load – low load<0).

Analysis of variance of the last simplified LMM showed: significant main effect of congruency (F (1, 333) = 5.393, p = 0.021) with amplitude of cost signal during congruent stimuli being smaller than during incongruent stimuli (congruent vs incongruent: $\Delta\hat{\mu}$ = 0.241, SE: 0.104, t (333) = 2.322, p = 0.021), non-significant main effect of flash presentation side (F (1, 333) = 0.126, p = 0.723), as well as no interaction between congruency and flash presentation side (F (1, 333) = 1.291, p = 0.257) (see Figure 3.10C and 3.10D). This simplified LMM is summarized in Table 3.16.

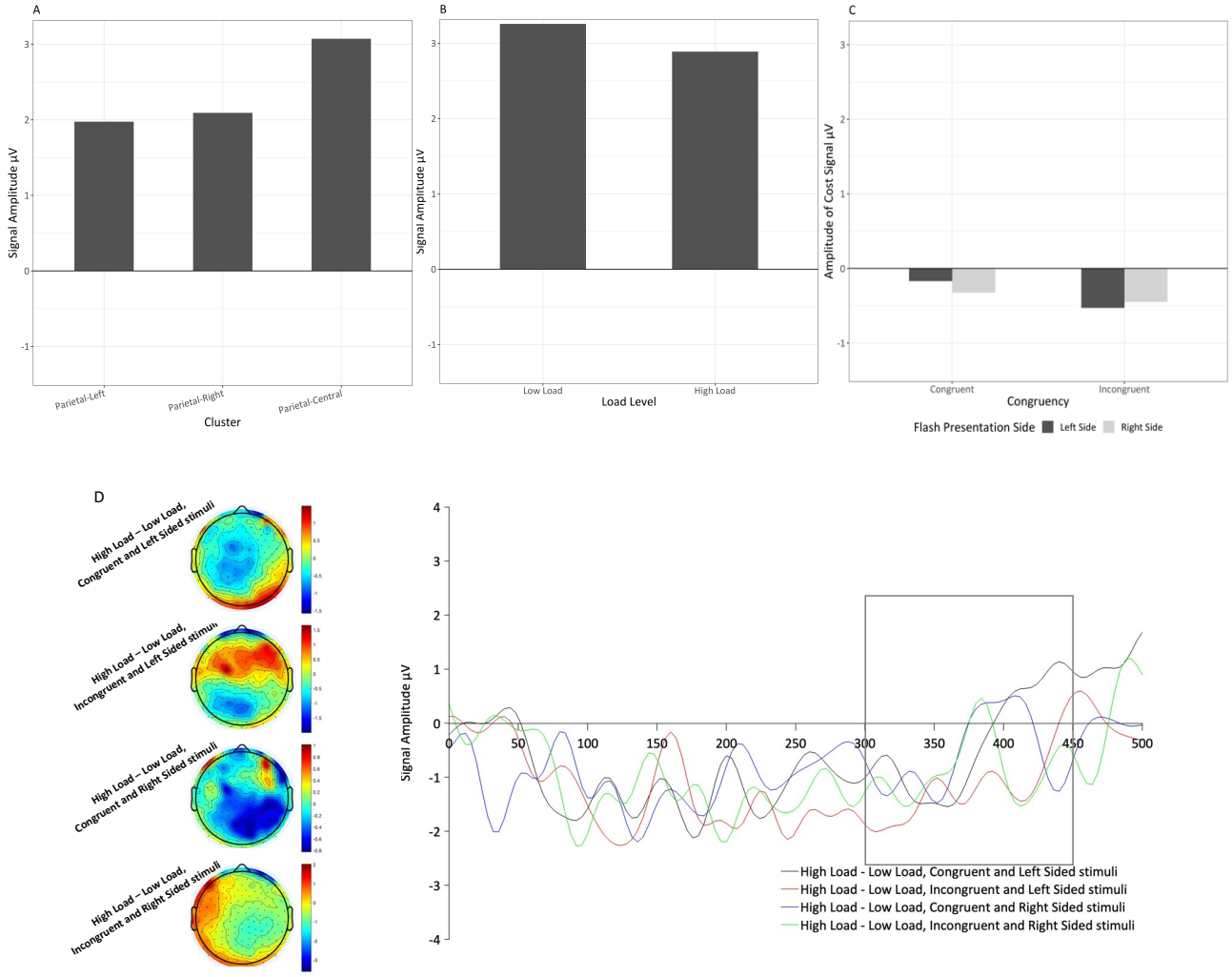

Figure 3.10. EEG during Dual-Task, P3 component: Panel A *displays signal amplitude, as a function of electrode clusters.* ***Panel B*** *displays signal amplitude in the selected cluster, as a function of load levels.* ***Panel C*** *displays amplitude of cost signal, as a function of congruency and flash presentation side.* ***Panel D*** *displays grand average waveforms and scalp maps in the following conditions: High Load – Low Load in Congruent and Left Sided Stimuli, High Load – Low Load in Incongruent and Left Sided Stimuli, High Load – Low Load in Congruent and Right Sided Stimuli, High Load – Low Load in Incongruent and Right Sided Stimuli. Grand average waveforms are derived by plotting the signal from electrode 119 (part of Parietal-Central Cluster). Scalp maps are derived by plotting average signal from all electrodes in the time window of P3 component, i.e. 300-450 msec.*

Predictors	*Estimates*	*SE*	*CI*
intercept	-0.17	0.13	-0.42 – 0.08
congruency (incongruent vs congruent)	-0.36	0.15	-0.65 – -0.07
flash presentation side (right vs left)	-0.15	0.15	-0.44 – 0.13
congruency (incongruent) X flash presentation side (right)	0.24	0.21	-0.17 – 0.64
Marginal R^2 = 0.014*; AIC* = 1173.266			

Table 3.16. EEG during Dual-Task: Simplified LMM for P3 component output.

In conclusion, we extracted: P1 component averaging the signal from Occipital-Central and Occipital-Right Clusters; N1 component averaging the signal from Frontal-Right Cluster; N2 component averaging the signal from Parietal-Left and Parietal-Right Clusters; P2 component and P3 components averaging the signal from Parietal-Central Cluster. For all the investigated components emerged a significant effect of attentional load levels. Specifically, signal amplitude was larger during high than during low attentional load in P1, N1 and N2 components, while it was smaller during high attentional load than during low attentional load in P2and P3 components. Crucially, H3.1 was confirmed for N2 and P3 components. Specifically, amplitude of cost signal during congruent stimuli was significantly larger than during incongruent stimuli in N2, while amplitude of cost signal during congruent stimuli was significantly smaller than during incongruent stimuli in P3. Moreover, also H3.2 was verified for N1 component. Specifically, amplitude of the cost signal related to left sided flashes was significantly smaller than the one related to right sided flashes in case of incongruent but not in the case of congruent stimuli.

3.6 Discussion

We conducted an experiment using a computer-based dual-task identical to that described in Experiment 2 of Chapter 2 and recording high-density EEG activity during resting-state and simultaneously with the task.

Dual-Task

Firstly, we analysed dual-task performance. The dual-task included a primary audiovisual integration task, characterized by briefly-presented stimuli inducing the SIFI on either the left or right side of the screen, along with a concurrent secondary task that required additional processing. Specifically, the secondary task was a visual discrimination task, that enabled us to manipulate attentional load *online*, as the stimuli used to vary the load were presented simultaneously with the lateralized audiovisual integration stimuli. This dual-task was selected for the present investigation because it is characterized by the absence of perceptual differences between high and low attentional load conditions. Instead, the variations are exclusively in the instructions, making it suitable for an EEG study and particularly appropriate for ERPs analysis (The Hillyard Principle, see Luck (2014)). Similarly, to Experiment 2 of Chapter 2 we expected: (H1.1) audiovisual integration accuracy would

be significantly lower and SIFI would emerge in incongruent audiovisual integration stimuli, namely 1F2S stimuli and 2F1S stimuli, (H1.2) the emergence of SIFI would significantly increase under high attentional load, (H1.3) especially in case of left sided flashes. This expectation was based on the premise that if the absence of load-induced spatial processing asymmetries observed in the two experiments of Chapter 2 was due to increased experimental noise related to the online setting, it would manifest differently in the lab setting.

Similarly, to the experiment in the online setting, we found that secondary task accuracy was significantly lower when participants were under high attentional load. Therefore, it was possible to confirm the effectiveness of the secondary task in inducing attentional load variations as expected. Moreover, H1.1 was clearly confirmed in the lab setting: audiovisual integration accuracy was significantly lower and SIFI emerged in incongruent audiovisual integration stimuli, i.e. 1F2S stimuli and 2F1S stimuli. Unlike the online setting, in the lab setting we observed a significant difference between incongruent 1F2S and 2F1S stimuli. This variation is however not unexpected, considering that fission and fusion illusion types are known to remarkably differ at an individual level. H1.2 was also confirmed in the lab setting: the occurrence of SIFI significantly increased under high attentional load. Finally, H1.3 found no support in the lab setting, just as in the online setting, as the emergence of SIFI under high attentional load did not display spatial asymmetry.

In conclusion, we successfully extended to the lab setting the fact that with our manipulations load-induced spatial processing asymmetries were clearly absent at the behavioural level.

EEG during Resting-State

Secondly, we conducted an analysis of EEG recorded during a resting-state period preceding the task.

More specifically, we assessed intrinsic functional connectivity using Liu et al. (2017)'s method to extract EEG-RSNs. This approach employs a semi-automatic data cleaning procedure coupled with an automatic analysis pipeline, comprising three steps: “standard head model creation”, “reconstruction of sources” and “ICA-based functional connectivity calculation”. ICA, a technique aimed at dividing data into maximally independent groups, forms a key part of this approach and allows a completely data-driven calculation of functional connectivity. We applied ICA in both its spatial (sICA) and temporal (tICA) variants, where sICA achieves maximum spatial independence and tICA guarantees temporal independence (Calhoun et al., 2001, 2009; Smith et al., 2012).

Subsequently, we performed a correlation analysis to see if “behavioural indexes” could be predicted by “brain indexes”. The behavioural indexes we focused on, identified as informative in the behavioural analysis, included: audiovisual integration accuracy across all incongruent 1F2S stimuli, audiovisual integration accuracy across all incongruent 2F1S stimuli, audiovisual integration d-prime across all cases of low attentional load and audiovisual integration d-prime across all cases of high attentional load. These behavioural indexes were correlated with brain indexes, namely, average functional connectivity values of specific EEG-RSNs and ROIs part of those networks, believed to be potentially involved in SIFI perception under conditions of increased attentional load on the base of the literature (see analysis section for further details about EEG-RSNs and ROIs selection). We expected (H2) significant correlations at both network and region of interest levels, yet due to the pioneering nature of our analysis, it was not possible to have expectations about the exact nature or direction of these correlations.

At the network level, as well as at the ROIs level, we found various significant correlations for both sICA and tICA functional connectivity. Here we focus the discussion on the ones we consider the most relevant.

First of all, the significant correlations between behavioural indexes and functional connectivity either in the AN, the VFN or the VPN, which are all networks that include areas dedicated to auditory or visual processing, were all observed in the gamma frequency band (30-80 Hz).

Gamma-band activity is known to work in sync with other frequency patterns like beta, playing a role in the anticipatory coordination of various brain regions, which is essential for the top-down shaping of perception (Engel et al., 2001). Furthermore, it has been associated to a wide range of cognitive functions, including feature binding (Herrmann et al., 2010) and early attention-based modulation during multisensory perception (Senkowski et al., 2005). During SIFI tasks pre-stimulus (Kaiser et al., 2019) and post-stimulus (Bhattacharya et al., 2002; Mishra et al., 2007) gamma-band activity over occipital regions predicts illusory perception. This might reflect a combination of feature binding and early attention-based modulation during multisensory perception. Additionally, it has been reported a positive correlation between gamma-aminobutyric acid (GABA) concentration in the superior temporal sulcus and both gamma power and SIFI perception (Balz et al., 2016), a finding that aligns with the well-known role of GABA neurotransmission in generating gamma-band activity.

Another finding we consider noteworthy is the presence of significant correlations between audiovisual integration accuracy in incongruent stimuli and sICA functional connectivity within the

VAN. Specifically, we found that audiovisual integration accuracy in 1F2S stimuli negatively correlated with sICA functional connectivity within the VAN in the theta frequency band. Conversely, audiovisual integration accuracy in 2F1S stimuli positively correlated with sICA functional connectivity in VAN in the alpha frequency band.

The fact that audiovisual integration accuracy in incongruent stimuli is predicted by functional connectivity in VAN is not surprising given its role during the detection of salient targets and the fact that incongruent stimuli might be particularly salient because they create a sensory conflict. The fact audiovisual integration accuracy in 1F2S and 2F1S stimuli is predicted by functional connectivity in different frequency bands is consistent with the distinct spatio-temporal activation patterns characterizing fission and fusion illusions (Mishra et al., 2007, 2008; Watkins et al., 2006, 2007). For instance, Watkins et al. (2007) found that while regions of the right superior temporal sulcus exhibit similar responses to both illusions, the primary visual cortex displays contrasting activation patterns: activity increases with 1F2S stimuli generating the fission illusion and diminishes with 2F2S stimuli generating the fusion illusion (Watkins et al., 2006, 2007).

Theta power is known to reflect the recruitment of executive control in interference situations and across different types of conflicts (Nigbur et al., 2011). Furthermore, its role has already been demonstrated in ambiguous audiovisual contexts (Michail et al., 2021; Morís Fernandez et al., 2018). Therefore, the level of functional connectivity in the theta band at rest may also be implicated in the conflict that arises during incongruent audiovisual integration stimuli, in which if the conflict between visual and auditory information is not solved, SIFI is generated. Alpha power is known to reflect inhibitory control (Jensen & Mazaheri, 2010; Klimesch et al., 2007). Additionally, it predicts illusory perception during SIFI tasks (Cecere et al., 2015; Keil & Senkowski, 2017). Therefore, an increase in the level of functional connectivity in the alpha band at rest might indicate higher in inhibitory abilities, which could assist in suppressing automatic responses, such as the illusory responses during incongruent audiovisual integration stimuli.

Finally, it is interesting the presence of significant correlations between audiovisual integration d-prime and tICA functional connectivity within the DAN and VAN. Specifically, we found that audiovisual integration d-prime in case of low load negatively correlated with tICA functional connectivity within DAN in the alpha frequency band. Conversely, audiovisual integration d-prime in case of high load positively correlated with tICA functional connectivity in VAN in the alpha frequency band. It is possible to speculate that this difference might derive from a different involvement of DAN and VAN depending on load level. It is possible that under low load conditions

mostly DAN drives allocation of attention in space, but when attentional load is increased, sustaining the task through top-down processes becomes more complex, and responses become more guided by the salience of the stimuli thanks to the VAN. The difference in the direction of correlation might be attributed to the fact that core regions of the VAN network potentially code for both matches and mismatches between expected and actual stimuli (Doricchi et al., 2022).

In conclusion, this analysis offers initial evidence that behavioural indexes of SIFI perception during increased attentional load can be predicted by brain indexes derived from EEG recordings during a resting-state period. These findings underscore the significance of intrinsic brain organization also in shaping SIFI perception and in how it is modulated when attentional load is varied in a multitasking scenario.

EEG during Dual-Task

Thirdly, we conducted an analysis of EEG recorded during dual-task. More specifically, in line with previous studies (Bonato et al., 2015; O'Connell et al., 2011; Romeo et al., 2019) and with the grand average visual inspection, we computed the following early ERP components: P1 (80-150 ms), N1 (90-140 ms), N2 (140-180 ms), P2 (150-230 ms) and P3 (300-450 ms). Additionally, we calculated a *cost waveform* considering the signal in the high load condition and subtracting the signal in the low load condition (high load – low load) (similar to: Bonato et al., 2015 - cost analysis).

To identify ERP modulations linked to the enhanced perception of SIFI under high attentional load we expected (H3.1) the cost waveform to be significantly different for congruent stimuli and incongruent stimuli (i.e., the ones in which SIFI is usually generated). Additionally, to confirm that spatial processing can be asymmetrically influenced by levels of attentional load during multitasking at the neural level we expected (H3.2) the cost waveform to be significantly different in incongruent stimuli (i.e., the one in which SIFI is usually generated) following left-sided stimuli or right-sided stimuli.

First of all, for all the investigated components emerged a significant effect of attentional load levels on signal amplitude. Specifically, signal amplitude was larger during high than during low attentional load in P1, N1 and N2 components, while it was smaller during high attentional load than during low attentional load in P2 and P3 components. It is important to emphasize that the dual-task employed was characterized by the lack of perceptual variances between high and low attentional load conditions. Consequently, this outcome stands as a pure measurement of the top-down attentional

load induced by dual-tasking. Additionally, it is worth noting that the administration of the dual-tasks in blocks, in which the two visual discrimination conditions were alternated (i.e., low load and high load), may have played against the increase especially of N1 amplitude observed in the high load condition, as this component is highly refractory (i.e., if a stimulus at a particular location is preceded by another stimulus at the same location at a short delay, the response to the second stimulus is greatly reduced) (Luck et al., 1990). The result relative to the early P1, N1 and N2 components replicates, for what concerns the direction of the effect, what found by previous studies (Bonato et al., 2015; Romeo et al., 2019). P1 components is known to be associated with selective attention (Hillyard et al., 1998; Luck et al., 2000) and with subject's state of arousal (Vogel & Luck, 2000). N1 component is known to be associated with spatial attention (Hillyard et al., 1998; Mangun, 1995) and with discriminative processing (Hopf et al., 2002; Ritter et al., 1979; Vogel & Luck, 2000). N2 component, especially when found over more posterior than anterior sites like in our case (i.e. "N2c"), is known to be associated with the process of categorizing a stimulus (Renault et al., 1982). Therefore, this finding confirms that all these cognitive processes, already during the earliest phases of stimulus processing, were affected by increased attentional load and, consequently, by the availability of unspecific attentional resources. Similarly, also the result relative to the late P2 and P3 components replicates what found by previous studies (O'Connell et al., 2011). P2 component and P3 component, especially when found over more posterior than anterior sites like in our case, are known to be associated with the processing of task-relevant stimuli. P2 usually occurs when the target is defined by fairly simple stimulus features, while P3 can occur for arbitrarily complex stimuli (Luck & Hillyard, 1994; Polich, 2011). Additionally, P3 amplitude variations have been associated to changes in task difficulty, and in the case of our finding, P3 amplitude might have decreased because participants become more uncertain about their responses with increased attentional load (Kok, 2001).

Secondly, we were able to identify ERP modulations linked to the enhanced perception of SIFI under high attentional load. H3.1 was indeed confirmed for N2 and P3 components. Specifically, amplitude of cost signal during congruent stimuli was significantly larger than during incongruent stimuli in N2. Differently, amplitude of cost signal during congruent stimuli was significantly smaller than during incongruent stimuli in P3. While interpreting the finding related to N2 remains challenging based on its functional significance, the interpretation of the finding concerning P3 can again be linked to task difficulty. Regarding P3, the amplitude difference between high load and low load was most

pronounced with incongruent stimuli, likely because participants encountered the highest level of uncertainty about their responses in this condition.

Finally, we were able to confirm that spatial processing can be asymmetrically influenced by levels of attentional load during multitasking at the neural level. H3.2 was indeed verified for N1 component. Specifically, amplitude of the cost signal related to left sided flashes was significantly smaller than the one related to right sided flashes in case of incongruent but not in the case of congruent stimuli. This means that the amplitude difference between high load and low load was most pronounced with incongruent stimuli presented on the right than on the left. If this finding was confirmed, it would imply that, during the initial stages of stimulus processing, neural markers for spatial processing operate asymmetrically in case of higher attentional engagement. However, these asymmetries might be compensated in later stages of stimulus processing. Consequently, with this specific paradigm, the allocation of attentional resources in space, as well as susceptibility to illusions, do not appear asymmetric at the behavioural level. Note that we refrained from interpreting N1 topography because, despite the potentially relevant implications, the absence of precise source localization imply we cannot conclusively determine that ERPs observed over the right hemisphere's electrodes originate from sources directly beneath them.

In conclusion, this analysis yielded several findings. Firstly, across all investigated components, there was a noticeable impact of attentional load levels on signal amplitude. Secondly, we identified N2 and P3 modulations associated with the presentation of incongruent stimuli, that are the ones in which SIFI is usually generated, during different levels of attentional load. Lastly, we established that spatial processing can be asymmetrically influenced by varying levels of attentional load during multitasking at the neural level, as indicated by N1 modulations, though further confirmation of these results is warranted. These findings offer valuable insights into the intricate relationship between spatial processing, multisensory perception and neural processes in a multitasking scenario.

3.7 Supplementary

Dual-Task: Model selection for block variable

For each model, a model selection was undertaken to decide how to handle a variable which coded for the block number, independently from the experimental condition characterizing the block.
In all cases we compared Akaike's Information Criterion (AIC) and the Bayesian Information Criterion (BIC) of a model “b0” without the block variable, a model “b” with the block variable coded as fixed effect, a model “b1” with the block variable coded as random intercept and a model “b2” with the block variable coded as random slope nested within participants. The “b2” model resulted significatively different from other models for the GLMM analysing secondary task accuracy and the GLMM assessing audiovisual integration accuracy (in all cases $p < .001$), exhibiting the lowest AIC and BIC values. When considering the LMM examining audiovisual integration d', the “b2” model resulted significatively different from other models ($p < .001$), exhibiting the lowest AIC (but not BIC). Following these results in all cases the block variable was coded as random slope nested within participants. This modelling choice captured the idea that time on task might have different effects at the individual level. Following this modelling choice any possible effect of increased attentional load should not be influenced by the confounding effect of reduced sustained attention over time on task.

Dual-Task: Effect of hand-used to respond

In the model with audiovisual integration accuracy and also in the model with audiovisual integration d' as dependent variable, we evaluated the following: 1) presence of a main effect of hand-used to respond, to assess whether there was a facilitation in responding with the dominant hand compared to the non-dominant hand 2) presence of an interaction between hand-used to respond and flash presentation side, to determine whether there was a stimulus-response compatibility effect, i.e. a facilitation in responding to stimuli presented on the right side with the dominant hand (which was consistently the right hand, as all participants were right-handed) and facilitation in responding to left-sided stimuli with the non-dominant hand (which was consistently the left hand, as all participants were right-handed). In the model with audiovisual integration accuracy as dependent variable, analysis of deviance highlighted no effect of hand-used to respond

(X^2 (1) = 2.846, p = 0.0916) as well as no interaction between hand-used to respond and flash presentation side (X^2 (1) = 0.000, p = 0.999). In the model with audiovisual integration d' as dependent variable, analysis of deviance highlighted no effect of hand-used to respond (F (1, 56) = 1.382, p = 0.245) as well as no interaction between hand-used to respond and flash presentation side (F (1, 669.56) = 0.043, p = 0.836).

CONCLUSIVE REMARKS AND FUTURE DIRECTIONS

The common thread weaving through the diverse contributions presented in this thesis was a detailed investigation into load-induced spatial processing modulations in multitasking scenarios. The work was motivated by the fact that these modulations could significantly impact real-life situations, influencing aspects ranging from safety, efficiency and user experience, in both clinical and healthy populations.

We started considering, in ***Chapter 1***, the damaged cognitive system, where these modulations are often extremely pronounced (e.g., Blini et al., 2016; Bonato, 2012; Bonato et al., 2010). Specifically, we tested the impact of attentional load upon spatial processing in an ultra-chronic right hemisphere damaged patient. Despite his ceiling performance in classic paper and pencil test, he showed load-induced spatial processing modulations and specifically biases toward the ipsilesional space (i.e. omissions in the contralesional space) when attentional load was increased. This finding confirmed once more that patients with apparently recovered forms of neglect may, instead, simply use compensatory strategies to counterbalance contralesional spatial processing deficits. In such cases, biases toward the ipsilesional space can be observed, but their detection is contingent on the task used, which must consume a significant amount of resources to the extent that compensation becomes impossible. Surprisingly, the effect was temporally retrospective. For the first time we presented lateralized targets before the stimuli used to implement the load manipulation. Therefore, targets were omitted as the result of increased attentional load even if they were not perceptually present during the load manipulation. This implies that the attentional load increase was so disruptive to affect the awareness of previously processed target stimuli. Additionally, the effect was modulated not only by top-down and primarily cognitive factors (i.e., changes in attentional load), but also by bottom-up and purely perceptual aspects (i.e. changes in target stimuli diameter). Puzzlingly, this patient never went below a certain amount of omissions. This possibly contributed to the very similar omission rate he showed as the result of the bottom-up and the top-down manipulation taken singularly or together.

The most significant limitation of this study was the uncertainty surrounding the generalizability of this patient's performance to a broader population. More specifically, questions remain about whether the novel effects observed are phenomena specific to this individual case or if they can be linked to the extended period that has elapsed since the stroke occurred also in other patients. This

ambiguity highlights the need for cautious interpretation of the results, as these findings may not uniformly apply to all stroke survivors. Additionally, it raises the need of conducting future studies with a broader cohort of patients to explore the prevalence and consistency of these effects across diverse stroke recovery profiles. It stresses the need to examine the presence of these effects during the acute phase through group studies, accompanied by longitudinal tracking to determine the timing of their emergence, if at all. This could provide insights into the temporal dynamics of stroke recovery and guide the timing and nature of interventions designed to mitigate the cognitive deficits associated with stroke. The challenge of conducting group studies however lies in the complexity of determining what constitutes a difficulty for one patient versus another. Therefore, to truly understand the implications of increasing task difficulty, it is essential to tailor this difficulty to each individual, such as through adaptive procedures that adjust the target size (e.g. similarly to: Lee et al., 2014; Wouters et al., 2009). Furthermore, an intriguing direction for future studies would be to integrate dual-task paradigms into patients' daily environments, for instance, through augmented reality techniques, in order to assess the role of an ecological context in the emergence of load-induced spatial processing modulations (e.g. similarly to: Mak et al., 2022).

In ***Chapter 2***, we investigated the unimpaired cognitive system. Clarifying whether load-induced spatial processing asymmetries exist in healthy adults was indeed essential to determine whether biases toward the ipsilesional space often observed in patients are to be considered remnants of contralesional spatial processing deficits or, rather, the manifestations of a spatial processing which is asymmetric already in the absence of neurological insults. Specifically, in two experiments, we tested the impact of attentional load upon spatial processing in large samples of healthy adults. We employed different versions of a rather complex dual-task paradigm, involving the parallel processing of multiple sources of information. To maximize the detection of spatial asymmetries we used stimuli capable of eliciting an audiovisual integration illusion (i.e., sound-induced flash illusion, Andersen et al., 2004; Shams et al., 2000, 2002). Although participants showed increased illusion rates when attentional load was increased, there were no differences between left- and right-sided stimuli. This finding spoke against the existence of load-induced spatial processing asymmetries in the unimpaired cognitive system, at least in the context of audiovisual integration illusions.

Future studies should explore whether load-induced spatial processing asymmetries remain undetected when utilizing stimuli that induce other types of audiovisual integration illusions or complex stimuli of an entirely different nature. An additional challenge would then to identify stimuli that are not only sufficiently complex but also more ecologically valid, again, in order to

assess the role of an ecological context in the emergence of load-induced spatial processing asymmetries (e.g. similarly to: Bartlett et al., 2020; Benedetto et al., 2013). Furthermore, an intriguing direction for future studies would be to test whether illusion rates are influenced by the modulation of endogenous or exogenous attention, independently from the impact of attentional load. Although various studies have indeed shown that endogenous spatial attention (Fairhall & Macaluso, 2009) as well as exogenous spatial attention (van der Stoep et al., 2015) play a role in shaping multisensory integration, to our knowledge, there are no studies directly targeting sound-induced flash illusion. This could entail, for example, employing central cues (e.g., arrows at the centre of the screen that instruct where to look) vs peripheral cues (e.g., sudden stimuli appearing at the target location).

Overall, the results of our behavioural experiments confirm that different task requirements are characterized by the common use of relatively unspecific attentional resources. When the attentional load increases, this general yet limited pool of resources is depleted, affecting performance (i.e., ability to compensate contralesional spatial processing deficits in the patient or ability to inhibit automatic illusory responses in healthy adults). However, these results seem also to suggest that the unimpaired cognitive system and the damaged cognitive system are not only quantitatively but also qualitatively distinct, as the decrease in performance was lateralized in the patient and symmetric in healthy adults. Consequently, assessing spatial processing in brain-damaged patients under high attentional load does not exacerbate asymmetries existing in the unimpaired cognitive system. Instead, it uncovers very subtle (yet potentially hazardous) deficits which are almost exclusively contralesional.

Finally, after having examined load-induced spatial processing asymmetries in the unimpaired cognitive system, as evidenced by task performance, we shifted our focus to the underlying neural processes. In ***Chapter 3***, firstly, we tested whether task performance in a dual-task paradigm identical to the one used in the behavioural experiments, could be predicted from intrinsic functional connectivity values within specific networks. This was done employing an innovative analysis approach that allows to extract functional connectivity from electroencephalography (EEG) recordings during resting-state. With regard to this, we have uncovered significant correlations between task performance and intrinsic functional connectivity, predominantly within networks related to auditory and visual processing, as well as the allocation of attentional resources in space. This finding offers preliminary evidence about the significance of intrinsic brain organization also in shaping illusory perception and in how it is modulated when attentional load is increased.

Additionally, we tested whether Event-Related Potential (ERP) modulations during in-task EEG recordings could be associated with task performance. With regard to this, we have identified N1, N2, and P3 modulations associated with the presentation of stimuli eliciting the sound-induced flash illusion during different levels of attentional load, with N1 modulations differing depending on the side of the flashes. This finding confirmed that load-induced spatial processing asymmetries, although not apparent in behavioural responses, could be discerned through ERP responses (similarly to: O'Connell et al., 2011).

Future studies are required to replicate and validate findings from both resting state functional connectivity and in-task ERP analyses. First of all, for what concern resting state analyses, functional connectivity could be correlated not only with behavioural indexes, but also with brain indexes present during in-task brain activity, such as ERPs (e.g. similarly to: Del Popolo Cristaldi et al., 2022; Li et al., 2015; Ma et al., 2023). In this way it will be possible to explore whether intrinsic functional connectivity predict load-induced spatial processing asymmetries, that seems to emerge exclusively through ERP responses. Additionally, intrinsic functional connectivity could be calculated using alternative methods, transitioning from a data-driven computation of connectivity to a computation of connectivity between predefined nodes of interest (Joel et al., 2011).

Moreover, for what concern in-task analyses, ERP modulations should be evaluated focusing exclusively on illusory trials or comparing illusory trials with non-illusory trials. Moreover, source localization analyses are essential to allow for a more comprehensive interpretation, particularly concerning flash presentation side effects. Finally, spectral analyses of in-task recordings could provide insights into the frequencies involved, particularly regarding the role of the alpha frequency, which appears to be implicated in both sound-induced flash illusion perception and load-induced spatial processing asymmetries (e.g. similarly to: Gallotto et al. 2020).

In conclusion, we have once again effectively utilized the multitasking approach to examine both damaged and unimpaired cognitive systems. Crucially, the utility of this method is not limited to the study of spatial processing; it extends to other cognitive functions, from memory to inhibitory abilities (Contemori et al., 2022; Saccani et al., 2022). Future studies could explore whether the qualitative distinction between impaired and unimpaired systems under multitasking conditions is replicated across other domains, or if there exists a continuum that ranges from baseline functionality to clinical impairment.

REFERENCES

Aglioti, S., Smania, N., Barbieri, C., & Corbetta, M. (1997). Influence of Stimulus Salience and Attentional Demands on Visual Search Patterns in Hemispatial Neglect. *Brain and Cognition*, *34*(3), 388–403. https://doi.org/10.1006/brcg.1997.0915

Albert, M. L. (1973). A simple test of visual neglect. *Neurology*, *23*(6), 658–658. https://doi.org/10.1212/WNL.23.6.658

Alsius, A., Navarra, J., Campbell, R., & Soto-Faraco, S. (2005). Audiovisual Integration of Speech Falters under High Attention Demands. *Current Biology*, *15*(9), 839–843. https://doi.org/10.1016/j.cub.2005.03.046

Alsius, A., Navarra, J., & Soto-Faraco, S. (2007). Attention to touch weakens audiovisual speech integration. *Experimental Brain Research*, *183*(3), 399–404. https://doi.org/10.1007/s00221-007-1110-1

Andersen, T. S., Tiippana, K., & Sams, M. (2004). Factors influencing audiovisual fission and fusion illusions. *Cognitive Brain Research*, *21*(3), 301–308. https://doi.org/10.1016/j.cogbrainres.2004.06.004

Andres, M., Geers, L., Marnette, S., Coyette, F., Bonato, M., Priftis, K., & Masson, N. (2019). Increased Cognitive Load Reveals Unilateral Neglect and Altitudinal Extinction in Chronic Stroke. *Journal of the International Neuropsychological Society*, *25*(6), 644–653. https://doi.org/10.1017/S1355617719000249

Anticevic, A., Repovs, G., Shulman, G. L., & Barch, D. M. (2010). When less is more: TPJ and default network deactivation during encoding predicts working memory performance. *NeuroImage*, *49*(3), 2638–2648. https://doi.org/10.1016/j.neuroimage.2009.11.008

Balz, J., Keil, J., Roa Romero, Y., Mekle, R., Schubert, F., Aydin, S., Ittermann, B., Gallinat, J., & Senkowski, D. (2016). GABA concentration in superior temporal sulcus predicts gamma power and perception in the sound-induced flash illusion. *NeuroImage*, *125*(12), 724–730. https://doi.org/10.1016/j.neuroimage.2015.10.087

Bartlett, M. L., Scott Gwinn, O., Thomas, N. A., & Nicholls, M. E. R. (2020). Cognitive load exacerbates rightward biases during computer maze navigation. *Brain and Cognition*, *140*, 105547. https://doi.org/10.1016/j.bandc.2020.105547

Barton, J. J. S., & Black, S. E. (1998). Line bisection in hemianopia. *Journal of Neurology, Neurosurgery & Psychiatry*, *64*(5), 660–662. https://doi.org/10.1136/jnnp.64.5.660

Basagni, B., De Tanti, A., Damora, A., Abbruzzese, L., Varalta, V., Antonucci, G., Bickerton, W. L., Smania, N., & Mancuso, M. (2017). The assessment of hemineglect syndrome with cancellation tasks: a comparison between the Bells test and the Apples test. *Neurological Sciences*, *38*(12), 2171–2176. https://doi.org/10.1007/s10072-017-3139-7

Bates, D., Mächler, M., Bolker, B., & Walker, S. (2015). Fitting Linear Mixed-Effects Models Using lme4. *Journal of Statistical Software*, *67*(1). https://doi.org/10.18637/jss.v067.i01

Beck, A., Robert A., Steer, R., & Brown, G. (1996). *Beck Depression Inventory–II.* Psychological assessment.

Beck, A. T., & Steer, R. A. (1993). *Beck Anxiety Inventory*. Psychological Corporation.

Bell, A. J., & Sejnowski, T. J. (1995). An Information-Maximization Approach to Blind Separation and Blind Deconvolution. *Neural Computation*, *7*(6), 1129–1159. https://doi.org/10.1162/neco.1995.7.6.1129

Bellgrove, M. A., Dockree, P. M., Aimola, L., & Robertson, I. H. (2004). Attenuation of spatial attentional asymmetries with poor sustained attention. *NeuroReport*, *15*(6), 1065–1069. https://doi.org/10.1097/00001756-200404290-00027

Bellgrove, M. A., Eramudugolla, R., Newman, D. l P., Vance, A., & Mattingley, J. B. (2013). Influence of attentional load on spatial attention in acquired and developmental disorders of attention. *Neuropsychologia*, *51*(6), 1085–1093. https://doi.org/10.1016/j.neuropsychologia.2013.01.019

Benedetto, S., Pedrotti, M., Bremond, R., & Baccino, T. (2013). Leftward attentional bias in a simulated driving task. *Transportation Research Part F: Traffic Psychology and Behaviour*, *20*, 147–153. https://doi.org/10.1016/j.trf.2013.07.006

Benwell, C. S. Y., Harvey, M., Gardner, S., & Thut, G. (2013). Stimulus- and state-dependence of systematic bias in spatial attention: Additive effects of stimulus-size and time-on-task. *Cortex*, *49*(3), 827–836. https://doi.org/10.1016/j.cortex.2011.12.007

Bertelson, P., Vroomen, J., De Gelder, B., & Driver, J. (2000). The ventriloquist effect does not depend on the direction of deliberate visual attention. *Perception & Psychophysics*, *62*(2), 321–332. https://doi.org/10.3758/BF03205552

Bhattacharya, J., Shams, L., & Shimojo, S. (2002). Sound-induced illusory flash perception: role of gamma band responses. *NeuroReport*, *13*(14), 1727–1730. https://doi.org/10.1097/00001756-200210070-00007

Blini, E., Romeo, Z., Spironelli, C., Pitteri, M., Meneghello, F., Bonato, M., & Zorzi, M. (2016). Multi-tasking uncovers right spatial neglect and extinction in chronic left-hemisphere stroke patients. *Neuropsychologia*, *92*, 147–157. https://doi.org/10.1016/j.neuropsychologia.2016.02.028

Bonato, M. (2012). Neglect and Extinction Depend Greatly on Task Demands: A Review. *Frontiers in Human Neuroscience*, *6*(7). https://doi.org/10.3389/fnhum.2012.00195

Bonato, M. (2015). Unveiling residual, spontaneous recovery from subtle hemispatial neglect three years after stroke. *Frontiers in Human Neuroscience*, *9*(7), 1–9. https://doi.org/10.3389/fnhum.2015.00413

Bonato, M., & Deouell, L. Y. (2013). Hemispatial Neglect: Computer-Based Testing Allows More Sensitive Quantification of Attentional Disorders and Recovery and Might Lead to Better Evaluation of Rehabilitation. *Frontiers in Human Neuroscience*, *7*. https://doi.org/10.3389/fnhum.2013.00162

Bonato, M., Priftis, K., Marenzi, R., Umiltà, C., & Zorzi, M. (2010). Increased attentional demands impair contralesional space awareness following stroke. *Neuropsychologia*, *48*(13), 3934–3940. https://doi.org/10.1016/j.neuropsychologia.2010.08.022

Bonato, M., Priftis, K., Marenzi, R., Umiltà, C., & Zorzi, M. (2012). Deficits of contralesional awareness: A case study on what paper-and-pencil tests neglect. *Neuropsychology*, *26*(1), 20–36. https://doi.org/10.1037/a0025306

Bonato, M., Priftis, K., Umiltà, C., & Zorzi, M. (2013). Computer-based attention-demanding testing unveils severe neglect in apparently intact patients. *Behavioural Neurology*, *26*(3), 179–181. https://doi.org/10.3233/BEN-2012-129005

Bonato, M., Romeo, Z., Blini, E., Pitteri, M., Durgoni, E., Passarini, L., Meneghello, F., & Zorzi, M. (2019). Ipsilesional Impairments of Visual Awareness After Right-Hemispheric Stroke. *Frontiers in Psychology*, *10*. https://doi.org/10.3389/fpsyg.2019.00697

Bonato, M., Spironelli, C., Lisi, M., Priftis, K., & Zorzi, M. (2015). Effects of Multimodal Load on Spatial Monitoring as Revealed by ERPs. *PLOS ONE*, *10*(9), e0136719. https://doi.org/10.1371/journal.pone.0136719

Bridges, D., Pitiot, A., MacAskill, M. R., & Peirce, J. W. (2020). The timing mega-study: Comparing a range of experiment generators, both lab-based and online. *PeerJ*, *8*, 1–29. https://doi.org/10.7717/peerj.9414

Brodie, E. E., & Pettigrew, L. E. L. (1996). Is left always right? Directional deviations in visual line bisection as a function of hand and initial scanning direction. *Neuropsychologia*, *34*(5), 467–470. https://doi.org/10.1016/0028-3932(95)00130-1

Brookes, M. J., Woolrich, M., Luckhoo, H., Price, D., Hale, J. R., Stephenson, M. C., Barnes, G. h R., Smith, S. M., & Morris, P. G. (2011). Investigating the electrophysiological basis of resting state networks using magnetoencephalography. *Proceedings of the National Academy of Sciences*, *108*(40), 16783–16788. https://doi.org/10.1073/pnas.1112685108

Brown, V. A. (2021). An Introduction to Linear Mixed-Effects Modeling in R. *Advances in Methods and Practices in Psychological Science*, *4*(1). https://doi.org/10.1177/2515245920960351

Calhoun, V. D., Adali, T., Pearlson, G. D., & Pekar, J. J. (2001). Spatial and temporal independent component analysis of functional MRI data containing a pair of task-related waveforms. *Human Brain Mapping*, *13*(1), 43–53. https://doi.org/10.1002/hbm.1024

Calhoun, V. D., Liu, J., & Adalı, T. (2009). A review of group ICA for fMRI data and ICA for joint inference of imaging, genetic, and ERP data. *NeuroImage*, *45*(1), S163–S172. https://doi.org/10.1016/j.neuroimage.2008.10.057

Caliandro, P., Vecchio, F., Miraglia, F., Reale, G., Della Marca, G., La Torre, G., Lacidogna, G., Iacovelli, C., Padua, L., Bramanti, P., & Rossini, P. M. (2017). Small-World Characteristics of Cortical Connectivity Changes in Acute Stroke. *Neurorehabilitation and Neural Repair*, *31*(1), 81–94. https://doi.org/10.1177/1545968316662525

Camilleri, J. A., Müller, V. I., Fox, P., Laird, A. R., Hoffstaedter, F., Kalenscher, T., & Eickhoff, S. B. (2018). Definition and characterization of an extended multiple-demand network. *NeuroImage*, *165*, 138–147. https://doi.org/10.1016/j.neuroimage.2017.10.020

Canuet, L., Ishii, R., Pascual-Marqui, R. D., Iwase, M., Kurimoto, R., Aoki, Y., Ikeda, S., Takahashi, H., Nakahachi, T., & Takeda, M. (2011). Resting-state EEG source localization and functional connectivity in schizophrenia-like psychosis of epilepsy. *PLoS ONE*, *6*(11). https://doi.org/10.1371/journal.pone.0027863

Cecere, R., Rees, G., & Romei, V. (2015). Individual Differences in Alpha Frequency Drive Crossmodal Illusory Perception. *Current Biology*, *25*(2), 231–235. https://doi.org/10.1016/j.cub.2014.11.034

Chang, C., Wang, E., Yang, J., Luan, X., Wang, Ai., & Zhang, M. (2023). Differences in eccentricity for sound-induced flash illusion in four visual fields. *Perception*, *52*(1), 56–73. https://doi.org/10.1177/03010066221136670

Choi, I., Lee, J. Y., & Lee, S. H. (2018). Bottom-up and top-down modulation of multisensory integration. *Current Opinion in Neurobiology*, *52*, 115–122. https://doi.org/10.1016/j.conb.2018.05.002

Cipora, K., Soltanlou, M., Reips, U. D., & Nuerk, H. C. (2019). The SNARC and MARC effects measured online: Large-scale assessment methods in flexible cognitive effects. *Behavior Research Methods*, *51*(4), 1676–1692. https://doi.org/10.3758/s13428-019-01213-5

Coccaro, A., Di Bono, M. G., Maffei, A., Orefice, C., Lievore, R., Mammarella, I., & Liotti, M. (2023). Resting State Dynamic Reconfiguration of Spatial Attention Cortical Networks and Visuospatial Functioning in Non-Verbal Learning Disability (NVLD): A HD-EEG Investigation. *Brain Sciences*, *13*(5), 731. https://doi.org/10.3390/brainsci13050731

Cocchini, G., & Beschin, N. (2022). The Fluff test: Improved scoring system to account for different degrees of contralesional and ipsilesional personal neglect in brain damaged patients. *Neuropsychological Rehabilitation*, *32*(1), 69–83. https://doi.org/10.1080/09602011.2020.1797828

Cocchini, G., Beschin, N., & Jehkonen, M. (2001). The Fluff Test: A simple task to assess body representation neglect. *Neuropsychological Rehabilitation*, *11*(1), 17–31. https://doi.org/10.1080/09602010042000132

Cocchini, G., Cubelli, R., Sala, S. D., & Beschin, N. (1999). Neglect Without Extinction. *Cortex*, *35*(3), 285–313. https://doi.org/10.1016/S0010-9452(08)70802-5

Contemori, G., Saccani, M. S., & Bonato, M. (2022). Multitasking Effects on Perception and Memory in Older Adults. *Vision*, *6*(3), 48. https://doi.org/10.3390/vision6030048

Corbetta, M., Patel, G., & Shulman, G. L. (2008). The Reorienting System of the Human Brain: From Environment to Theory of Mind. *Neuron*, *58*(3), 306–324. https://doi.org/10.1016/j.neuron.2008.04.017

Corbetta, M., & Shulman, G. L. (2002). Control of goal-directed and stimulus-driven attention in the brain. *Nature Reviews Neuroscience*, *3*(3), 201–215. https://doi.org/10.1038/nrn755

Corbetta, M., & Shulman, G. L. (2011). Spatial Neglect and Attention Networks. *Annual Review of Neuroscience*, *34*(1), 569–599. https://doi.org/10.1146/annurev-neuro-061010-113731

Cousineau, D., Goulet, M. A., & Harding, B. (2021). Summary Plots With Adjusted Error Bars: The superb Framework With an Implementation in R. *Advances in Methods and Practices in Psychological Science*, *4*(3), 251524592110351. https://doi.org/10.1177/25152459211035109

Crawford, J. R., & Garthwaite, P. H. (2005). Testing for Suspected Impairments and Dissociations in Single-Case Studies in Neuropsychology: Evaluation of Alternatives Using Monte Carlo Simulations and Revised Tests for Dissociations. *Neuropsychology*, *19*(3), 318–331. https://doi.org/10.1037/0894-4105.19.3.318

Crawford, J. R., Garthwaite, P. H., & Porter, S. (2010). Point and interval estimates of effect sizes for the case-controls design in neuropsychology: Rationale, methods, implementations, and proposed reporting standards. *Cognitive Neuropsychology*, *27*(3), 245–260. https://doi.org/10.1080/02643294.2010.513967

Crawford, J. R., Howell, D. C., & Garthwaite, P. H. (1998). Payne and Jones Revisited: Estimating the Abnormality of Test Score Differences Using a Modified Paired Samples t Test. *Journal of Clinical and Experimental Neuropsychology*, *20*(6), 898–905. https://doi.org/10.1076/jcen.20.6.898.1112

Damasio, A. R., Damasio, H., & Chui, H. C. (1980). Neglect following damage to frontal lobe or basal ganglia. *Neuropsychologia*, *18*(2), 123–132. https://doi.org/10.1016/0028-3932(80)90058-5

Damoiseaux, J. S., Rombouts, S. A. R. B., Barkhof, F., Scheltens, P., Stam, C. J., Smith, S. M., & Beckmann, C. F. (2006). Consistent resting-state networks across healthy subjects. *Proceedings of the National Academy of Sciences*, *103*(37), 13848–13853. https://doi.org/10.1073/pnas.0601417103

de Cheveigné, A. (2020). ZapLine: A simple and effective method to remove power line artifacts. *NeuroImage*, *207*, 116356. https://doi.org/10.1016/j.neuroimage.2019.116356

de Haas, B., Kanai, R., Jalkanen, L., & Rees, G. (2012). Grey matter volume in early human visual cortex predicts proneness to the sound-induced flash illusion. *Proceedings of the Royal Society B: Biological Sciences*, *279*(1749), 4955–4961. https://doi.org/10.1098/rspb.2012.2132

de Leeuw, J. R. (2015). jsPsych: A JavaScript library for creating behavioral experiments in a web browser. *Behavior Research Methods*, *47*(1), 1–12. https://doi.org/10.3758/s13428-014-0458-y

de Leeuw, J. R., Gilbert, R. A., & Luchterhandt, B. (2023). jsPsych: Enabling an Open-Source Collaborative Ecosystem of Behavioral Experiments. *Journal of Open Source Software*, *8*(85), 5351. https://doi.org/10.21105/joss.05351

de Pasquale, F., Della Penna, S., Snyder, A. Z., Lewis, C., Mantini, D., Marzetti, L., Belardinelli, P., Ciancetta, L., Pizzella, V., Romani, G. L., & Corbetta, M. (2010). Temporal dynamics of spontaneous MEG activity in brain networks. *Proceedings of the National Academy of Sciences*, *107*(13), 6040–6045. https://doi.org/10.1073/pnas.0913863107

DeBruine, L. M., & Barr, D. J. (2021). Understanding Mixed-Effects Models Through Data Simulation. *Advances in Methods and Practices in Psychological Science*, *4*(1), 251524592096511. https://doi.org/10.1177/2515245920965119

Del Popolo Cristaldi, F., Buodo, G., Duma, G. M., Sarlo, M., & Mento, G. (2022). Unbalanced functional connectivity at rest affects the ERP correlates of affective prediction in high intolerance of uncertainty individuals: A high density EEG investigation. *International Journal of Psychophysiology*, *178*, 22–33. https://doi.org/10.1016/j.ijpsycho.2022.06.006

Del Popolo Cristaldi, F., Granziol, U., Bariletti, I., & Mento, G. (2022). Doing Experimental Psychological Research from Remote: How Alerting Differently Impacts Online vs. Lab Setting. *Brain Sciences*, *12*(8), 1061. https://doi.org/10.3390/brainsci12081061

Delorme, A., & Makeig, S. (2004). EEGLAB: an open source toolbox for analysis of single-trial EEG dynamics including independent component analysis. *Journal of Neuroscience Methods*, *134*(1), 9–21. https://doi.org/10.1016/j.jneumeth.2003.10.009

Deouell, L. Y., Sacher, Y., & Soroker, N. (2005). Assessment of spatial attention after brain damage with a dynamic reaction time test. *Journal of the International Neuropsychological Society*, *11*(6), 697–707. https://doi.org/10.1017/S1355617705050824

Dey, A., & Sommers, M. S. (2015). Age-related differences in inhibitory control predict audiovisual speech perception. *Psychology and Aging*, *30*(3), 634–646. https://doi.org/10.1037/pag0000033

Dodds, C. M., van Belle, J., Peers, P. V., Dove, A., Cusack, R., Duncan, J., & Manly, T. (2008). The effects of time-on-task and concurrent cognitive load on normal visuospatial bias. *Neuropsychology*, *22*(4), 545–552. https://doi.org/10.1037/0894-4105.22.4.545

Doricchi, F., Lasaponara, S., Pazzaglia, M., & Silvetti, M. (2022). Left and right temporal-parietal junctions (TPJs) as “match/mismatch” hedonic machines: A unifying account of TPJ function. *Physics of Life Reviews*, *42*, 56–92. https://doi.org/10.1016/j.plrev.2022.07.001

Dufour, A., Touzalin, P., & Candas, V. (2007). Time-on-task effect in pseudoneglect. *Experimental Brain Research*, *176*(3), 532–537. https://doi.org/10.1007/s00221-006-0810-2

Duma, G. M., Di Bono, M. G., & Mento, G. (2021). Grounding adaptive cognitive control in the intrinsic, functional brain organization: An HD-EEG resting state investigation. *Brain Sciences*, *11*(11). https://doi.org/10.3390/brainsci11111513

Durfee, A. Z., & Hillis, A. E. (2023). Unilateral Spatial Neglect Recovery Poststroke. *Stroke*, *54*(1), 10–19. https://doi.org/10.1161/STROKEAHA.122.041710

Engel, A. K., Fries, P., & Singer, W. (2001). Dynamic predictions: Oscillations and synchrony in top–down processing. *Nature Reviews Neuroscience*, *2*(10), 704–716. https://doi.org/10.1038/35094565

Eramudugolla, R., Kamke, M. R., Soto-Faraco, S., & Mattingley, J. B. (2011). Perceptual load influences auditory space perception in the ventriloquist aftereffect. *Cognition*, *118*(1), 62–74. https://doi.org/10.1016/j.cognition.2010.09.009

Esposito, E., Shekhtman, G., & Chen, P. (2021). Prevalence of spatial neglect post-stroke: A systematic review. *Annals of Physical and Rehabilitation Medicine*, *64*(5), 101459. https://doi.org/10.1016/j.rehab.2020.10.010

Fairhall, S. L., & Macaluso, E. (2009). Spatial attention can modulate audiovisual integration at multiple cortical and subcortical sites. *European Journal of Neuroscience*, *29*(6), 1247–1257. https://doi.org/10.1111/j.1460-9568.2009.06688.x

Ferber, S., & Karnath, H. O. (2001). How to assess spatial neglect - Line bisection or cancellation tasks? *Journal of Clinical and Experimental Neuropsychology*, *23*(5), 599–607. https://doi.org/10.1076/jcen.23.5.599.1243

Ferree, T. C. (2006). Spherical Splines and Average Referencing in Scalp Electroencephalography. *Brain Topography*, *19*, 43–52. https://doi.org/10.1007/s10548-006-0011-0

Fimm, B., Willmes, K., & Spijkers, W. (2006). The effect of low arousal on visuo-spatial attention. *Neuropsychologia*, *44*(8), 1261–1268. https://doi.org/10.1016/j.neuropsychologia.2006.01.027

Fox J., & Weisberg S. (2019). *An R Companion to Applied Regression.* (Third edition). Sage. https://socialsciences.mcmaster.ca/jfox/Books/Companion/.

Fox, M. D., & Raichle, M. E. (2007). Spontaneous fluctuations in brain activity observed with functional magnetic resonance imaging. *Nature Reviews Neuroscience*, *8*(9), 700–711. https://doi.org/10.1038/nrn2201

Friedrich, F., & Margolin, D. I. (1993). Response Time Measures of Hemi-inattention: A Longitudinal Case Report. *Neuropsychiatry, Neuropsychology & Behavioral Neurology* , *6*(1), 54–59.

Friston, K. J. (2011). Functional and Effective Connectivity: A Review. *Brain Connectivity*, *1*(1), 13–36. https://doi.org/10.1089/brain.2011.0008

Fruhmann Berger, M., Johannsen, L., & Karnath, H. O. (2008). Time course of eye and head deviation in spatial neglect. *Neuropsychology*, *22*(6), 697–702. https://doi.org/10.1037/a0013351

Fu, S., Fedota, J. R., Greenwood, P. M., & Parasuraman, R. (2010). Dissociation of visual C1 and P1 components as a function of attentional load: An event-related potential study. *Biological Psychology*, *85*(1), 171–178. https://doi.org/10.1016/j.biopsycho.2010.06.008

Fu, S., Zinni, M., Squire, P. N., Kumar, R., Caggiano, D. M., & Parasuraman, R. (2008). When and where perceptual load interacts with voluntary visuospatial attention: An event-related potential and dipole modeling study. *NeuroImage*, *39*(3), 1345–1355. https://doi.org/10.1016/j.neuroimage.2007.09.068

Gallotto, S., Duecker, F., Ten Oever, S., Schuhmann, T., De Graaf, T. A., & Sack, A. T. (2020). Relating alpha power modulations to competing visuospatial attention theories. *NeuroImage*, 207, 116429. https://doi.org/10.1016/j.neuroimage.2019.116429

Gao, Z., Chen, B., Sun, T., Chen, H., Wang, K., Xuan, P., & Liang, Z. (2020). Implementation of stimuli with millisecond timing accuracy in online experiments. *PLoS ONE*, *15*(7), 1–14. https://doi.org/10.1371/journal.pone.0235249

Gauthier, L., Dehaut, F., & Joanette, Y. (1989). The bells test: A quantitative and qualitative test for visual neglect. *International Journal of Clinical Neuropsychology*, *11*, 49–54.

Gazzaley, A., Cooney, J. W., Rissman, J., & D'Esposito, M. (2005). Top-down suppression deficit underlies working memory impairment in normal aging. *Nature Neuroscience*, *8*(10), 1298–1300. https://doi.org/10.1038/nn1543

Germine, L., Nakayama, K., Duchaine, B. C., Chabris, C. F., Chatterjee, G., & Wilmer, J. B. (2012). Is the Web as good as the lab? Comparable performance from Web and lab in cognitive/perceptual experiments. *Psychonomic Bulletin & Review*, *19*(5), 847–857. https://doi.org/10.3758/s13423-012-0296-9

Glickman, M. E., Rao, S. R., & Schultz, M. R. (2014). False discovery rate control is a recommended alternative to Bonferroni-type adjustments in health studies. *Journal of Clinical Epidemiology*, *67*(8), 850–857. https://doi.org/10.1016/j.jclinepi.2014.03.012

Green, P., & MacLeod, C. J. (2016). SIMR: an R package for power analysis of generalized linear mixed models by simulation. *Methods in Ecology and Evolution*, *7*(4), 493–498. https://doi.org/10.1111/2041-210X.12504

Guilbert, A. (2023). Clinical assessment of unilateral spatial neglect dissociations and heterogeneities: A narrative synthesis. *Neuropsychology*, *37*(4), 450–462. https://doi.org/10.1037/neu0000841

Halligan, P. W., Marshall, J. C., & Wade, D. T. (1989). Visuospatial neglect: underlying factors and test sensitivity. *The Lancet*, *334*(8668), 908–911. https://doi.org/10.1016/S0140-6736(89)91561-4

Hamilton, R. H., Wiener, M., Drebing, D. E., & Branch Coslett, H. (2013). Gone in a flash: Manipulation of audiovisual temporal integration using transcranial magnetic stimulation. *Frontiers in Psychology*, *4*. https://doi.org/10.3389/fpsyg.2013.00571

Handy, T. C., Soltani, M., & Mangun, G. R. (2001). Perceptual Load and Visuocortical Processing: Event-Related Potentials Reveal Sensory-Level Selection. *Psychological Science*, *12*(3), 213–218. https://doi.org/10.1111/1467-9280.00338

Hartig, F. (2022). *DHARMa: Residual Diagnostics for Hierarchical (Multi-Level / Mixed) Regression Models* (0.4.6). https://CRAN.R-project.org/package=DHARMa

Hata, M., Kazui, H., Tanaka, T., Ishii, R., Canuet, L., Pascual-Marqui, R. D., Aoki, Y., Ikeda, S., Kanemoto, H., Yoshiyama, K., Iwase, M., & Takeda, M. (2016). Functional connectivity assessed by resting state EEG correlates with cognitive decline of Alzheimer's disease - An eLORETA study. *Clinical Neurophysiology*, *127*(2), 1269–1278. https://doi.org/10.1016/j.clinph.2015.10.030

Haueisen, J., Ramon, C., Eiselt, M., Brauer, H., & Nowak, H. (1997). Influence of tissue resistivities on neuromagnetic fields and electric potentials studied with a finite element model of the head. *IEEE Transactions on Biomedical Engineering*, *44*(8), 727–735. https://doi.org/10.1109/10.605429

Hautus, M. J. (1995). Corrections for extreme proportions and their biasing effects on estimated values ofd'. *Behavior Research Methods, Instruments, & Computers*, *27*(1), 46–51. https://doi.org/10.3758/BF03203619

Hedrich, T., Pellegrino, G., Kobayashi, E., Lina, J. M., & Grova, C. (2017). Comparison of the spatial resolution of source imaging techniques in high-density EEG and MEG. *NeuroImage*, *157*, 531–544. https://doi.org/10.1016/j.neuroimage.2017.06.022

Heilman, K. M., Watson, R. T., & Valenstein, E. (2002). Spatial neglect. In *The Cognitive and Neural Bases of Spatial Neglect* (pp. 2–30). Oxford University PressOxford. https://doi.org/10.1093/acprof:oso/9780198508335.003.0001

Herrmann, C. S., Fründ, I., & Lenz, D. (2010). Human gamma-band activity: A review on cognitive and behavioral correlates and network models. *Neuroscience & Biobehavioral Reviews*, *34*(7), 981–992. https://doi.org/10.1016/j.neubiorev.2009.09.001

Hester, R., & Garavan, H. (2005). Working memory and executive function: The influence of content and load on the control of attention. *Memory & Cognition*, *33*(2), 221–233. https://doi.org/10.3758/BF03195311

Hilbig, B. E. (2016). Reaction time effects in lab- versus Web-based research: Experimental evidence. *Behavior Research Methods*, *48*(4), 1718–1724. https://doi.org/10.3758/s13428-015-0678-9

Hillyard, S. A., Vogel, E. K., & Luck, S. J. (1998). Sensory gain control (amplification) as a mechanism of selective attention: electrophysiological and neuroimaging evidence. *Philosophical Transactions of the Royal Society of London. Series B: Biological Sciences*, *353*(1373), 1257–1270. https://doi.org/10.1098/rstb.1998.0281

Hirst, R. J., McGovern, D. P., Setti, A., Shams, L., & Newell, F. N. (2020). What you see is what you hear: Twenty years of research using the Sound-Induced Flash Illusion. *Neuroscience and Biobehavioral Reviews*, *118*, 759–774. https://doi.org/10.1016/j.neubiorev.2020.09.006

Hirst, R. J., Setti, A., Kenny, R. A., & Newell, F. N. (2019). Age-related sensory decline mediates the Sound-Induced Flash Illusion: Evidence for reliability weighting models of multisensory perception. *Scientific Reports*, *9*(1), 1–12. https://doi.org/10.1038/s41598-019-55901-5

Hopf, J. M., Vogel, E., Woodman, G., Heinze, H. J., & Luck, S. J. (2002). Localizing Visual Discrimination Processes in Time and Space. *Journal of Neurophysiology*, *88*(4), 2088–2095. https://doi.org/10.1152/jn.2002.88.4.2088

Hopfinger, J. B., & West, V. M. (2006). Interactions between endogenous and exogenous attention on cortical visual processing. *NeuroImage*, *31*(2), 774–789. https://doi.org/10.1016/j.neuroimage.2005.12.049

Husain, M. (2019). Visual Attention: What Inattention Reveals about the Brain. *Current Biology*, *29*(7), 262–264. https://doi.org/10.1016/j.cub.2019.02.026

Jacobs, S., Brozzoli, C., & Farnè, A. (2012). Neglect: A multisensory deficit? *Neuropsychologia*, *50*(6), 1029–1044. https://doi.org/10.1016/j.neuropsychologia.2012.03.018

Jensen, O., & Mazaheri, A. (2010). Shaping Functional Architecture by Oscillatory Alpha Activity: Gating by Inhibition. *Frontiers in Human Neuroscience*, *4*. https://doi.org/10.3389/fnhum.2010.00186

Jiang, J., Bruss, J., Lee, W. T., Tranel, D., & Boes, A. D. (2023). White matter disconnection of left multiple demand network is associated with post-lesion deficits in cognitive control. *Nature Communications*, *14*(1), 1740. https://doi.org/10.1038/s41467-023-37330-1

Joel, S. E., Caffo, B. S., van Zijl, P. C. M., & Pekar, J. J. (2011). On the relationship between seed-based and ICA-based measures of functional connectivity. *Magnetic Resonance in Medicine*, *66*(3), 644–657. https://doi.org/10.1002/mrm.22818

Kaiser, M., Senkowski, D., Busch, N. A., Balz, J., & Keil, J. (2019). Single trial prestimulus oscillations predict perception of the sound-induced flash illusion. *Scientific Reports*, *9*(1). https://doi.org/10.1038/s41598-019-42380-x

Kalnins, A. (2018). Multicollinearity: How common factors cause Type 1 errors in multivariate regression. *Strategic Management Journal*, *39*(8), 2362–2385. https://doi.org/10.1002/smj.2783

Kamke, M. R., Vieth, H. E., Cottrell, D., & Mattingley, J. B. (2012). Parietal disruption alters audiovisual binding in the sound-induced flash illusion. *NeuroImage*, *62*(3), 1334–1341. https://doi.org/10.1016/j.neuroimage.2012.05.063

Karnath, H. O., Rennig, J., Johannsen, L., & Rorden, C. (2011). The anatomy underlying acute versus chronic spatial neglect: a longitudinal study. *Brain*, *134*(3), 903–912. https://doi.org/10.1093/brain/awq355

Keil, J. (2020). Double Flash Illusions: Current Findings and Future Directions. *Frontiers in Neuroscience*, *14*(4), 1–8. https://doi.org/10.3389/fnins.2020.00298

Keil, J., Müller, N., Hartmann, T., & Weisz, N. (2014). Prestimulus Beta Power and Phase Synchrony Influence the Sound-Induced Flash Illusion. *Cerebral Cortex*, *24*(5), 1278–1288. https://doi.org/10.1093/cercor/bhs409

Keil, J., & Senkowski, D. (2017). Individual Alpha Frequency Relates to the Sound-Induced Flash Illusion. *Multisensory Research*, *30*(6), 565–578. https://doi.org/10.1163/22134808-00002572

Kinsbourne, M. (1987). Mechanisms of Unilateral Neglect. In *Advances in Psychology* (pp. 69–86). North-Holland. https://doi.org/10.1016/S0166-4115(08)61709-4

Klimesch, W., Sauseng, P., & Hanslmayr, S. (2007). EEG alpha oscillations: The inhibition–timing hypothesis. *Brain Research Reviews*, *53*(1), 63–88. https://doi.org/10.1016/j.brainresrev.2006.06.003

Kok, A. (2001). On the utility of P3 amplitude as a measure of processing capacity. *Psychophysiology*, *38*(3), 557–577. https://doi.org/10.1017/S0048577201990559

Kotowski, K., Stapor, K., & Leski, J. (2019). Improved robust weighted averaging for event-related potentials in EEG. *Biocybernetics and Biomedical Engineering*, *39*(4), 1036–1046. https://doi.org/10.1016/j.bbe.2019.09.002

Kuroki, D. (2021). A new jsPsych plugin for psychophysics, providing accurate display duration and stimulus onset asynchrony. *Behavior Research Methods*, *53*(1), 301–310. https://doi.org/10.3758/s13428-020-01445-w

Kuznetsova, A., Brockhoff, P. B., & Christensen, R. H. B. (2017). lmerTest Package: Tests in Linear Mixed Effects Models. *Journal of Statistical Software*, *82*(13), 1–26. https://doi.org/10.18637/jss.v082.i13

Lacadie, C. M., Fulbright, R. K., Arora, J., Constable, R. T., & Papademetris, X. (2008). Brodmann Areas defined in MNI space using a new Tracing Tool in BioImage Suite. *Organization for Human Brain Mapping*.

Làdavas, E., Petronio, A., & Umiltà, C. (1990). The Deployment of Visual Attention in the Intact Field of Hemineglect Patients. *Cortex*, *26*(3), 307–317. https://doi.org/10.1016/S0010-9452(13)80083-4

Lai, M., Demuru, M., Hillebrand, A., & Fraschini, M. (2018). A comparison between scalp- and source-reconstructed EEG networks. *Scientific Reports*, *8*(1), 12269. https://doi.org/10.1038/s41598-018-30869-w

Lamble, D., Kauranen, T., Laakso, M., & Summala, H. (1999). Cognitive load and detection thresholds in car following situations: safety implications for using mobile (cellular) telephones while driving. *Accident Analysis & Prevention*, *31*(6), 617–623. https://doi.org/10.1016/S0001-4575(99)00018-4

Lange, K., Kühn, S., & Filevich, E. (2015). "Just Another Tool for Online Studies" (JATOS): An easy eolution for setup and management of web servers supporting online studies. *PLOS ONE*, *10*(6), e0130834. https://doi.org/10.1371/journal.pone.0130834

Lavan, N., Chan, W. Y., Zhuang, Y., Mareschal, I., & Shergill, S. S. (2022). Direct eye gaze enhances the ventriloquism effect. *Attention, Perception, and Psychophysics*, *84*(7), 2293–2302. https://doi.org/10.3758/s13414-022-02468-5

Lavie, N. (2005). Distracted and confused?: Selective attention under load. *Trends in Cognitive Sciences*, *9*(2), 75–82. https://doi.org/10.1016/j.tics.2004.12.004

Lavie, N. (2010). Attention, Distraction, and Cognitive Control Under Load. *Current Directions in Psychological Science*, *19*(3), 143–148. https://doi.org/10.1177/0963721410370295

Lee, Y. C., Yu, W. H., Lin, Y. F., Hsueh, I. P., Wu, H. C., & Hsieh, C. L. (2014). Reliability and Responsiveness of the Activities of Daily Living Computerized Adaptive Testing System in Patients With Stroke. *Archives of Physical Medicine and Rehabilitation*, *95*(11), 2055–2063. https://doi.org/10.1016/j.apmr.2014.04.025

Leski, J. M. (2002). Robust weighted averaging [of biomedical signals]. *IEEE Transactions on Biomedical Engineering*, *49*(8), 796–804. https://doi.org/10.1109/TBME.2002.800757

Li, F., Liu, T., Wang, F., Li, H., Gong, D., Zhang, R., Jiang, Y., Tian, Y., Guo, D., Yao, D., & Xu, P. (2015). Relationships between the resting-state network and the P3: Evidence from a scalp EEG study. *Scientific Reports*, *5*(1), 15129. https://doi.org/10.1038/srep15129

Li, Q., Joo, S. J., Yeatman, J. D., & Reinecke, K. (2020). Controlling for Participants' Viewing Distance in Large-Scale, Psychophysical Online Experiments Using a Virtual Chinrest. *Scientific Reports*, *10*(1), 1–11. https://doi.org/10.1038/s41598-019-57204-1

Lisi, M., Bonato, M., & Zorzi, M. (2015). Pupil dilation reveals top–down attentional load during spatial monitoring. *Biological Psychology*, *112*, 39–45. https://doi.org/10.1016/j.biopsycho.2015.10.002

List, A., Brooks, J. L., Esterman, M., Flevaris, A. V., Landau, A. N., Bowman, G., Stanton, V., Vanvleet, T. M., Robertson, L. C., & Schendel, K. (2008). Visual hemispatial neglect, re-assessed. *Journal of the International Neuropsychological Society*, *14*(02), 243–256. https://doi.org/10.1017/S1355617708080284

Liu, Q., Farahibozorg, S., Porcaro, C., Wenderoth, N., & Mantini, D. (2017). Detecting large-scale networks in the human brain using high-density electroencephalography. *Human Brain Mapping*, *38*(9), 4631–4643. https://doi.org/10.1002/hbm.23688

Liu, Q., Ganzetti, M., Wenderoth, N., & Mantini, D. (2018). Detecting Large-Scale Brain Networks Using EEG: Impact of Electrode Density, Head Modeling and Source Localization. *Frontiers in Neuroinformatics*, *12*. https://doi.org/10.3389/fninf.2018.00004

Luck, S. J. (2014). *An introduction to the event-related potential technique.* (Second Edition). MIT press.

Luck, S. J., Heinze, H. J., Mangun, G. R., & Hillyard, S. A. (1990). Visual event-related potentials index focused attention within bilateral stimulus arrays. II. Functional dissociation of P1 and N1 components. *Electroencephalography and Clinical Neurophysiology*, *75*(6), 528–542. https://doi.org/10.1016/0013-4694(90)90139-B

Luck, S. J., & Hillyard, S. A. (1994). Electrophysiological correlates of feature analysis during visual search. *Psychophysiology*, *31*(3), 291–308. https://doi.org/10.1111/j.1469-8986.1994.tb02218.x

Luck, S. J., Woodman, G. F., & Vogel, E. K. (2000). Event-related potential studies of attention. *Trends in Cognitive Sciences*, *4*(11), 432–440. https://doi.org/10.1016/S1364-6613(00)01545-X

Ma, H. L., Zeng, T. A., Jiang, L., Zhang, M., Li, H., Su, R., Wang, Z. X., Chen, D. M., Xu, M., Xie, W. T., Dang, P., Bu, X. O., Zhang, T., & Wang, T. Z. (2023). Altered resting-state network connectivity patterns for predicting attentional function in deaf individuals: An EEG study. *Hearing Research*, *429*, 108696. https://doi.org/10.1016/j.heares.2023.108696

Macaluso, E., Noppeney, U., Talsma, D., Vercillo, T., Hartcher-O'Brien, J., & Adam, R. (2016). The Curious Incident of Attention in Multisensory Integration: Bottom-up vs. Top-down. *Multisensory Research*, *29*(6), 557–583. https://doi.org/10.1163/22134808-00002528

Magnotti, J. F., Smith, K. B., Salinas, M., Mays, J., Zhu, L. L., & Beauchamp, M. S. (2018). A causal inference explanation for enhancement of multisensory integration by co-articulation. *Scientific Reports*, *8*(1). https://doi.org/10.1038/s41598-018-36772-8

Magstim EGI. (2021). *EGI® Net Amp GES-400*. https://www.egi.com/

Mak, J., Kocanaogullari, D., Huang, X., Kersey, J., Shih, M., Grattan, E. S., Skidmore, E. R., Wittenberg, G. F., Ostadabbas, S., & Akcakaya, M. (2022). Detection of Stroke-Induced Visual Neglect and Target Response Prediction Using Augmented Reality and Electroencephalography. *IEEE Transactions on Neural Systems and Rehabilitation Engineering*, *30*, 1840–1850. https://doi.org/10.1109/TNSRE.2022.3188184

Makowski, D. (2018). The psycho Package: an Efficient and Publishing-Oriented Workflow for Psychological Science. *The Journal of Open Source Software*, *3*(22), 470. https://doi.org/10.21105/joss.00470

Mangun, G. R. (1995). Neural mechanisms of visual selective attention. *Psychophysiology*, *32*(1), 4–18. https://doi.org/10.1111/j.1469-8986.1995.tb03400.x

Manly, T., Dobler, V. B., Dodds, C. M., & George, M. A. (2005). Rightward shift in spatial awareness with declining alertness. *Neuropsychologia*, *43*(12), 1721–1728. https://doi.org/10.1016/j.neuropsychologia.2005.02.009

Mantini, D., Corbetta, M., Perrucci, M., Romani, G., & Delgratta, C. (2009). Large-scale brain networks account for sustained and transient activity during target detection. *NeuroImage*, *44*(1), 265–274. https://doi.org/10.1016/j.neuroimage.2008.08.019

Mantini, D., Corbetta, M., Romani, G. L., Orban, G. A., & Vanduffel, W. (2013). Evolutionarily Novel Functional Networks in the Human Brain? *The Journal of Neuroscience*, *33*(8), 3259–3275. https://doi.org/10.1523/JNEUROSCI.4392-12.2013

Mantini, D., Franciotti, R., Romani, G. L., & Pizzella, V. (2008). Improving MEG source localizations: An automated method for complete artifact removal based on independent component analysis. *NeuroImage*, *40*(1), 160–173. https://doi.org/10.1016/j.neuroimage.2007.11.022

Mantini, D., Perrucci, M. G., Del Gratta, C., Romani, G. L., Corbetta, M., & Raichle, M. E. (2007). Electrophysiological signatures of resting state networks in the human brain. Proceedings of the National Academy of Sciences, 104(32), 13170-13175. https://doi.org/10.1073/pnas.0700668104

Marino, M., Liu, Q., Samogin, J., Tecchio, F., Cottone, C., Mantini, D., & Porcaro, C. (2019). Neuronal dynamics enable the functional differentiation of resting state networks in the human brain. *Human Brain Mapping*, *40*(5), 1445–1457. https://doi.org/10.1002/hbm.24458

Mégevand, P., Molholm, S., Nayak, A., & Foxe, J. J. (2013). Recalibration of the Multisensory Temporal Window of Integration Results from Changing Task Demands. *PLoS ONE*, *8*(8), e71608. https://doi.org/10.1371/journal.pone.0071608

Michail, G., & Keil, J. (2018). High cognitive load enhances the susceptibility to non-speech audiovisual illusions. *Scientific Reports*, *8*(1), 11530. https://doi.org/10.1038/s41598-018-30007-6

Michail, G., Senkowski, D., Niedeggen, M., & Keil, J. (2021). Memory Load Alters Perception-Related Neural Oscillations during Multisensory Integration. *The Journal of Neuroscience*, *41*(7), 1505–1515. https://doi.org/10.1523/JNEUROSCI.1397-20.2020

Mishra, J., Martinez, A., & Hillyard, S. A. (2008). Cortical processes underlying sound-induced flash fusion. *Brain Research*, *1242*, 102–115. https://doi.org/10.1016/j.brainres.2008.05.023

Mishra, J., Martinez, A., Sejnowski, T. J., & Hillyard, S. A. (2007). Early Cross-Modal Interactions in Auditory and Visual Cortex Underlie a Sound-Induced Visual Illusion. *The Journal of Neuroscience*, *27*(15), 4120–4131. https://doi.org/10.1523/JNEUROSCI.4912-06.2007

Moore, T., & Zirnsak, M. (2017). Neural Mechanisms of Selective Visual Attention. *Annual Review of Psychology*, *68*(1), 47–72. https://doi.org/10.1146/annurev-psych-122414-033400

Morís Fernandez, L., Torralba, M., & Soto-Faraco, S. (2018). Theta oscillations reflect conflict processing in the perception of the McGurk illusion. *European Journal of Neuroscience*, *48*(7), 2630–2641. https://doi.org/10.1111/ejn.13804

Morys-Carter, W. L. (2021). *ScreenScale. Pavlovia.* https://doi.org/10.17605/OSF.IO/8FHQK

Mulert, C., Jäger, L., Schmitt, R., Bussfeld, P., Pogarell, O., Möller, H. J., Juckel, G., & Hegerl, U. (2004). Integration of fMRI and simultaneous EEG: towards a comprehensive understanding of localization and time-course of brain activity in target detection. *NeuroImage*, *22*(1), 83–94. https://doi.org/10.1016/j.neuroimage.2003.10.051

Naert, L., Bonato, M., & Fias, W. (2018). Asymmetric Spatial Processing Under Cognitive Load. *Frontiers in Psychology*, *9*. https://doi.org/10.3389/fpsyg.2018.00583

Nasreddine, Z. S., Phillips, N. A., Bédirian, V., Charbonneau, S., Whitehead, V., Collin, I., Cummings, J. L., & Chertkow, H. (2005). The Montreal Cognitive Assessment, MoCA: A Brief Screening Tool For Mild Cognitive Impairment. *Journal of the American Geriatrics Society*, *53*(4), 695–699. https://doi.org/10.1111/j.1532-5415.2005.53221.x

Nigbur, R., Ivanova, G., & Stürmer, B. (2011). Theta power as a marker for cognitive interference. *Clinical Neurophysiology*, *122*(11), 2185–2194. https://doi.org/10.1016/j.clinph.2011.03.030

O'Connell, R. G., Schneider, D., Hester, R., Mattingley, J. B., & Bellgrove, M. A. (2011). Attentional Load Asymmetrically Affects Early Electrophysiological Indices of Visual Orienting. *Cerebral Cortex*, *21*(5), 1056–1065. https://doi.org/10.1093/cercor/bhq178

O'Dowd, A., Hirst, R. J., Setti, A., Donoghue, O. A., Kenny, R. A., & Newell, F. N. (2023). The temporal precision of audiovisual integration is associated with longitudinal fall incidents but not sensorimotor fall risk in older adults. *Scientific Reports*, *13*(1), 7167. https://doi.org/10.1038/s41598-023-32404-y

Olbrich, S., Tränkner, A., Chittka, T., Hegerl, U., & Schönknecht, P. (2014). Functional connectivity in major depression: Increased phase synchronization between frontal cortical EEG-source estimates. *Psychiatry Research - Neuroimaging*, *222*, 91–99. https://doi.org/10.1016/j.pscychresns.2014.02.010

Oldfield, R. C. (1971). The assessment and analysis of handedness: The Edinburgh inventory. *Neuropsychologia*, *9*(1), 97–113. https://doi.org/10.1016/0028-3932(71)90067-4

Paladini, R. E., Wieland, F. A. M., Naert, L., Bonato, M., Mosimann, U. P., Nef, T., Müri, R. M., Nyffeler, T., & Cazzoli, D. (2020). The Impact of Cognitive Load on the Spatial Deployment of Visual Attention: Testing the Role of Interhemispheric Balance With Biparietal Transcranial Direct Current Stimulation. *Frontiers in Neuroscience*, *13*. https://doi.org/10.3389/fnins.2019.01391

Pascual-Marqui, R. D., Lehmann, D., Koukkou, M., Kochi, K., Anderer, P., Saletu, B., Tanaka, H., Hirata, K., John, E. R., Prichep, L., Biscay-Lirio, R., & Kinoshita, T. (2011). Assessing interactions in the brain with exact low-resolution electromagnetic tomography. *Philosophical Transactions of the Royal Society A: Mathematical, Physical and Engineering Sciences*, *369*(1952), 3768–3784. https://doi.org/10.1098/rsta.2011.0081

Peelen, M. V., & Kastner, S. (2014). Attention in the real world: toward understanding its neural basis. *Trends in Cognitive Sciences*, *18*(5), 242–250. https://doi.org/10.1016/j.tics.2014.02.004

Peers, P., Cusack, R., & Duncan, J. (2006). Modulation of spatial bias in the dual task paradigm: Evidence from patients with unilateral parietal lesions and controls. *Neuropsychologia*, *44*(8), 1325–1335. https://doi.org/10.1016/j.neuropsychologia.2006.01.033

Pérez, A., Peers, P. V., Valdés-Sosa, M., Galán, L., García, L., & Martínez-Montes, E. (2009). Hemispheric modulations of alpha-band power reflect the rightward shift in attention induced by enhanced attentional load. *Neuropsychologia*, *47*(1), 41–49. https://doi.org/10.1016/j.neuropsychologia.2008.08.017

Pérez, A., Pentón, L. G., & Valdés-Sosa, M. (2008). *Rightward shift in temporal order judgements in the wake of the attentional blink*. *29*(1), 35–54. https://www.redalyc.org/articulo.oa?id=16929102

Perrin, F., Pernier, J., Bertrand, O., & Echallier, J. F. (1989). Spherical splines for scalp potential and current density mapping. *Electroencephalography and Clinical Neurophysiology*, *72*(2), 184–187. https://doi.org/10.1016/0013-4694(89)90180-6

Pluta, S. R., Rowland, B. A., Stanford, T. R., & Stein, B. E. (2011). Alterations to multisensory and unisensory integration by stimulus competition. *Journal of Neurophysiology*, *106*(6), 3091–3101. https://doi.org/10.1152/jn.00509.2011

Polich, J. (2011). Neuropsychology of P300. In *The Oxford handbook of event-related potential components* (pp. 159–188). Oxford University Press. https://doi.org/10.1093/oxfordhb/9780195374148.013.0089

Posner, M., Walker, J. A., Friedrich, F. J., & Rafal, R. D. (1984). Effects of parietal injury on covert orienting of attention. *The Journal of Neuroscience*, *4*(7), 1863–1874. https://doi.org/10.1523/JNEUROSCI.04-07-01863.1984

Priftis, K., Di Salvo, S., & Zara, D. (2019). The importance of time limits in detecting signs of left visual peripersonal neglect: a multiple single-case, pilot study. *Neurocase*, *25*(5), 209–215. https://doi.org/10.1080/13554794.2019.1658788

Pronk, T., Hirst, R. J., Wiers, R. W., & Murre, J. M. J. (2022). Can we measure individual differences in cognitive measures reliably via smartphones? A comparison of the flanker effect across device types and samples. *Behavior Research Methods*, *55*(4), 1641–1652. https://doi.org/10.3758/s13428-022-01885-6

Psychology Software Tools. (2012). *E-Prime*. https://pstnet.com/

R Core Team. (2022). *R: A Language and Environment for Statistical Computing* (4.2.2). https://www.R-project.org/

Rauss, K. S., Pourtois, G., Vuilleumier, P., & Schwartz, S. (2009). Attentional load modifies early activity in human primary visual cortex. *Human Brain Mapping*, *30*(5), 1723–1733. https://doi.org/10.1002/hbm.20636

Rauss, K. S., Pourtois, G., Vuilleumier, P., & Schwartz, S. (2012). Effects of attentional load on early visual processing depend on stimulus timing. *Human Brain Mapping*, *33*(1), 63–74. https://doi.org/10.1002/hbm.21193

Renault, B., Ragot, R., Lesevre, N., & Remond, A. (1982). Onset and Offset of Brain Events as Indices of Mental Chronometry. *Science*, *215*(4538), 1413–1415. https://doi.org/10.1126/science.7063853

Rengachary, J., d'Avossa, G., Sapir, A., Shulman, G. L., & Corbetta, M. (2009). Is the Posner Reaction Time Test More Accurate Than Clinical Tests in Detecting Left Neglect in Acute and Chronic Stroke? *Archives of Physical Medicine and Rehabilitation*, *90*(12), 2081–2088. https://doi.org/10.1016/j.apmr.2009.07.014

Ritter, W., Simson, R., Vaughan, J. H. G., & Friedman, D. (1979). A brain event related to the making of a sensory discrimination. *Science*, *2031*(4387), 1358–1361.

Romeo, Z., Bonato, M., Zorzi, M., & Spironelli, C. (2019). Electrophysiological correlates of spatial processing during multitasking. *Neuropsychologia*, *133*, 107152. https://doi.org/10.1016/j.neuropsychologia.2019.107152

Romeo, Z., Mantini, D., Durgoni, E., Passarini, L., Meneghello, F., & Zorzi, M. (2021). Electrophysiological signatures of resting state networks predict cognitive deficits in stroke. *Cortex*, *138*, 59–71. https://doi.org/10.1016/j.cortex.2021.01.019

Rorden, C., Bonilha, L., Fridriksson, J., Bender, B., & Karnath, H. O. (2012). Age-specific CT and MRI templates for spatial normalization. *NeuroImage*, *61*(4), 957–965. https://doi.org/10.1016/j.neuroimage.2012.03.020

Rorden, C., Guerrini, C., Swainson, R., Lazzeri, M., & Baylis, G. C. (2008). Event related potentials reveal that increasing perceptual load leads to increased responses for target stimuli and decreased responses for irrelevant stimuli. *Frontiers in Human Neuroscience*, *2*. https://doi.org/10.3389/neuro.09.004.2008

Rorden, C., Karnath, H. O., & Bonilha, L. (2007). Improving Lesion-Symptom Mapping. *Journal of Cognitive Neuroscience*, *19*(7), 1081–1088. https://doi.org/10.1162/jocn.2007.19.7.1081

Russell, C., Malhotra, P., Deidda, C., & Husain, M. (2013). Dynamic attentional modulation of vision across space and time after right hemisphere stroke and in ageing. *Cortex*, *49*(7), 1874–1883. https://doi.org/10.1016/j.cortex.2012.10.005

Russell, V. L. (2022). *Estimated Marginal Means, aka Least-Squares Means* (1.8.3). https://CRAN.R-project.org/package=emmeans

Saccani, M. S., Contemori, G., Corolli, C., & Bonato, M. (2022). Transforming a Concept in a Tool: Diagnostic and Prognostic Value of Tasks Depleting Cognitive Resources. *Frontiers in Psychology*, *12*. https://doi.org/10.3389/fpsyg.2021.787374

Salthouse, T. A., & Meinz, E. J. (1995). Aging, Inhibition, Working Memory, and Speed. *The Journals of Gerontology Series*, *50*(6), 297–306. https://academic.oup.com/psychsocgerontology/article-lookup/doi/10.1093/geronb/50B.6.P297

Samogin, J., Liu, Q., Marino, M., Wenderoth, N., & Mantini, D. (2019). Shared and connection-specific intrinsic interactions in the default mode network. *NeuroImage*, *200*, 474–481. https://doi.org/10.1016/j.neuroimage.2019.07.007

Samogin, J., Marino, M., Porcaro, C., Wenderoth, N., Dupont, P., Swinnen, S. P., & Mantini, D. (2020). Frequency-dependent functional connectivity in resting state networks. *Human Brain Mapping*, *41*(18), 5187–5198. https://doi.org/10.1002/hbm.25184

Sarri, M., Greenwood, R., Kalra, L., & Driver, J. (2009). Task-related modulation of visual neglect in cancellation tasks. *Neuropsychologia*, *47*(1), 91–103. https://doi.org/10.1016/j.neuropsychologia.2008.08.020

Schendel, K. L., & Robertson, L. C. (2002). Using Reaction Time to Assess Patients With Unilateral Neglect and Extinction. *Journal of Clinical and Experimental Neuropsychology*, *24*(7), 941–950. https://doi.org/10.1076/jcen.24.7.941.8390

Schidelko, L. P., Schünemann, B., Rakoczy, H., & Proft, M. (2021). Online Testing Yields the Same Results as Lab Testing: A Validation Study With the False Belief Task. *Frontiers in Psychology*, *12*. https://doi.org/10.3389/fpsyg.2021.703238

Scurry, A. N., Lovelady, Z., Lemus, D. M., & Jiang, F. (2021). Impoverished Inhibitory Control Exacerbates Multisensory Impairments in Older Fallers. *Frontiers in Aging Neuroscience*, *13*. https://doi.org/10.3389/fnagi.2021.700787

Semmelmann, K., & Weigelt, S. (2017). Online psychophysics: reaction time effects in cognitive experiments. *Behavior Research Methods*, *49*(4), 1241–1260. https://doi.org/10.3758/s13428-016-0783-4

Senkowski, D., Talsma, D., Herrmann, C. S., & Woldorff, M. G. (2005). Multisensory processing and oscillatory gamma responses: effects of spatial selective attention. *Experimental Brain Research*, *166*, 411–426. https://doi.org/10.1007/s00221-005-2381-z

Shams, L., Iwaki, S., Chawla, A., & Bhattacharya, J. (2005). Early modulation of visual cortex by sound: An MEG study. *Neuroscience Letters*, *378*(2), 76–81. https://doi.org/10.1016/j.neulet.2004.12.035

Shams, L., Kamitani, Y., & Shimojo, S. (2000). What you see is what you hear. *Nature*, *408*(6814), 788–788. https://doi.org/10.1038/35048669

Shams, L., Kamitani, Y., & Shimojo, S. (2002). Visual illusion induced by sound. *Cognitive Brain Research*, *14*(1), 147–152. https://doi.org/10.1016/S0926-6410(02)00069-1

Shams, L., Kamitani, Y., Thompson, S., & Shimojo, S. (2001). Sound alters visual evoked potentials in humans. *Neuroreport*, *12*(17), 3849–3852. https://doi.org/10.1097/00001756-200112040-00049

Smith, S. M., Miller, K. L., Moeller, S., Xu, J., Auerbach, E. J., Woolrich, M. W., Beckmann, C. F., Jenkinson, M., Andersson, J., Glasser, M. F., Van Essen, D. C., Feinberg, D. A., Yacoub, E. S., & Ugurbil, K. (2012). Temporally-independent functional modes of spontaneous brain activity. *Proceedings of the National Academy of Sciences*, *109*(8), 3131–3136. https://doi.org/10.1073/pnas.1121329109

Smitha, K. A., Akhil Raja, K., Arun, K. M., Rajesh, P. G., Thomas, B., Kapilamoorthy, T. R., & Kesavadas, C. (2017). Resting state fMRI: A review on methods in resting state connectivity analysis and resting state networks. *The Neuroradiology Journal*, *30*(4), 305–317. https://doi.org/10.1177/1971400917697342

Sockeel, S., Schwartz, D., Pélégrini-Issac, M., & Benali, H. (2016). Large-Scale Functional Networks Identified from Resting-State EEG Using Spatial ICA. *PLOS ONE*, *11*(1), e0146845. https://doi.org/10.1371/journal.pone.0146845

Somers, D. C., & Sheremata, S. L. (2013). Attention maps in the brain. *WIREs Cognitive Science*, *4*(4), 327–340. https://doi.org/10.1002/wcs.1230

Spaccavento, S., Cellamare, F., Falcone, R., Loverre, A., & Nardulli, R. (2017). Effect of subtypes of neglect on functional outcome in stroke patients. *Annals of Physical and Rehabilitation Medicine*, *60*(6), 376–381. https://doi.org/10.1016/j.rehab.2017.07.245

Stevenson, R. A., Zemtsov, R. K., & Wallace, M. T. (2012). Individual differences in the multisensory temporal binding window predict susceptibility to audiovisual illusions. *Journal of Experimental Psychology: Human Perception and Performance*, *38*(6), 1517–1529. https://doi.org/10.1037/a0027339

Taberna, G. A., Samogin, J., Zhao, M., Marino, M., Guarnieri, R., Morales, E. C., Ganzetti, M., Liu, Q., & Mantini, D. (Under Review). Large-scale analysis of neural activity and connectivity from high-density electroencephalographic data. *Computers in Medicine and Biology*.

Talsma, D., Doty, T. J., & Woldorff, M. G. (2006). Selective Attention and Audiovisual Integration: Is Attending to Both Modalities a Prerequisite for Early Integration? *Cerebral Cortex*, *17*(3), 679–690. https://doi.org/10.1093/cercor/bhk016

Talsma, D., Senkowski, D., Soto-Faraco, S., & Woldorff, M. G. (2010). The multifaceted interplay between attention and multisensory integration. *Trends in Cognitive Sciences*, *14*(9), 400–410. https://doi.org/10.1016/j.tics.2010.06.008

Talsma, D., & Woldorff, M. G. (2005). Selective Attention and Multisensory Integration: Multiple Phases of Effects on the Evoked Brain Activity. *Journal of Cognitive Neuroscience*, *17*(7), 1098–1114. https://doi.org/10.1162/0898929054475172

Ten Brink, A. F., Verwer, J. H., Biesbroek, J. M., Visser-Meily, J. M. A., & Nijboer, T. C. W. (2017). Differences between left- and right-sided neglect revisited: A large cohort study across multiple domains. *Journal of Clinical and Experimental Neuropsychology*, *39*(7), 707–723. https://doi.org/10.1080/13803395.2016.1262333

The MathWorks Inc. (2016). *MATLAB version: 9.1.0 (R2016b)*. https://www.mathworks.com

The MathWorks Inc. (2023). *MATLAB version: 9.14.0 (R2023a)*. https://www.mathworks.com

Thompson, C. G., Kim, R. S., Aloe, A. M., & Becker, B. J. (2017). Extracting the Variance Inflation Factor and Other Multicollinearity Diagnostics from Typical Regression Results. *Basic and Applied Social Psychology*, *39*(2), 81–90. https://doi.org/10.1080/01973533.2016.1277529

Thompson, W. F., Russo, .F A., & Quinto, L. (2008). Audio-visual integration of emotional cues in song. *Cognition & Emotion*, *22*(8), 1457–1470. https://doi.org/10.1080/02699930701813974

Tiego, J., Testa, R., Bellgrove, M. A., Pantelis, C., & Whittle, S. (2018). A Hierarchical Model of Inhibitory Control. *Frontiers in Psychology*, *9*. https://doi.org/10.3389/fpsyg.2018.01339

Tosoni, A., Capotosto, P., Baldassarre, A., Spadone, S., & Sestieri, C. (2023). Neuroimaging evidence supporting a dual-network architecture for the control of visuospatial attention in the human brain: a mini review. *Frontiers in Human Neuroscience*, *17*. https://doi.org/10.3389/fnhum.2023.1250096

Upshaw, J. N., Leitner, D. W., Rutherford, B. a J., Miller, H. B. D., & Libben, M. R. (2019). Allocentric Versus Egocentric Neglect in Stroke Patients: A Pilot Study Investigating the Assessment of Neglect Subtypes and Their Impacts on Functional Outcome Using Eye Tracking. *Journal of the International Neuropsychological Society*, *25*(05), 479–489. https://doi.org/10.1017/S1355617719000110

Upton, G. J. G. (1992). Fisher's Exact Test. *Journal of the Royal Statistical Society*, *155*(3), 395. https://doi.org/10.2307/2982890

van den Heuvel, M. P., & Hulshoff Pol, H. E. (2010). Exploring the brain network: A review on resting-state fMRI functional connectivity. *European Neuropsychopharmacology*, *20*(8), 519–534. https://doi.org/10.1016/j.euroneuro.2010.03.008

van der Stoep, N., van der Stigchel, S., & Nijboer, T. C. W. (2015). Exogenous spatial attention decreases audiovisual integration. *Attention, Perception, & Psychophysics*, *77*(2), 464–482. https://doi.org/10.3758/s13414-014-0785-1

van Kessel, M. E., van Nes, I. J. W., Geurts, A. C. H., Brouwer, W. H., & Fasotti, L. (2013). Visuospatial asymmetry in dual-task performance after subacute stroke. *Journal of Neuropsychology*, *7*(1), 72–90. https://doi.org/10.1111/j.1748-6653.2012.02036.x

van Wassenhove, V., Grant, K. W., & Poeppel, D. (2007). Temporal window of integration in auditory-visual speech perception. *Neuropsychologia*, *45*(3), 598–607. https://doi.org/10.1016/j.neuropsychologia.2006.01.001

Varela, F., Lachaux, J. P., Rodriguez, E., & Martinerie, J. (2001). The brainweb: Phase synchronization and large-scale integration. *Nature Reviews Neuroscience*, *2*(4), 229–239. https://doi.org/10.1038/35067550

Vecera, S. P., & Rizzo, M. (2003). Spatial attention: normal processes and their breakdown. *Neurologic Clinics*, *21*(3), 575–607. https://doi.org/10.1016/S0733-8619(02)00103-2

Villarreal, S., Linnavuo, M., Sepponen, R., Vuori, O., Bonato, M., Jokinen, H., & Hietanen, M. (2022). Computer-Based Assessment: Dual-Task Outperforms Large-Screen Cancellation Task in

Detecting Contralesional Omissions. *Frontiers in Psychology*, *12*. https://doi.org/10.3389/fpsyg.2021.790438

Vogel, E. K., & Luck, S. J. (2000). The visual N1 component as an index of a discrimination process. *Psychophysiology*, *37*(2), 190–203. https://doi.org/10.1111/1469-8986.3720190

Vossel, S., Geng, J. J., & Fink, G. R. (2014). Dorsal and Ventral Attention Systems. *The Neuroscientist*, *20*(2), 150–159. https://doi.org/10.1177/1073858413494269

Vroomen, J., Bertelson, P., & De Gelder, B. (2001). The ventriloquist effect does not depend on the direction of automatic visual attention. *Perception & Psychophysics*, *63*(4), 651–659. https://doi.org/10.3758/BF03194427

Vuilleumier, P., & Rafal, R. (1999). "Both" means more than "two": localizing and counting in patients with visuospatial neglect. *Nature Neuroscience*, *2*(9), 783–784. https://doi.org/10.1038/12150

Wang, A., Sang, H., He, J., Sava-Segal, C., Tang, X., & Zhang, M. (2019). Effects of Cognitive Expectation on Sound-Induced Flash Illusion. *Perception*, *48*(12), 1214–1234. https://doi.org/10.1177/0301006619885796

Watkins, S., Shams, L., Josephs, O., & Rees, G. (2007). Activity in human V1 follows multisensory perception. *NeuroImage*, *37*(2), 572–578. https://doi.org/10.1016/j.neuroimage.2007.05.027

Watkins, S., Shams, L., Tanaka, S., Haynes, J.-D., & Rees, G. (2006). Sound alters activity in human V1 in association with illusory visual perception. *NeuroImage*, *31*(3), 1247–1256. https://doi.org/10.1016/j.neuroimage.2006.01.016

Watson, D., Clark, A., & Tellegen, A. (1988). Development and validation of brief measures of positive and negative affect: The PANAS scales. *Journal of Personality and Social Psychology*, *54*(6), 1063–1070. https://doi.org/10.1037/0022-3514.54.6.1063

Wee, J. Y. M., & Hopman, W. M. (2008). Comparing Consequences of Right and Left Unilateral Neglect in a Stroke Rehabilitation Population. *American Journal of Physical Medicine & Rehabilitation*, *87*(11), 910–920. https://doi.org/10.1097/PHM.0b013e31818a58bd

Weintraub, S., & Mesulam, M. M. (1985). Mental state assessment of young and elderly adults in behavioral neurology. *Principles of Behavioral Neurology*, 71–123.

Whittingham, K. M., McDonald, J. S., & Clifford, C. W. G. (2014). Synesthetes show normal sound-induced flash fission and fusion illusions. *Vision Research*, *105*, 1–9. https://doi.org/10.1016/j.visres.2014.08.010

Wilson, B., Cockburn, J., & Halligan, P. (1987). Development of a behavioral test of visuospatial neglect. *Archives of Physical Medicine and Rehabilitation*, *68*(2), 98–102.

Wolters, C. H., Grasedyck, L., & Hackbusch, W. (2004). Efficient computation of lead field bases and influence matrix for the FEM-based EEG and MEG inverse problem. *Inverse Problems*, *20*(4), 1099–1116. https://doi.org/10.1088/0266-5611/20/4/007

Wouters, H., de Koning, I., Zwinderman, A. H., van Gool, W. A., Schmand, B., Buiter, M., & Lindeboom, R. (2009). Adaptive Cognitive Testing in Cerebrovascular Disease and Vascular Dementia. *Dementia and Geriatric Cognitive Disorders*, *28*(5), 471–477. https://doi.org/10.1159/000250593

Yi, C., Chen, C., Si, Y., Li, F., Zhang, T., Liao, Y., Jiang, Y., Yao, D., & Xu, P. (2020). Constructing large-scale cortical brain networks from scalp EEG with Bayesian nonnegative matrix factorization. *Neural Networks*, *125*, 338–348. https://doi.org/10.1016/j.neunet.2020.02.021

Yoshida, T., Mizuno, K., Miyamoto, A., Kondo, K., & Liu, M. (2022). Influence of right versus left unilateral spatial neglect on the functional recovery after rehabilitation in sub-acute stroke patients. *Neuropsychological Rehabilitation*, *32*(5), 640–661. https://doi.org/10.1080/09602011.2020.1798255

Yuan, H., Ding, L., Zhu, M., Zotev, V., Phillips, R., & Bodurka, J. (2016). Reconstructing Large-Scale Brain Resting-State Networks from High-Resolution EEG: Spatial and Temporal Comparisons with fMRI. *Brain Connectivity*, *6*(2), 122–135. https://doi.org/10.1089/brain.2014.0336

Ziegler, E., Chellappa, S. L., Gaggioni, G., Ly, J. Q. M., Vandewalle, G., André, E., Geuzaine, C., & Phillips, C. (2014). A finite-element reciprocity solution for EEG forward modeling with realistic individual head models. *NeuroImage*, *103*, 542–551. https://doi.org/10.1016/j.neuroimage.2014.08.056

Zimmer, U., & Macaluso, E. (2007). Processing of multisensory spatial congruency can be dissociated from working memory and visuo-spatial attention. *European Journal of Neuroscience*, *26*(6), 1681–1691. https://doi.org/10.1111/j.1460-9568.2007.05784.x